Polymères Malléables Capables de Mémoire de Forme, d'Autoréparation et de Mouvement Contrôlés par des Stimuli

par

Xili Lu

Thèse présentée au Département de chimie en vue
de l'obtention du grade de docteur ès sciences (Ph.D.)
FACULTÉ DES SCIENCES, UNIVERSITÉ DE SHERBROOKE

présentée au State Key Laboratory of Polymer Materials Engineering en vue
de l'obtention du grade de Docteur (Ph.D.)
FACULTÉ DES SCIENCES, SICHUAN UNIVERSITY

Sherbrooke, Québec, Canada, Mai 2018

Malleable Polymers Capable of Stimuli-controlled Shape Memory, Self-healing and Motion

by

Xili Lu

Presented to the Department of Chimie
for the Degree of Doctor of Philosophy (Ph.D.)
FACULTÉ DES SCIENCES, UNIVERSITÉ DE SHERBROOKE

Presented to State Key Laboratory of Polymer Materials Engineering
for the Degree of Doctor of Philosophy (Ph.D.)
FACULTY OF SCIENCES, SICHUAN UNIVERSITY

Sherbrooke, Québec, Canada, May 2018

Le 23 Mai 2018

le jury a accepté la thèse de monsieur Xili Lu
dans sa version finale.

Membres du jury

Professeur Yue Zhao
Directeur de recherche
Département de chimie

Professeur Hesheng Xia
Codirecteur de recherche
Université de Sichuan

Professeur Yves Dory
Président-rapporteur
Département de chimie

Professour Armand Soldera
Évaluateur interne
Département de chimie

Professeur Jérôme Claverie
Évaluateur interne
Université de Sherbrooke

Professeur Christian Pellerin
Évaluateur externe
Université de Montréal

SOMMAIRE

Mots clés: polymères stimuli-répondants, polymères de mémoire de forme, polymères autoréparables, actionneurs polymères, polymères cristallins liquides

Dans la nature, des systèmes biologiques peuvent percevoir des changements environnementaux et répondre en modifiant leurs propriétés pour s'adapter aux changeants. Inspirés par la nature, les scientifiques ont développé une variété de nouveaux polymères stimuli-répondants qui sont capables de réagir aux stimuli environnementaux de manière contrôlée. Trois exemples représentatifs sont les polymères à mémoire de forme (SMP), les polymères autoréparables (SHP) et les actionneurs polymères, lesquels sont sujets de cette thèse. D'une part, les SHP sont une classe de matériaux intelligents qui ont la capacité de réparer les dommages par l'exposition à des stimuli externes. Cette fonction permet aux matériaux d'amél orer la sécurité ainsi que l'efficacité d'utilisation de l'énergie. Au cours des dernières années, il y a un développement rapide dans ce domaine de recherche. De nombreux matériaux autoréparables sont rapportés, dont une grande partie est basée sur l'utilisation des liaisons covalentes dynamiques telles que la liaison Diels-Alder, le disulfure, le trithiocarbonate et la chimie de transestérification. Cependant, les méthodes de déclenchement auto-cicatrisant sont limitées à l'utilisation de quelques stimuli, y compris le chauffage direct dans la plupart des cas, ainsi que l'exposition à la lumière, au champ électrique, au champ magnétique, au changement de pH ou d'humidité. Il est encore nécessaire de développer de nouvelles méthodes pour activer et contrôler les SHP. D'autre part, avec les matériaux autoréparables développés jusqu'à présent, l'effet auto-cicatrisant est souvent limité aux petites fissures, alors que les grandes fractures induites par une défo mation ré ultant d'une charge externe sont difficiles à gué ir. Généralement, les dommages sont accompagnés d'une déformation plastique et, dans beaucoup de cas, si la forme originale de la pièce ne peut être récupérée, les grandes fissures ou fractures, avec les surfaces s'éloignant l'une de l'autre, ne peuvent pas être réparées Afin de résoud e ce problème, la fonction de mémoire de forme est introduite dans les matériaux pour faciliter l'autoré p ration. En plus de la mémoire de forme et de l'auto-guérison, les systèmes

biologiques possèdent une autre fonctionnalité optimisée dans son évolution : la réactivité mécanique. C'est la capacité de détecter les changements environnementaux et de convertir les stimuli environnementaux (par exemple, l'humidité, la lumière ou le toucher) en mouvements. Aussi inspirés par cette fonction, les scientifiques ont développé un autre type de matériaux réactifs aux stimuli: les actionneurs polymères, qui ont la capacité de changer de forme sous l'effet de stimulation, et donc d'effectuer un travail méc an que aux échelles nano, micro et macroscopique. Les actionneurs polymères ont suscité un intérêt grandissant ces dernières années en raison de leur large éventail d'applications dans les systèmes de microfabrication, de robots souples, de médecine et de laboratoire-sur-puce. Cependant, les actionneurs polymères pouvant présenter des mouvements macroscopiques robustes, auto-propulsifs (continus) avec une vitesse de déplacement réglable et une direction de déplacement contrôlable sont très rares. Le sujet principal de cette thèse est d'apprendre de la nature à concevoir, fabriquer et étudier des polymères dynamiques qui présentent des caract ́er stiques intelligentes, c'est-à-dire la mémoire de forme, l'autoréparation et les mouvements contrôlés par des stimuli. Nous avons utilisé des ultrasons pour d ́e lencher un processus d'auto-guérison assisté par un effet de mémoire de forme. L'utilisation d'ultrasons pour contrôler l'autoréparation présente plusieurs avantages par rapport à d'autres stimuli, tels que l'activation à distance, le contrôle spatiotemporel et, plus important encore, la pénétration profonde dans les tissus biologiques. De plus, nous avons développé des actionneurs cristallins liquides azobenzènes qui sont malléables et peuvent afficher des mouvements macroscopiques sophistiqués avec une direction de déplacement contrôlable et une vitesse de déplacement réglable. Les travaux de recherche accomplis dans cette thèse couvrent principalement ces deux sujets, rapportés dans trois chapitres.

Dans notre première ́etude sur les SHP sous l'effet des ultrasons, nous avons démontré un nouveau concept d'auto-guérison assistée par un effet de mémoire de forme en utilisant des polymères dynamiques. Les polymères sont conçus comme des réseaux de polyuréthane (PU) avec des segments de poly(ε-caprolactone) (PCL) et des unités Diels-Alder (DA) (furan-maléimide) incorporés en alternance dans les chaînes entre des points de réticulation. L'intégration d'un certain nombre de caractéristiques et propriétés souhaitables dans le

même matériau peut être obtenue, telles que de bonnes propriétés mécaniques, une efficacité de guérison élevée, une grande sensibilité aux ultrasons, une excellente performance de la fermeture de fissure assistée par mémoire de forme, ainsi qu'un processus de guérison à distance et avec un contrôle spatial. Les actions de mémoire de forme déclenchées par les ultrasons focalisés de haute intensité (HIFU) peuvent fermer les fissures, ce qui constitue la condition préalable à la formation de liens entre les surfaces endommagées pendant le processus de cicatrisation. Des réactions rétro-DA et de remaniement déclenchées par HIFU sont les principales raisons de la guérison efficace des polymères réticulés par des liaisons covalentes dynamiques. La réparation localisée et sur demande peut être facilement réalisée par HIFU, à distance et de manière et contrôlée, en déposant l'énergie acoustique uniquement dans la zone endommagée avec une grande précision et des effets secondaires minimaux. Ce qui est démontré dans cette étude, et ce pour la première fois, c'est l'autoréparation assistée par la mémoire de forme déclenchée par HIFU et renforcée par l'utilisation de polymères dynamiques basé sur une réaction réversible de Diels-Alder, ainsi que la stratégie de conception d'architecture moléculaire, applicable à une large gamme de matériaux dynamiques pour des applications potentielles telles que des composants sous tension mécanique à long terme et des dispositifs médicaux antifatigues.

Dans la deuxième étude concernant les actionneurs polymères, nous avons conçu et synthétisé un élastomère cristallin liquide malléable contenant des unités mésogènes d'azobenzène dans le squelette de chaîne (ALCE) en utilisant une réticulation covalente dynamique à base de transestérification. Nous avons démontré que par pré-stockage de l'énergie de déformation mécanique dans les films ALCE, une force de contraction sans précédent peut être générée par l'irradiation de la lumière UV en raison de la libération photoinduite de l'énergie stockée en plus de la conversion directe d'énergie optique en énergie mécanique issue de la photoisomérisation trans-cis de l'azobenzène. La force mécanique forte permet de réaliser des mouvements continus des actionneurs polymères de grande taille sous la forme de roues ou de «moteurs» ruban-ressorts qui peuvent être poussés vers l'avant ou tirés vers l'arrière par la lumière UV actinique, avec une vitesse de rotation déterminé par la quantité de l'énergie de déformation pré-stockée dans l'ALCE.

Cette approche de l'amplification de la force mécanique photoinduite est générale pour les élastomères ou les réseaux de polymères cristallins liquides contenant des azobenzènes et peut aider leur exploitation pour des applications.

Sur la base du second projet, afin de renforcer le photocontrôle des actionneurs polymères cristallins liquides, nous avons doté les réseaux dynamiques d'une réponse au proche infrarouge (NIR) en plus de la réponse à la lumière UV-Vis, en ajoutant des nanobâtonnets d'or dans la matrice polymère (AuNR -ALCN). Nous avons mesuré la force de contraction induite par la lumière NIR et UV pour investiguer ces deux mécanismes photo-répondants différents. De plus, en utilisant des structures de bicouche, nous avons réalisé un contrôle de la direction de mouvement des AUNR-ALCN. Grace à ce renforcement du photocontrôle, nous avons pu manipuler certains «athlètes» en plastique pour exécuter des tâches de mouvement spécifiques et programmées, telles que le « push up » et le « sit up », en inscrivant des alignements moléculaires dans différentes régions des actionneurs bicouches. En outre, en utilisant la propriété de récupération de forme rapide du film bicouche, nous avons démontré un marcheur capable de ramper vers l'avant comme une chenille, sur un substrat à cliquet, contrôlé par la lumière. Enfin, une « grue » polymère a été fabriqué et des mouvements macroscopiques robotiques ont été réalisés pour produire un travail mécanique (saisir, soulever, baisser et relâcher un objet). Ce travail fournit non seulement de nouvelles perspectives sur la fabrication des actionneurs photoactifs, mais fait également un pas important vers des applications potentielles des actionneurs polymères photocontrôlables.

ABSTRACT

Keywords: stimuli-responsive polymers, shape memory polymers, self-healing polymers, polymer actuators, liquid crystalline polymers

In nature, biological systems can perceive environmental change and respond by changing one or more performance parameters to adapt themselves to the changed environment. Inspired by these biological systems, scientists have developed a variety of novel stimuli-responsive polymers that are able to perform a desired function in response to environmental stimuli in a controlled and predetermined modality. Three representative examples are shape-memory polymers (SMPs), self-healing polymers (SHPs) and polymeric actuators that are subjects of this thesis. On the one hand, SHPs are a class of smart materials that have the ability to repair damage upon exposure to external stimuli (triggers). This kind of material has advantages in improving material security, enhancing energy utilization efficiency and reducing environmental pollution. In recent years there is a rapid development in this research field; a variety of "intrinsically" self-healing materials based on covalent dynamic chemical bonds (such as Diels-Alder bond, disulfide, trithiocarbonate and transesterification chemistry) that can repair themselves via reversible bond breaking and reformation have been produced. However, the self-healing triggering methods are limited to the use of a handful of stimuli, including direct heating in most cases, as well as exposure to light, electric field, magnetic field, pH change or moisture. There is still a need to develop novel triggering methods to control SHPs. On the other hand, with the self-healing materials developed so far, self-healing effect is limited to small cracks while deformation-induced large cracks resulting from external force are difficult to heal. In most situations, damage is caused or accompanied by plastic deformation. Deformed parts usually require manual operation to recover to their original shapes, which wastes time and energy. Moreover, if the original shape cannot be recovered, the damages separated by large cracks cannot be repaired. In order to resolve this problem, shape memory function is introduced into the materials to assist the self-healing effect. In addition to shape memory and self-healing, biological systems possess another evolutionarily optimised functionality: mechanical responsiveness. That is the ability to sense environmental changes and convert environmental stimuli (e.g., humidity, light or

touch) into motions. Inspired by nature, scientists have also developed another kind of stimuli-responsive materials: polymer actuators, which have the ability to change their shape in response to changing environmental conditions and thus perform mechanical work on the nano-, micro-, and macroscales. Polymer actuators have been attracting broad and growing interest in recent years because of their wide range of applications in microfabrication, microrobots, medicine, and lab-on-a-chip systems. However, stimuli-responsive polymer actuators that are able to exhibit robust, self-propelling (continuous), macroscopic motions with tunable moving speed and controllable moving direction are elusive. The main topic of this thesis is to learn from nature to design, fabricate and investigate covalent dynamic polymers that display smart features, such as stimuli-controlled shape memory, self-healing and biomimetic motions. We utilized ultrasound to trigger shape recovery assisted self-healing of covalently cross-linked dynamic polymers. Using ultrasound to control self-healing has several advantages compared to other stimuli, such as remote activation, spatiotemporal control and, more importantly, deep penetration into biological tissues. Moreover, we developed malleable azobenzene liquid crystalline actuators that can display sophisticated macroscopic motions with controllable moving direction and tunable moving speed. The research works accomplished in this thesis mainly covers these two topics, reported in three chapters.

In our first study regarding ultrasound-healable SHPs, we demonstrated a novel concept of ultrasound-triggered shape memory assisted self-healing of covalently cross-linked dynamic polymers. The polymers are designed as polyurethane (PU) networks with poly(ε-caprolactone) (PCL) and Diels-Alder (DA) adducts (furan-maleimide) alternately incorporated in the backbone of polymer chains between adjacent crosslinking points. Integration of a number of desirable features and properties into the same material could be achieved, such as good mechanical properties, high healing efficiency, sensitive ultrasound-responsiveness, excellent performance of shape memory-assisted crack closure, remote and spatially controllable healing process. The shape memory actions triggered by high-intensity-focused-ultrasound (HIFU) can close the crack, which provides the prerequisite for the bond formation between the damage surfaces during the healing process. HIFU triggered retro-DA reactions and DA reshuffling reactions are the main

reasons for the effective healing of covalently cross-linked dynamic polymers. The localized, on-demand repairing can be easily achieved by HIFU via depositing the acoustic energy only in the damaged area with pinpoint accuracy and minimum side effects in a remote and controlled way. The modality, i.e., HIFU-triggered shape memory assisted healing of polymers based on reversible Diels−Alder reaction, as well as the unique molecular architecture design strategy, can be extended to a wide range of dynamic materials for potential applications such as long-term load-bearing engineering components and anti-fatigue medical devices.

In the second study concerning polymer actuators, we designed and synthesized reprocessable liquid crystalline elastomers containing azobenzene mesogens in the chain backbone (ALCE) using transesterification-based dynamic covalent crosslinking. We demonstrated that by pre-storing mechanical strain energy in ALCE films, unprecedented contraction force can be generated by UV light irradiation as a result of the phototriggered release of the stored energy in addition to the direct optical to mechanical energy conversion stemming from the *trans-cis* photoisomerization of azobenzene. The strong mechanical force enables sophisticated continuous motions of large-size polymer actuators in the form of wheels or spring-like "motors" that can be either pushed forward or pulled backward by the actinic UV light, with tunable rolling speed determined by the amount of pre-stored strain energy in the ALCE. This approach to amplifying the photoinduced mechanical force is general for azobenzene-containing liquid crystal elastomers or networks and should help their exploitation for applications.

On the basis of the second project, in order to further enhance the photocontrol of actuations of the liquid crystalline polymers, we endowed the azobenzene liquid crystalline dynamic networks with both NIR and UV-Vis light responsiveness by doping AuNRs into the polymer matrix (namely AuNR-ALCNs). We used isostrain experiments to measure the NIR- and UV- lightinduced contraction force of the AuNR-ALCNs to investage these two different photoresponsive mechanisms. Moreover, by taking advantages of bilayer structures, we successfully controlled the motion directions of AuNR-ALCNs. Based on this enhanced photoresponsiveness, we could manipulate some plastic "athletes" to execute localized-programmable specified motion tasks, such as push up and sit up, by locally

encoding molecular alignments in different regions of the bilayer actuators. Besides, a light-driven caterpillar-inspired walker that can crawl forward on a ratcheted substrate was demonstrated as a biomimetic application by making use of the rapid shape-change recover property of the bilayer film. Finally, the light-triggered molecular level changes, i.e., LC phase transition and photoisomerization of azobenzene, were successfully added up to converted into sophisticated, combinational robot-like, macroscopic motions to produce useful work, in the from of a photo-operated polymer crane grasping, lifting up, lowering down, and releasing an object. This work not only provides new insights into the fabrication of multiple responsive LC actuations but also takes a significant step forward towards potential applications of light-driven polymer actuators in artificial muscle and biomimetic soft robots.

摘要

关键词：刺激响应聚合物，形状记忆聚合物，自修复高分子，聚合物致动器，液晶高分子

在自然界中，生物系统可以感知环境变化和实时改变一个或多个性能参数来使自己适应环境的改变。受这些生物系统的启发，科学家开发了各种新型刺激响应聚合物，它们能够以受控和预定的方式对环境刺激变化做出响应，进而展示预设的功能。形状记忆聚合物（SMPs），自修复聚合物（SHPs）和聚合物致动器是本论文的研究的三个代表性实例。一方面，自修复聚合物是一类在外部刺激作用下可以自我修复损伤的智能材料。这种材料在提高材料安全性，提高能源利用效率和减少环境污染方面具有很大优势。近年来，该研究领域发展迅速，各种基于共价动态化学键（例如 Diels-Alder 键，二硫键，三硫代碳酸酯和酯交换化学）的“本征型”自修复材料已经被报道，它们可以通过动态键的可逆断裂和重组来修复自身损伤。然而，自修复刺激方式很有限，包括在大多数情况下的直接加热，以及光，电场，磁场，pH 变化或水分。新型的刺激自修复方法仍待开发。另一方面，目前为止已经开发的自修复材料，自愈效果仅限于小裂纹，而由外力引起的伴随变形的大裂纹难以愈合。在大多数情况下，材料损伤往往伴随着塑性变形。变形部件通常需要手动操作和调平才能恢复到原来的形状，浪费时间和能源。在某些特殊情况下，变形部件甚至不能拆下来进行维修。此外，如果原始形状无法恢复，则不能修复由裂缝分离的损伤。为了解决这个问题，形状记忆功能被引入到材料中以辅助自修复效果。除了形状记忆和自我修复这两个突出的特征之外，生物系统还具有另一个进化上优化的功能——机械响应性，即感测环境变化并将环境刺激（例如，湿度，光或触感）转化为运动的能力。受生物系统机械响应特征的影响，科学家已经开发出另一种刺激响应材料——聚合物致动器，它们具有对环境条件变化作出响应来改变其形状的能力，从而在纳米，微米和宏观尺度做功（运动）。近年来，聚合致动器由于它们在微细加工，微型机器人，医药和实验室芯片系统中等领域中具有广泛应用前景，进而引起广泛和日益增长的兴趣。 然而，能够显示稳定、自推进（连续）、速度可调和运

动方向可控的宏观运动的刺激响应聚合物致动器，仍然在很大程度上未被探索。本论文的主要内容是向自然界学习，设计、制备和研究具有形状记忆、自修复和仿生运动能力等智能特征的共价动态聚合物。我们利用超声波引发共价交联动态聚合物的形状记忆功能来辅助材料的自修复。使用超声波引发材料自修复与其他刺激相比具有几个优点，如远程激活、时空控制性，更重要的是超声在生物组织中良好穿透性。此外，我们开发了可加工的偶氮苯液晶致动器，其可刺激响应运动具有可控移动方向和可调移动速度。第二部分着重于开发具有可加工能力和机械响应性的新型液晶聚合物致动器，并且可以通过光来控制其运动。

在我们第一项关于超声刺激材料自修复的研究中，我们证明了一种超声触发形状记忆辅助共价交联动态聚合物自修复的新概念。聚合物分子结构设计：聚（ε-己内酯）（PCL）和 Diels-Alder（DA）加合物（呋喃——马来酰亚胺）交替地嵌入在相邻交联点之间的聚合物主链上，以此构成含动态键的聚氨酯（PU）网络。在本项研究中，我们实现了将多种所需特征和性质整合同一材料中，例如良好的机械性能，高自修复效率，敏感的超声响应性，优良的形状记忆辅助裂纹愈合性能，远程的空间可控的自修复过程。由 HIFU 触发的形状记忆行为可以关闭裂纹，这为自修复过程中裂纹表面之间的结合形成提供了先决条件。HIFU 引发逆转 DA 反应或 DA 重组反应是共价交联动态聚合物有效愈合的主要原因。HIFU 可以通过仅在受损区域中以精确的准确度和最小的副作用，远程地和受控地沉积声能来轻松实现局部的按需修复。HIFU 触发形状记忆辅助动态聚合物自修复的这种策略以及独特的聚合物分子结构设计方法可以扩展到广泛的动态材料，用于潜在的应用，如长期承重工程部件和抗疲劳医疗器械。

在关于聚合物致动器的第二项研究中，我们使用基于酯交换的动态共价交联设计并合成了在主链中含有偶氮苯的可再加工的可延展的液晶弹性体（LCEs）。我们证明了通过在 ALCE 薄膜中预先存储机械应变能量，薄膜在 UV 光照射可以产生前所未有的收缩力。这些力除了来自偶氮苯的顺式-反式光异构化引发的光能-机械能转化外，也来自于储存能量的光触释放。我们利用这些储存了机械应变能量的薄膜制

备了轮状或弹簧状“马达”，在紫外光的驱动下，这些马达呈现方向可控速度可调的复杂连续光驱运动：通过构造不同的致动器结构来控制运动方向以及通过调控聚合物薄膜储存能量来调节马达的运动速度。这种扩大光诱导机械力的方法对于含偶氮苯的液晶弹性体或网络就有通用性，并且有助于它们的应用开发。

在第二个研究项目的基础上，为了进一步增强液晶聚合物的光控驱动，我们通过掺杂 AuNRs 到聚合物基体来同时赋予偶氮苯液晶动态聚合物网络近红外（NIR）光和紫外-可见（UV-Vis）光响应性（命名为 AuNR-ALCNs）。我们通过等应变机械应力测试测量 AuNR-ALCNs 的 UV 光和 NIR 光响应力来研究这两种不同的光响应行为和机制。此外，通过利用双层膜结构的光响应特点，我们成功实现对致动器运动方向的控制。在此基础上，通过在双层膜致动器不同区域局部地编码液晶分子排列，实验成功实现操控塑料“运动员”执行不同的运动任务，如俯卧撑和仰卧起坐等。此外，通过利用双层膜快速恢复形状变化的性能，实验实现了塑料“毛毛虫”在棘齿型基板上进行光驱动爬行的仿生应用。最后，光引发的分子水平的变化，即液晶相转变和偶氮苯异构化反应，在实验中成功协同叠加并转化成复杂的类机器人的组合型宏观运动，实现了聚合物起重机在光操控下执行一系列运动任务，包括抓取、提升、降低和释放一个管状重物。这项工作不仅为制造多重响应的液晶致动器提供了新的见解，还使光响应聚合物致动器在人工肌肉和仿生柔性机器人的应用方面迈出了重要一步。

ACKNOWLEDGEMENT

First of all, I would like to extend my sincere gratitude to my supervisor, Professor Yue Zhao, for his constant guidance and encouragement in my research and in the pursuit of my Ph.D degree during these years. It is my great honor to have a chance to study in his group at the Université de Sherbrooke, his perceptive insights into scientific research and charming personality have a great influence on me. I also would like to thank my co-supervisor Prof. Hesheng Xia in Sichuan University, for all of his patient guidance and very helpful suggestions during the years before I came to Canada.

I would like to thank all the professors and staff working in the Department of Chemistry at the Université de Sherbrooke, for their kind help during my Ph.D study in the Université de Sherbrooke. I also would like to thank Prof. Christian Pellerin (Université de Montréal), and Profs. Jérôme Claverie, Yves Dory and Armand Soldera to read my thesis and serving in the jury. Special thanks go to Dr. Daniel Fortin for his help in conducting WAXS experiments and many useful discussions.

My sincere thanks also go to all my group members, both past and present, as they have contributed immensely to my personal and professional time at Sherbrooke, the group has been a source of friendship as well as good advice and collaboration: Mrs. Xia Tong, Prof. Qiang Yan, Dr. Olivier Boissière, Dr. Xin Zhao, Dr. Shengwei Guo, Dr. Bin Yu, Dr. Shangyi Fu, Dr. Hu Zhang, Dr. Guo Li, Dr. Rong Yang, Mr. Damien Habault, Mr. Jun Xiang, Mr. Weizheng Fan, Mrs. Aurélie Lespes, Mrs. Amelie Auge, Mr. Farhad Farnia, Mr. Feijie Ge, Mr. Liangliang Dong and Mr. Ricardo Da Silva Lemos. Especially, I thank Mrs. Xia Tong for the great help in all characterization works and assistance in starting all the measurements in the lab. Same thanks go to all group members and colleagues in Prof. Xia's laboratory in Sichuan University.

I would like to give my thanks and respect to the Chinese Scholar Council (CSC) for awarding me a scholarship that allow my living and study in Canada. I also would like to thank all the members of the Education Office of the Chinese Embassy in Canada.

Sincere gratitude to my parents and my relatives for all their love and encouragement during my study in Canada.

Finally, I would like to acknowledge the following organizations for their financial support: Major Project of Chinese Ministry of Education (313036), the Programme of Introducing Talents of Discipline to Universities (B13040), National Natural Science Foundation of China (51203102, 51010004, 51433006), the Young Talent Team Science and Technology Innovation Project of Sichuan Province (2016TD0010), Natural Sciences and Engineering Research Council of Canada (NSERC), Le Fonds de recherche du Québec: Nature et technologies (FQRNT) and the Université de Sherbrooke.

TABLE OF CONTENTS

LIST OF ABBREVIATIONS

AFM: atomic force microscope

AFT: addition-fragmentation chain transfer

ALCEs: azobenzene liquid-crystalline elastomers

AuNP: gold nanoparticles

AuNR: gold nanorods

Bip: 2,6-bisbenzimidazolylpyridine

BPO: benzoyl peroxide

BOPP: biaxially oriented polypropylene

CAA: cinnamylidene acetic acid

CB: carbon black

CNT: carbon nanotubes

CTAB:hexadecyltrimethylammonium bromide

DA: Diels Alder

DMA: dynamic thermomechanical analysis

DSC: differential scanning calorimetry

endo-DCPD: endo-dicyclopentadiene

FM: furan-maleimide

FTIR: fourier transform infrared spectroscopy

G': storage modulus

G'': loss modulus

GO: graphene oxide

HDCNs: hemiaminal dynamic covalent networks

HIFU: high intensity focused ultrasound

IPN: interpenetrating polymer network

LC: liquid-crystalline

LCEs: liquid-crystalline elastomers

LCNs: liquid crystalline polymer networks

LCP: liquid crystalline polymer

MDI: 4, 4'-methylene diphenyl diisocyanate

NIR light: near infrared light

NMP: N-methyl-2-pyrrolidone

NMR: nuclear magnetic resonance

ODA: 4,4′-oxydianiline

PBA: poly(n-butyl acrylate)

PCL: poly(ε-caprolactone)

PDMA: poly(N,N-dimethylacrylamide)

PEG: polyethylene glycol

PHTs: poly(hexahydrotriazine)s

P(MMA-BA): p(methyl methacrylate-co-butyl acrylate)

PNC: polymer carbon nanotube nanocomposite

PU: polyurethane

PVA: polyvinyl alcohol

R_f: shape fixity ratio

R_r: shape recovery ratio

RAFT: reversible addition-fragmentation chain transfer polymerization

SAXS: small-angle X-ray scattering

SM: shape memory

SMA: shape-memory alloy

SMP: shape memory polymer

SMPs: shape memory polymers

SHPs: self-healing polymers

SPR: surface plasmon resonance

TBD: triazobicyclodecene

TDS: thiuram disulfide

TEM: transmission electron microscopy

T_g: glass transition temperature

THF: tetrahydrofuran

T_m: melting temperature

T_{ni}: liquid crystal nematic-isotropic transition

T_{si} : liquid crystal smectic-isotropic phase transition

TTC: trithiocarbonates

T_{trans}: transition temperature

UV light: ultraviolet light

Vis light: visible light

WAXS: wide-angle X-ray scattering

XRD: X-ray diffractio

LIST OF TABLES

LIST OF FIGURES

INTRODUCTION

Stimuli-responsive polymers can be defined as the ‘‘smart’’ polymers that are capable of performing a desired function in response to external stimuli, such as light, ultrasound, temperature, magnetic or electric field, pH, ionic strength, biomolecules, and so on (1,2). These materials are playing a more and more important role in a wide range of fields, such as shape memory polymers (SMPs), self-healing polymers (SHPs), actuators, drug delivery, as well as biosensors, soft robotics, artificial muscles, coatings and textiles. Generally, these smart polymers can adapt to surrounding environmental changes, usually slight changes are sufficient to induce significant response in the polymer's structure and properties, like macroscopic shape, mechanical strength, mode of motions, transportation of ions and molecules, wettability and color (1,3-5). In the following sections we will focus on the relevant literatures about stimuli-responsive (stimuli-controlled) SMPs, SHPs and polymer actuators that are the research topics of this thesis.

I. Shape Memory Polymers

As one of the most important stimuli-responsive materials, SMPs are polymer materials that are able to recover their original (permanent) shape from a deformed shape (temporary state) upon exposure to external stimuli (triggers) (6), such as temperature, electric or magnetic field (7), light (8), ultrasound (9) or solvent (10). Generally, SMPs comprise physical or chemical cross-linkers and molecular switches. The cross-linkers are employed to keep the integrity of the polymer during deformation, prevent chain relaxation and thus “remember” the permanent shape, while the molecular switches (vitrification or crystallization of polymer chains) are responsible for retaining and release of the deformation. Once the SMPs are deformed in the “switch on” state, the deformation can be kept by “switch off” of the chain mobility, and the deformation will be retained until the chain mobility of the polymer is switched on again. Two important quantities, shape fixity ratio (R_f) and shape recovery ratio (R_r), are used to describe shape-memory effects. The shape fixity ratio is defined as the ability of switching domains to fix the temporary deformation, while the shape recovery ratio represents the ability of the polymer to memorize its permanent shape.

$$Rf = \frac{\varepsilon_p}{\varepsilon_m} \qquad Rr = \frac{\varepsilon_m - \varepsilon_p}{\varepsilon_m}$$

where ε_m represents the maximum strain applied on the material, and ε_p is defined as the recovery strain upon exposure to a stimulus.

Among various SMPs, thermo-responsive SMPs are the most studied ones, in which the shape memory behavior is controlled by heating and cooling. In order to endow SMPs with more controllability and expand their applications, much attention has recently been paid to develop novel SMPs triggered by stimuli other than heat.

I.I. Thermo-responsive SMPs

Typically, thermo-responsive SMPs contain two phases: the reversible phase (soft segment) and the stable phase (hard segment). The reversible phase generally is derived from physical crosslinking or entanglement of the polymer chains, and the transition temperature is low. For amorphous polymers, the reversible phase undergoes a reversible transition between glassy state, viscous fluid state and rubbery state with temperature change. For crystalline polymer, the reversible phase changes between crystalline and molten state. The stable phase, which is used to remember the initial shape, can be physical crosslinking or chemical crosslinking. The typical shape memory process of thermo-responsive SMPs as follows. 1) When the temperature of the polymer rises to 15~20 ºC above the reversible phase transition temperature (T_{trans}), the reversible phase undergoes softening or melting and the modulus of the polymer decreases by 1~2 orders of magnitude due to stronger polymer chain relaxation. 2) Mechanical force is applied to deform the SMPs to a prescribed shape. In this process, chain segments in the reversible phase are deformed while the stable phase is still in the solid phase. The relative motion of the whole polymer chains is restricted by the stable phases, which enable the polymer to remember the original shape. 3) Maintain the external force and cool the polymer below the transition temperature (room temperature or 15~20 ºC below T_{trans}) to make the polymer crystallize or vitrify to limit the molecular motion. The polymer shape is fixed with a slight creep after the external force is

removed, and the strain energy is stored in the polymer. 4) When the temperature is raised above T_{trans}, the stored energy releases and the polymer returns to the original shape.

I.II. Light-responsive SMPs

Generally, light-responsive SMPs can be mainly divided into two kinds, including those based on reversible photochemical reactions (8,11,12) and those relied on photothermal effect (13-27). For the former, its shape fixation and shape recovery rely on reversible photochemical reactions and do not involve any thermal effect. For the latter, by incorporating functional fillers into the SMP matrix, the fillers can transform light energy into heat and subsequently elevate the surrounding temperature of the polymer matrix above its T_{trans} to triggers the shape recovery process. Compared with the traditional SMPs, the most important advantages of light-responsive SMPs are that 1) spatial control of shape memory behavior is feasible because the light beam can be delivered to selected regions; 2) remote control is easily achievable as light is able to travel a long distance and 3) light-controlled processes can be terminated and resumed at any time just by turning off or turning on the exciting light (4).

I.II.I. Light-responsive SMPs Based on Reversible Photochemical Reactions

In this kind of SMPs, photo-responsive units capable of photoinduced reversible [2+2] cycloaddition reactions are usually employed to serve as molecular switches. Upon exposure to two different wavelengths of light, the SMPs undergo a reversible photo-controlled crossliking/decrosslinking to adjust the crosslinking density and change the T_g and modulus, allowing the material to switch between “soft” and “rigid” states. Soft state usually bases on a slightly crosslinked SMP with a low T_g which provides the original shape. Rigid state is obtained by increasing the crosslinking density using photo-crosslinking recation with a certain wavelength of light. And the high T_g rigid state can be employed to fix the temporary shape at room temperature. Upon exposure to the incident light with other wavelength, the de-crosslinking of the polymer network allows the material to recover its original shape. Lendlein and coworkers (8) made the demonstration of the first light-responsive SMPs by incorporation of photo-responsive cinnamic moieties into polymer structures to serve as molecular switches. In this way, the polymer

can be deformed and fixed into preprogrammed shape such as stretched film and tube, arche or spring ribbon by UV light irradiation (Figure 1). These temporary shapes are stable for a long time even at 50 ºC, and the polymer can recover their permanent shapes at ambient temperatures upon exposure to UV light with a different wavelength.

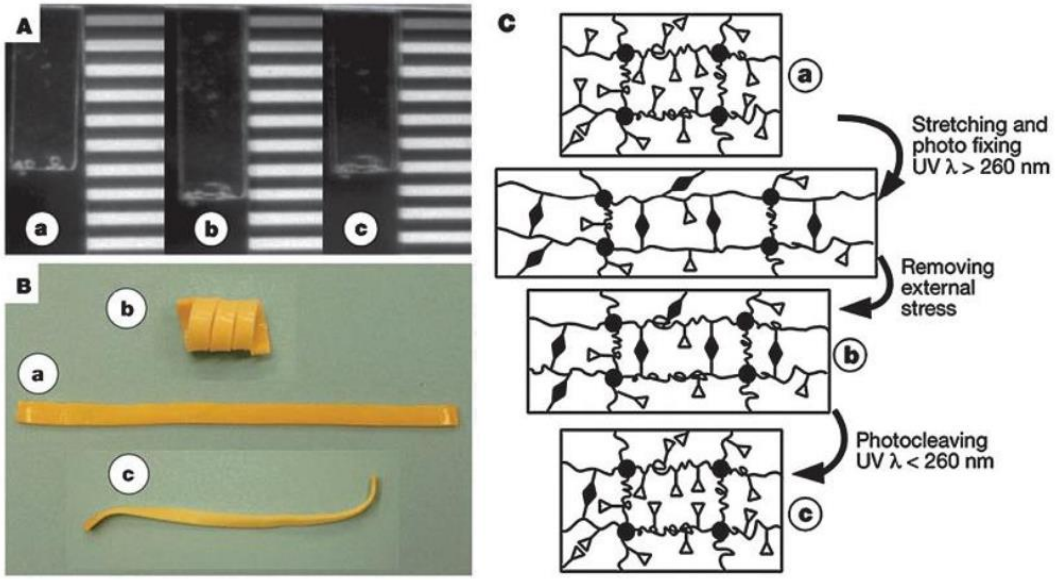

Figure 1. Shape-memory behavior of light-responsive polymers. (A) The cinnamic acid-containing polymer film, with both sides of the specimen exposed to UV light for photo-crosslinking (fixation of a temporary shape) and photo-decrosslinking (recovery of the original shape). a, Permanet shape; b, temporary shape; c, recovered original shape. (B) An IPN polymer sheet containing cinnamylidene acetic acid (CAA) moieties, with only one side of the specimen exposed to UV light for temporary shape fixation. a, Permanent shape; b, spring-like temporary shape; c, recovered shape achieved by exposure to UV light of $\lambda < 260$ nm for 60 min. (C) The proposed mechanism of shape-memory effect of the light-responsive SMP based on the photoreversible [2+2] cycloaddition reactions of cinnamic acid. [8]

I.II.II. Light-responsive SMPs Based on Photothermal Effect

For most of stimuli-responsive SMPs, the key point of an appropriate stimulus to trigger the shape recovery behavior is that it can raise the polymer temperature above the transition temperature to

allow the transformation from temporary shape to original shape. It is demonstrated that photothermal effect is a highly efficient stimulus to trigger shape recovery behavior in a remote and spatiotemporal way. Up to date, many light-absorbing and heat-generating species including gold nanoparticles (AuNP), gold nanorods (AuNR), carbon nanotubes (CNT), graphene, organic dyes and ligands have been employed to obtain the photothermal effect to trigger shape recovery of SMPs. These light-absorption species can efficiently convert light energy into heat via a non-radiative energy dissipation of electrons from excited state to ground state.

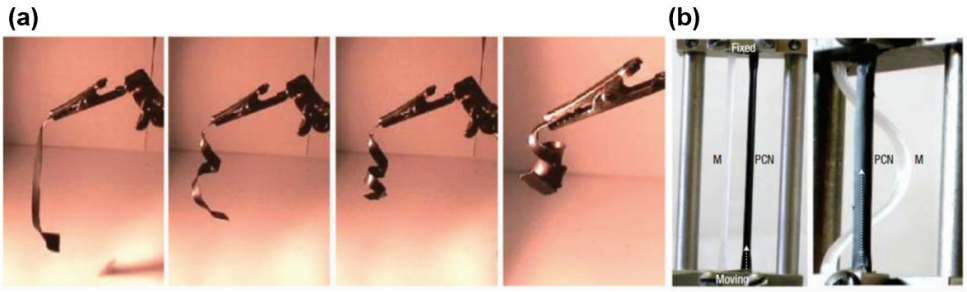

Figure 2 . (a) Optical images showing shape recovery of the material under infrared light (NIR) irradiation. (b) Comparison of the actuation behavior before (left) and after (right) NIR irradiation. Neat Morthane undergoes bending but does not recover. On the contrary, a CNT (1 wt%) nanocomposite (PCN) undergoes contraction and lifts a 60 g weight (moving bottom clamp) 3.3 cm with ~588 N of force under NIR irradiation (white arrow showing moving direction), producing a work of ~19 J. [17]

In 2004, Vaia et al. reported a polyurethane-based Morthane/CNTs nanocomposite displaying shape-memory behavior upon exposure to infrared light (Figure 2) (17). The stretched temporary shape was kept by strain-induced polymer chain crystallization, with a melting temperature around 48 °C. Upon exposure to infrared light, the non-radiative decay of infrared photons absorbed by CNT generated heat and elevated the temperature of the composite above T_m of the crystalline domains, thus allowing remotely triggered shape recovery. As shown in Figure 2a, directional recovery of the sample can be controlled: the initial absorption, non-radiative energy decay and associated heating mainly take place in the near-surface region of the ribbon due to the strong infrared absorption of CNT. The resulting non-homogeneous shape recovery within the sample

caused it to 'curl' towards the light source. Moreover, under near-infrared irradiation, the PCN (polymer CNT nanocomposite) with 300% elongation exerted ~19 J to lift 60 g weight more than 3 cm with ~588 N of force (Figure 2b), while the neat Morthane remains unchanged due to its infrared transparency.

Gold nanoparticles (AuNPs) and gold nanorods (AuNRs) have also been employed as functional fillers to achieve light-controlled shape memory behaviors due to several advantages: 1) high molar absorption coefficients (~10^7-10^9 $M^{-1}cm^{-1}$ for nanoparticle diameter from 5 nm to 40 nm); 2) the absorption spectra are tunable in a wide range depending on their size and shape, limited spectral range (500 – 550 nm) for AuNPs and wide spectral range (700 – 1100 nm) for AuNRs. The photothermal property of these gold nanofillers arises from their localized surface plasmon resonance (SPR) attributes. The electrons on surface of the gold nanofillers are subjected to a periodically varying distortion in alternating electric field against the restoring force generated by the positive nuclei, and the electrical field drives the electrons to collectively oscillate in phase if the frequency of incident light matches the intrinsic frequency of the surface electrons (28-32). Gold nanospheres or AuNPs usually display a quite narrow absorbance in the visible range owing to the isotropic form. Once anisotropy is introduced into the geometric structure of these gold nanofillers, such as AuNRs, the absorption spectra will greatly shift to longer wavelength. AuNR has two SPR: one is related to the transverse oscillating electrons and the other to the longitudinal oscillating electrons. The former displays a visible light absorption spectrum similar to gold nanoparticles while the latter absorbs near infrared with wavelength from 700 nm to 1100 nm upon increasing the aspect ratio (length over diameter) (30).

Our group (13) developed an optically and spatiotemporally controllable SHP/AuNPs nanocomposite. In that system, PCL-grafted AuNPs were embedded in cross-linked PCL matrix. By taking advantage of the localized photothermal effect stemming from the SPR absorption of AuNPs, an optically triggered and spatiotemporally selective shape memory behavior was achieved, with an elongated cross-linked PCL/AuNPs film contracting stepwise and lifting up an object (Figure 3). Since the shape memory behavior can be halted "on demand" just by turning off the light irradiation, multiple intermediate shapes can easily be achieved.

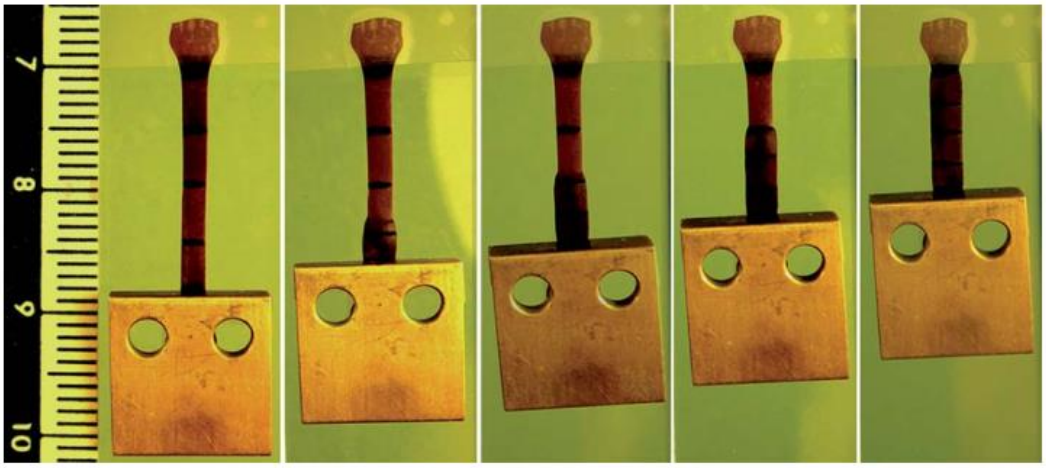

Figure 3. Series of image showing a spatiotemporally controllable shape recovery process at room temperature by separated light irradiation in four sections (successively from the bottom section to the top section) of a cross-linked PCL/AuNP sheet of 100% strain, with the film stepwise lifting up an object 350 times its own weight. [13]

I.III. Magneto-responsive SMPs

As one kind of remotely-controlled stimuli, magnetic field induced heating has attracted widespread attention in stimuli-responsive SMPs. Magnetically responsive SMP composites are composed of thermo-responsive SMP matrix and magnetic particles as the fillers. The magnetic particles can generate heat upon exposure to alternating magnetic field and heat SMP above its phase transition temperature, enabling the recovery of the permanent shape. The magnetic particles usually used in SMPs are γ-Fe_2O_3, Fe_3O_4 and NdFeB (33). Among them, Fe_3O_4 is the most used one because it is biocompatible, non-toxic, easy to be synthesized in large-scale and easy to control (34-36).

Zhou and coworkers (36) reported a biodegradable nanocomposite that display excellent shape-memory performances in hot water or under an alternating magnetic field with a frequency of 20 kHz and a field strength of 6.8 kA m^{-1} (Figure 4). They synthesized the PCL/Fe_3O_4 nanocomposite by using benzoyl peroxide (BPO) as a crosslinking initiator.

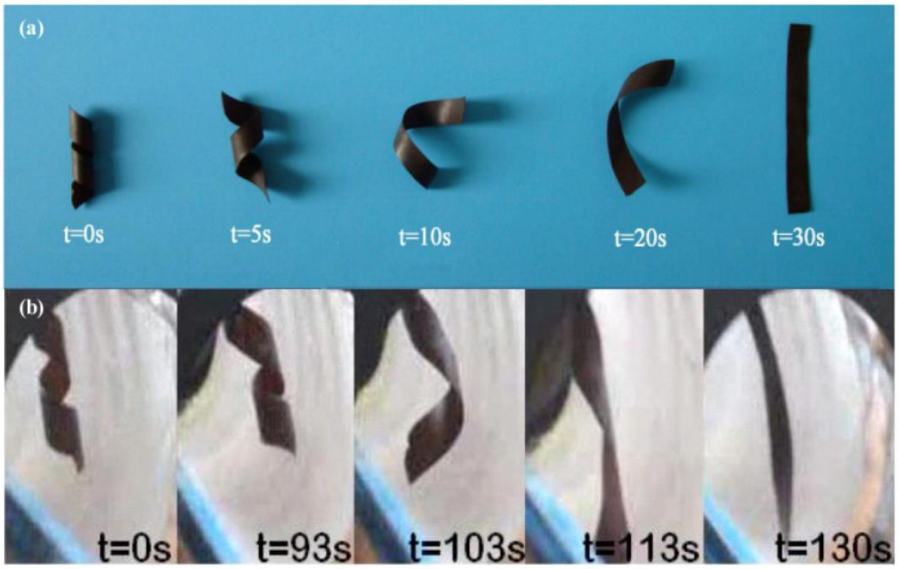

Figure 4. A serie of photographs showing the deploying helical ribbon (a) in hot water and (b) under an alternating magnetic field. The composites with 15 wt% Fe_3O_4 and 2.5 wt% BPO were immersed to 55 °C hot water and exposed to an alternating magnetic field with with f = 20 kHz and H = 6.8 kA m^{-1}. [36]

I.IV. Electrically Responsive SMPs

At present, there are few reports about SMPs with intrinsic electrical conductivity. Most of the reported SMPs are insulators and do not have intrinsic electrical conductivity. The conductivity of the electrically responsive SMPs is achieved by adding an appropriate amount of conductive fillers to the shape memory polymer matrix. Well-dispersed conductive fillers can form a network when the content reaches a certain threshold which can increase thoroughly the electrical conductivity of the materials. When the composites are exposed to an appropriate electrical field, electrical current flows through the conductive network, generating heat through “Joule effect”, which triggers the polymer matrix to experience glass transition or melting transition (37, 38).

The typical shape memory process of electrically responsive SMP composite material is: when the SMP is heated to above the glass transition temperature (T_g), external force is imposed to deform the material; maintain the external force unchanged and cool the material to "freeze" the stress and

deformation; when the voltage is applied to the material, the current flows through the conductive network of composite material and then generate heat to raise the temperature of the material above the glass transition or melting transition temperature; the "frozen" stress releases and the material recovers the original shape.

The conductive fillers for electrically responsive SMPs can be classified into two categories: metal fillers and carbonaceous fillers. From the point of view of the conductive ability of the filler itself, metal filler is best for improving the conductivity of the composite material. Metal fillers include gold, silver, copper and so on. However, metal filler is not only expensive and easily oxidized, but also have high critical concentration, which will have a negative impact on the mechanical properties of composite materials. Besides, due to the difference in density, metal filler is difficult to disperse well within the polymer. Therefore, electrically responsive SMPs with metal fillers are reported rarely. At present, most of the conductive fillers that have been reported are carbonaceous fillers, including carbon black (CB) (39), carbon nanotube (CNT) and chopped carbon fiber.

Jan et al. (39) reported the effects of carbon black (CB) on shape memory performance of polyurethane (PU) nanocomposites. The results showed there is a strong correlation between soft segment crystallinity and shape memory effect. The author also found that the CB fillers interfered with crystallization owing to the comparable dimension of the particles and the typical crystal lamellae. When the CB content is higher than 3 wt%, the composites failed to show useful shape memory performance due to brittleness. Better shape memory performance were achieved at higher strain owing to strain induced crystallization of the soft segment. Zhang and coworkers (40) quantitatively measured the electrical and shape memory properties of the polyvinyl alcohol (PVA) with different content of CNTs (wt.%). The results showed that even a low content of CNTs could provide a high level of conductivity. Nishikawa et al. (41) studied the shape memory behavior of thermosetting PU composites with different content of carbon fiber. The results showed that with the increase of carbon fiber content, the deformation recovery rate of the material decreased and the residual strain increased. By analyzing the finite element model of the composite, it was found that the irreversible strain of the polymer in end region of the fiber has negative influence on the performance of the shape memory polymer composite.

I.V. Ultrasound-responsive SMPs

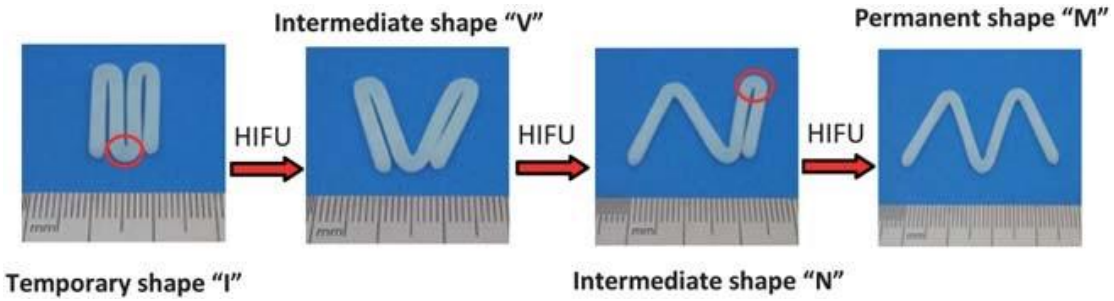

Figure 5. Spatiotemporally controllable shape memory behavior of cross-linked P(MMA-BA) upon exposure to HIFU (output power 25 W) at room temperature. The specimen with an original shape "M" was deformed to a temporary shape "I", and then three folded points were irradiated with HIFU at three different times to trigger the recover of the original shape in three steps and two intermediate shapes can be readily obtained. [9]

Our groups (9) also developed a novel strategy enabling the simultaneous triggering of shape memory polymers (SMPs) and release of loaded drugs by using high intensity focused ultrasound (HIFU) as the stimulus (Figure 5). HIFU, whose ultrasound beam can be concentrated into a focal spot (diameter ~3 mm), was originally developed as an extracorporeal tool to treat tumors owing to its thermal effect. The acoustic energy can convert into mechanical energy through viscous shearing oscillation and relaxation of polymer chains, which can subsequently be absorbed by an SMP resulting in rise of temperature. Despite HIFU usually requires a liquid media to transfer the acousticly induced thermal energy, the remote heating modality of HIFU is a unique advantage compared with the other indirect heating stimuli that can only heat SMP composites incorporated with heat generating species.

II. Stimuli-responsive Self-healing Polymers

In nature, biological systems are evolutionarily optimised to exhibit remarkable functions. One of their most brilliant features is the ability of self-repairing and regeneration of functions in response to the infliction of injury by external mechanical forces. It is identified that all the examined plants and animals contains first and second self-sealing phase. Taking plants for example, the rapid self-

sealing prevents the plants from infection by pathogenic germs and desiccation, which provides enough time for the subsequent self-repairing of the damage, closure of wound and regeneration of functions of the plant organs. Inspired by a variety of self-healing and self-sealing processes in plants, scientists have successfully transferred these different functional principles into the design and synthesis of self-repairing materials. The concept of self-healing polymers was firstly proposed in the 1980s (42) as an approach of repairing invisible microcracks for improving the service time and safety of materials. To date, the developed SHPs can be divided into two kinds: (i) extrinsic self-healing polymers, which repair themselves with the help of deliberately pre-embedded repairing agents, and (ii) intrinsic self-healing polymers, which enable injury healing without any additional repairing agent. Extrinsic self-healing polymers based on an initial healing mechanism were firstly developed by White and coworkers (43). These materials utilized microcapsules embedded in epoxy matrixes to release liquid repairing agents to repair the damaged regions. This kind of self-healing material was prepared by embedding liquid endo-DCPD (endo-dicyclopentadiene) monomers and 1st generation Grubbs' catalyst particles into a thermosetting matrix. These microcapsules can break and release the liquid DCPD monomers into the crack once the thermosetting material ruptures, and then contact with the dispersed catalyst to undergo ring-opening metathesis polymerization, resulting in the formation of a crosslinked network to adhere the crack surfaces back together. In contrast, intrinsic self-healing behavior depends on the physical, chemical and supramolecular interactions within polymer chains and groups. Generally, intrinsic self-healing polymers contain autonomous SHPs and stimuli-responsive SHPs. In principle, autonomous SHPs are much desirable since the self-repairing behavior can take place at ambient conditions without any external intervention and input. However, despite the increasing interest, autonomous SHPs are generally limited to soft materials with low mechanical properties due to the weak interactions of non-covalent dynamic bonds such as hydrogen bonding (44-48), metal-ligand coordination (49,50), π-π stacking (51-53), electrostatic interaction (54-57), ion migration (58), molecular recognition (59,60) and hydrophobic association (61). Different from soft supramolecular polymers whose dynamic non-covalent bonds can undergo breaking and reformation at room temperature across cut or crack surfaces for healing, strong or hard materials are generally covalently cross-linked polymers with high T_g or T_m and, therefore, the autonomous

self-healing mechanism does not work no matter how long the damage surfaces are kept in contact due to weak chain mobility. In order to address this challenge, it also attracts great interest to develop stimuli-responsive SHPs, in which external energy or stimuli, such as heat, light, electricity, electromagnetic field, ions and pH are often applied (62) to initiate or activate the healing process. For this kind of SHPs, covalent dynamic bonds take charge in conducting the self-healing behavior, such as DA bonds (63), thiuram disulfide moieties (64), alkoxyamine units (65), coumarin derivatives (66), acylhydrazone bonds (67), disulfide bonds (68), Ru-catalyzed shuffling of C=C motifs (69), among others. When the SHPs are exposed to the stimuli, the dynamic bonds undergo bond breaking and reformation between the crack surfaces enabling regeneration of the network and healing of the damage.

II.I. Thermo-responsive SHPs

Thermo-responsive SHPs usually contain thermally reversible dynamic bonds, i.e., DA bonds (63), alkoxyamine moieties (65) and Ru-catalyzed shuffling of C=C bonds (69). As a famous thermally reversible reaction, Diels–Alder (DA) reaction has been widely used in the field of thermo-responsive SHPs. At room temperature, the DA partners (a conjugated diene and a substituted alkene) undergo cycloaddition reactions; at high temperature, the DA adducts experience retro-Diels–Alder reactions. The choice of DA reaction for SHPs stems from the facts that: 1) DA reactions have a desired property of being self-contained reversible reactions, where all atoms exist both in the starting materials and the products (70), which is an excellent advantage for the stability of materials; 2) the equilibrium position of reversible DA reactions, therefore, responds to temperature, solvent, and concentration but is not influenced by ancillary molecules such as water (71), making possible the healing process of the dynamic polymers taking place in water or in vivo; 3) the furan-maleimide cycloaddition product shows a relatively low decoupling temperature via retro-DA reaction (> 75 ℃) (71,72); 4) furan derivatives come from renewable natural resources and are thus likely to play an icreasingly important role on sustainable approaches for recycle materials and green chemistry (73).

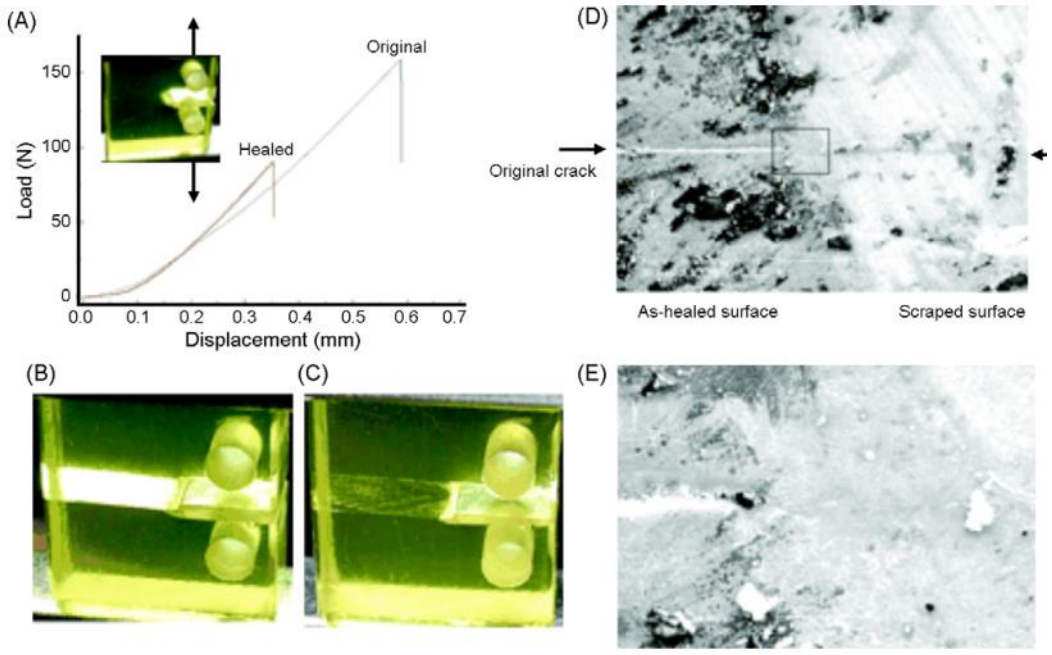

Figure 6. (a) Healing efficiency of DA bond-containing polymer achieved via fracture toughness testing of compact tension test samples; (b) photograph of a damaged sample before heating; (c) photograph of the sample after heating; (d) SEM picture of the surface of a repaired specimen: the left part shows the as-healed surface and the right part shows the scraped surface; (e) enlarged image of the selective region in (d). [63]

The first healing system based on Diels-Alder chemistry was designed by Chen et al. (63) through utilization of the DA and retro DA reaction between furan and maleimide derivatives. The material was synthesized by polymerization of multi-furan monomers and multi-maleimide monomers, leading to a macromolecular network formed by dynamic covalent bonds. The results showed that this material had mechanical properties equaling those of commercial epoxy resins, indicating their promising utilization in the field of engineering composite materials. Upon heating to 120-150 ºC, these materials displayed a 57% healing efficiency, which is significant for a covalently crosslinked epoxy without any additional healing agent. The failure of fully healing was owing to complete sample fracture into two separate pieces, which resulted in poor contact between the two fracture surfaces during the repairing process (Figure 6). Perhaps the most significant property of

this system is that it can intrinsically repair itself multiple times, greatly improving the serving time of the polymer. Indeed, the healing efficiency of the third crack was 80% that of the second crack after two full cycles of fracture and healing.

II.II. Light-responsive SHPs

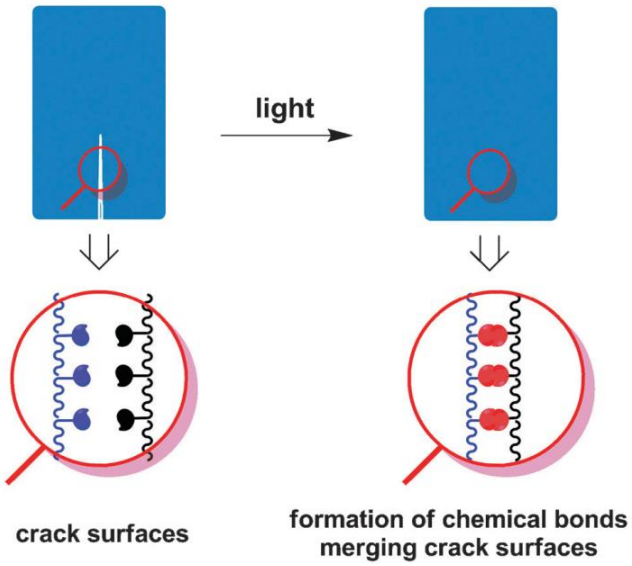

Figure 7. Schematic illustration of light-induced self-repairing of a crack, requiring the reformation of chemical bonds and fusion/entanglement of polymer chains between crack surfaces. [4]

When polymers suffer a damage, such as formation and propagation of a frature or crack, breaking of polymer chains or chemical bonds are the main reason to cause the damage of the materials. Therefore, reformation of chemical bonds (either covalent or noncovalent) between the crack surfaces is essential for an effective self-healing of damage. As shown in Figure 7, utilizing light to activate the self-repairing process includes the phototriggered formation of new chemical bonds and diffusion/entanglement of polymer chains across the fracture or crack surfaces. (4) In recent years, three basic methods for light-responsive SHPs based on different chemistries have been demonstrated. The first method uses a reversible photocyclization to trigger crack closure; the second method consists in employing photo-sensitive dynamic bonds to conduct the repairing of

the crack; and the third one takes advantage of a photothermal effect that reshuffles non-covalent chemical bonds or enhances the wetting, diffusion and reentanglement of the polymer chains between the crack surfaces.

II.II.I. Light-responsive SHPs Based on Reversible Photocyclization

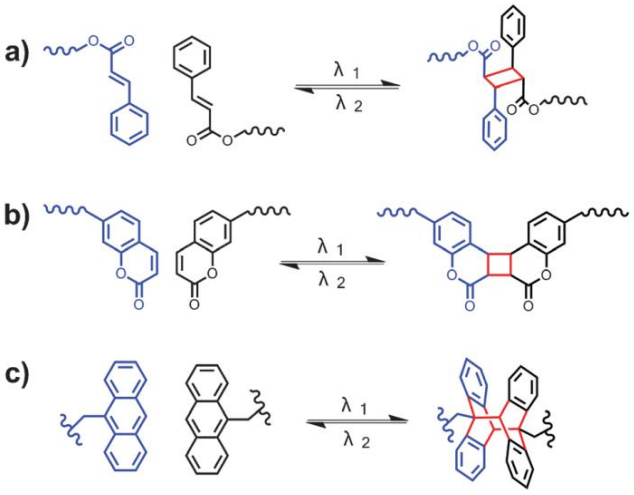

Figure 8. Reversible photo-dimerization (at λ_1) and photo-cleavage (at λ_2) upon exposure to UV light at two different wavelengths ($\lambda_1 > \lambda_2$) for (a) cynnamoyl, (b) coumarin and (c) anthracene. [4]

Inspired by the employment of thermally reversible DA reactions for SHPs (63), a lot of researches have studied the utilization of reversible photocyclization based on the reversible photodimerization and photocleavage of chromophores, e.g. cinnamoyl, coumarin and anthracene (66,74-78). As illustrated in Figure 8, the alternative type of cycloaddition reactions are photoinitiated, undergoing either [2+2] cycloaddition (for coumarine and cinnamoyl) or [4+4] cycloaddition (for anthracene) upon exposure to UV light with a certain wavelength and cleavage upon illumination with a shorter wavelength of light. In all the reported studies, the dimer form of these photoreactive groups served as crosslinkers in polymer networks. Upon exposure to UV light with appropriate wavelengths, the free photoactive groups (e.g. coumarin) incorporated in the polymer structure would undergo the desirable photocyclization and thus covalently cross-linked the two crack surfaces enabling the optical self-repairing. For the purpose of improving the optical self-healing efficiency, it is very important to pre-treat the two crack surfaces by irradiating the

polymer with shorter wavelengths of light to cleave the dimers to liberate sufficient photoactive groups on the fracture or crack surfaces. Besides, cleavage of the dimers also de-crosslink the polymer network to provide better polymer chain mobility on the fracture surfaces.

As early as 2004, Chung and coworkers (76) developed a light-responsive self-healing polymer by incorporating cinnamoyl groups into the polymer structures. In this polymer, the cinnamoyl groups undergo photochemical cycloaddition to form cyclobutane dimers, enabling the formation of cross-linked networks. It was theoretically deduced that the cyclobutane groups of the dimers would undergo preferential breaking during crack propagation owing to the high value of ring strain. Upon exposure to UV light with appropriate wavelength (>310 nm), the liberated cinnamoyl groups underwent photochemical cycloaddition to reform the cyclobutane dimers to serve as cross-links, recovering mechanical properties of the polymer. This process could be monitored by the distinctive C=C and C=O peaks in IR spectroscopy. The result showed that when crack propagation occurred, the cyclobutane underwent breaking and the original cinnamoyl peaks appeared. Upon UV illumination, the cinnamoyl groups would undergo cycloaddition again and mechanical properties of the polymer could be recover. Through measuring the flexural strengths of original, damaged and optically healed specimens, a modest self-healing efficiency of ~14%, which was calculated using the ratio of flexural strength of the healed specimen over that of the original specimen, was ahieved after exposure to UV light for 10 minutes. A better healing efficiency of ~26% could be obtained by heating the samples to 100 ℃ during UV light irradiation due to the increase of polymer chain mobility. Moreover, the healing efficiency also could be tuned by changing the content of the photo-crosslinkable cinnamoyl groups in the polymer struture.

II.II.II. Light-responsive SHPs Based on Photo-sensitive Dynamic Bonds

Recently, a novel strategy that uses photo-sensitive dynamic bonds for light-triggered self-healing of polymers has been reported (64,78-84). As shown in Figure 9, upon illumination with UV light, the photo-sensitive dynamic bonds, such as disulfide (64,79,83,85), allyl sulfide (84), and trithiocarbonates (80), undergo a reshuffling reaction. The self-healing mechanism of this kind of SHPs is as follows. When the polymer is irradiated with light, the dynamic covalent bonds

experience bond dissociation, enabling the generation of reactive radicals on the crack interfaces. During or after light irradiation, the photogenerated reactive radicals at different chain terminals undergo fast recombination to form new chemical bonds, part of which are formed between macromolecule chains locating at opposite sides of the crack surfaces, leading to the fusion and healing of cracks.

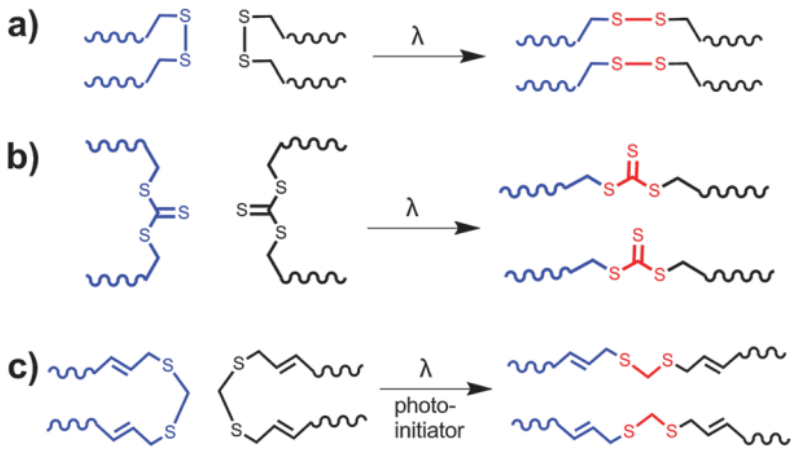

Figure 9. Photo-sensitive dynamic bonds used for light-responsive self-healing: (a) disulfide, (b) trithiocarbonates, and (c) allyl sulfide. [4]

Matyjaszewski et al. (80) prepared a poly(n-butyl acrylate) (PBA) network with trithiocarbonates (TTC) located in the main chain backbone (Figure 10a). Upon exposure to UV light, the TTC units dissociate and generate radicals that will undergo reshuffling/exchange reaction to repair the material. In the experiment of model reactions between two low-molecular-weight TTC compounds, the result showed that the TTC units can undergo radical exchange reaction in acetonitrile upon exposure to UV light (λ= 330 nm, 0.9 mW cm^{-2}). Under similar conditions, pieces of the covalently crosslinked dynamic material could be re-jointed through pressing them with a good contact in acetonitrile and illuminating them with UV light for several hours (Figure 10b). The healed sample showed a tensile modulus (65 ± 11 kPa) which was similar to that of the initial sample (69 ± 6 kPa). The healing effect of the polymers in dry state was also studied, and the result showed that the healing efficiency decrease as the absence of solvent would decrease the chain mobility of the material (Figure 10c). It demonstrated that longer UV exposure time (48 hours) of

a partially cut specimen resulted in better healing efficiency, even though small defects remained in regions where the contact between the interfaces was not intimate.

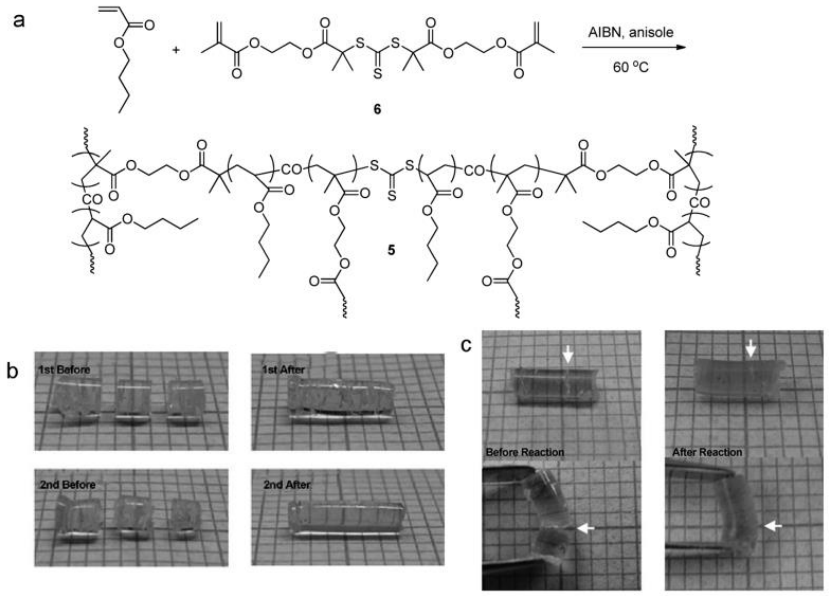

Figure 10. (a) Synthesis of a TTC-containing crosslinked polymer through RAFT polymerization and (b and c) photographs of material samples that were cut and repaired under N_2 upon exposure to UV light (λ= 330 nm, 0.9 mW cm^{-2}) in the presence of (b) acetonitrile and (c) in bulk state. [80]

Although the use of TTC units to SHPs can provide a significant healing effect, the healing process is carried out under a protective N_2 atmosphere owing to the high reactivity of the radical intermediates. In order to allow photo-triggered repairing of materials to go on under mild conditions, i.e., exposure to visible light in the air at room temperature (RT), Matyjaszewski and coworkers further synthesized a thiuram disulfide (TDS)-containing polymer that can self-heal under such milder conditions by generating stable reshuffling radicals (64). These materials were rationally designed to display a low T_g (~50 to ~34 ºC) so as to obtain good chain mobility for self-healing at room temperature without any solvent. As seen from Figure 11a-c, the light-triggered healing of the polymer was evaluated by cutting a bull cylindrical specimen into two pieces and then bringing them into contact. Upon exposure to visible light by utilizing a commercial tabletop lamp in the air and at RT, the TDS units underwent reshuffling reaction to

repair the cutting surfaces, leading to merging of the two polymer pieces. The result also showed that the sample could recover almost the original mechanical properties when the light exposure time was long enough (24 h, Figure 11 d and e).

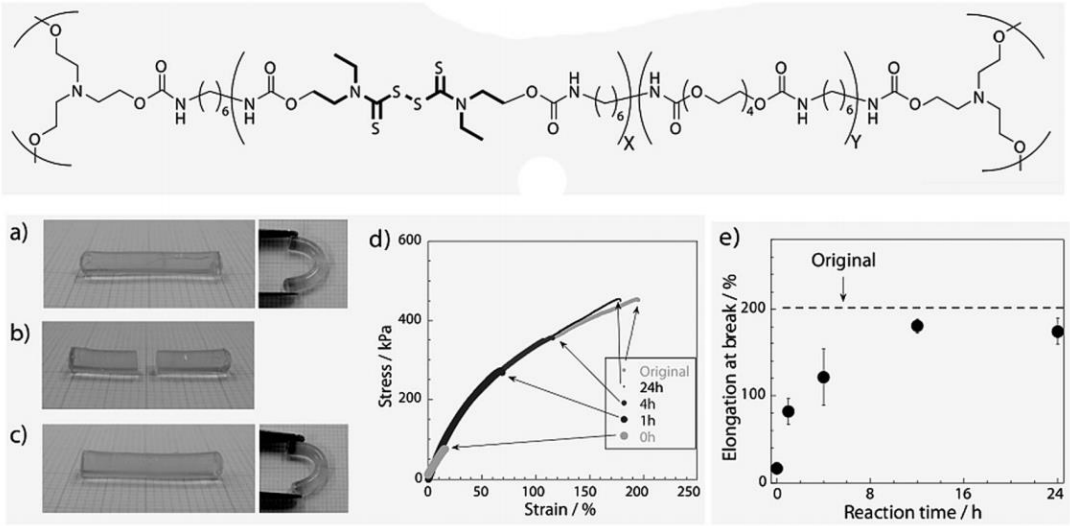

Figure 11. Polymer architecture of the PU network containing TDS units and the results showing light-responsive self-healing: (a) a cylindrical sample cut into two parts; (b) separate pieces; (c) self-repared, single-piece cylindrical sample under visible light illumination; (d) stress-strain behaviors and (e) elongation value at break for the initial and light-repaired specimens with different light illumintion times. [64]

II.II.III. Light-responsive SHPs Based on Photothermal Effect

Rowan and coworkers (81) reported metallosupramolecular polymers that can be repaired by photothermal effect. As shown in Figure 12, an oligomer-based monomer containing a rubbery, amorphous poly(ethylene-co-butylene) core with 2,6-bis(1'-methylbenzimidazolyl)-pyridine (Mebip) ligands at the polymer chain ends was synthesized. Then these telechelic macromonomers assembled through ligand-metal ion binding, such as Zn^{2+} or La^{3+}, to form metallosupramolecular polymers. This polymer system is dynamic because the assembling and breaking of the metal–ligand bonds are reversible, which enables depolymerization of the polymer under treatment with certain external stimulus (such as light and heat). Under irradiation with UV light, the ligand-metal

bonds are electronically excited and convert light energy into heat which can elevate the temperature of the irradiated region to above 175 ℃ . At this high temperature, the ligand–metal motifs are temporary disengaged, resulting in an accompanying reversible decrease of the materials' molecular weight and viscosity, allowing effective diffusion of the species in the crack region or across the fracture surfaces. Upon turning off light, the temperature of the material decreases and the reformation of ligand–metal bonds enables self-healing of the polymer.

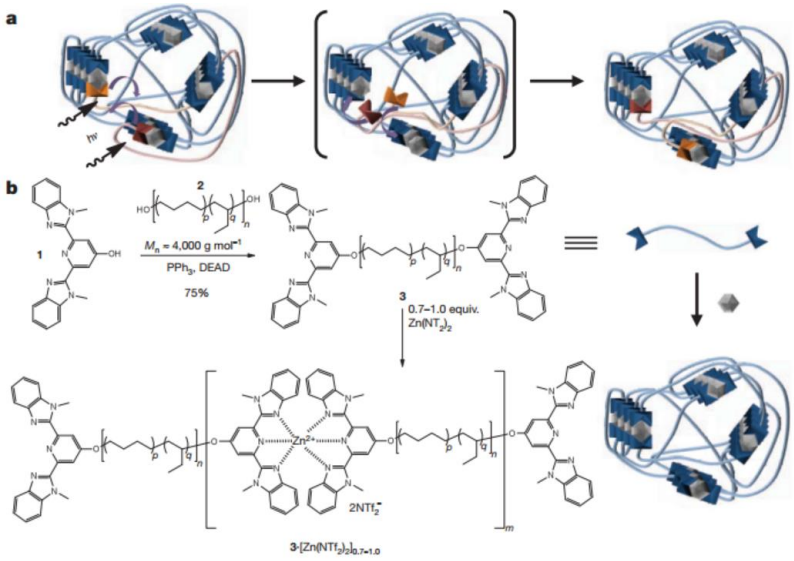

Figure 12. Light-triggered self-healing mechanism and synthesis routes of metallosupramolecular polymers. (a) Schematic showing optical repairing of a metallosupramolecular, phase-separated polymer. (b) Synthesis steps to the metallosupramolecular polymers. [81]

II.III. Electrically Triggered SHPs

In recent years, a promising alternative method for triggering the self-healing process of polymers has been developed. By introducing conductive fillers into polymer matrix, the composites are able to display resistive heating to repair the defect upon employment of an electric field. When a fracture appears in the composite, the resistance increase due to the decrease of routes available for the electrons to travel. When a constant electric field is applied, resistive heat will generate at the site of damage owing to increase of resistance. This localized heating initiates

entanglement/diffusion of polymer chains or reshuffling reactions of dynamic bonds between the crack surfaces, which repairs the specimen and restores its initial mechanical and electrical performances. This strategy not only allows for localized repairing but also develops a non-destructive approach to detect the composite's internal defects based on an electronic feedback mechanism, enabling diagnosing of invisible cracks and fractures that otherwise can develop without being noticed.

In 2007, Hahn and coworkers (86) reported a series of polymers and their composites that display self-healing feature under electrically triggered heating based on thermally reversible Diels-Alder reactions. The polymers showed great self-healing performance in solid state. The composites were prepared by curing the monomers between carbon fiber textile layers in autoclave. In order to evaluate the self-healing performance of the materials, micro fractures were introduced on the surface of material by using Instron machine to hold the specimen at 1% strain for 1 min at room temperature. The self-repairing ability of the material was confirmed by the vanishing of microfractures after heating. Resistance heating of the material and its universality in self-repairing composites was also investigated to lay fundamental work for electrically triggered self-healing composites. In 2008, Park et al. (87) reported a similar self-healing composite system comprising of a dicyclopentadiene-based polymer and a graphite/epoxy substrate. They introduced microcracks into the composites using three-point bending tests and studied the healing ability by convective heating and electrically resistive heating. The result showed that the fractures were repaired within minutes upon resistive heating at temperature ranging from 70 to 100 ℃ , leading to a better healing effect of the composite with less surface scars than specimens repaired by traditional heating.

II.IV. Electromagnetic Field-responsive SHPs

Unlike conductive composites that require electrical contacts to achieve resistive heating, magnetic fillers can be introduced into the polymer and triggered remotely (avoiding direct contacts) upon application of an electromagnetic field. This approach of inductive heating was originally developed for biomedical engineering, where magnetic nanoparticles were injected directly into

the pathological tissues and subsequently heated by employment of a high-frequency magnetic field (88). In 2003, Nemat-Nasser (89) and coworkers developed an electromagnetic field-responsive SHPs by incorporating straight copper wires and copper coils into fiber-reinforced polymeric composites. The incorperated elements provide the composites with remotely controlled electromagnetic responsiveness. In the composites, the fiber/wire generated heat upon exposure to electromagnetic field to repair the internal fractures through thermo-reversible covalent bonds (Diels-Alder bonds).

III. Stimuli-responsive Polymer Actuators

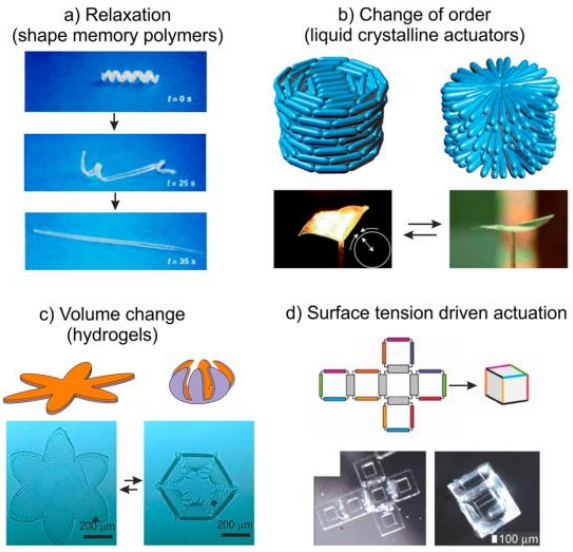

Figure 13. Four main classes of polymer actuators based on different actuation mechanisms [90]: (a) relaxation induced shape recovery (shape memory polymers) [6]; (b) change of molecular order (liquid crystalline polymers) [99]; (c) volume change (hydrogels) [100]; and (d) surface-tension-driven actuators [101].

Polymer actuators are a class of devices and materials that have the ability to change their shape in response to external stimuli and thus perform mechanical motions and produce useful work on the nano-, micro-, and macroscales (90). Polymer actuators have been attracting broad and growing interest in recent years because they may find a wide range of applications in artificial muscles,

microrobots and lab-on-a-chip systems (90-95). There are many examples of polymer actuators based on shape memory polymers, liquid crystalline elastomers and hydrogels (96,97). The polymers used as actuators can be soft (viscoelastic state) or hard (glassy state) lying on their physical and chemical interactions between the polymer chains and groups which enable the fabrication of soft actuators for application in biological engineering and hard actuators for application in artificial muscles, respectively (98). There are plenty of stimuli-responsive polymers that can be used for the fabrication of actuators controlled by changing temperature, humidity, pH, biosignals, or light (1).

The polymer actuators can be categorized into four groups based on their actuation mechanisms. The first group of actuators comprises those based on the elastic shape recover of shape memory polymers (Figure 13a). These polymers are deformed above the transition temperature and "frozen" in a temporary shape by cooling to low temperature. Upon elevating the temperature, they undergo elastic relaxation to perform mechanical work. The actuation from such shape memory polymers is irreversible, even though a few examples of reversible actuation based on two-way shape memory polymers are reported (102-104). The second class of actuators is based on the change of molecular orientation of liquid-crystalline polymers (LCPs) (Figure 13b), which can be either a transition between different ordered states or a transition from an ordered state to a disordered one. The actuation of LCPs is typically reversible. The actuation of the third group of actuators is based on a reversible change in the volume (Figure 13c). This kind of actuators are usually hydrogels, which are able to swell and shrink. The fourth group of actuators make use of surface tension as the driving force to perform actuation behavior (Figure 13d). The change of surface tension is derived from the melting of crystalline polymers. Typically, such actuators are small to ensure the surface tension is large enough for inducing mechanical work. That is because when the size of the actuators is decreased to the microscale or nanoscale, the role of surface tension becomes remarkable, which allows the fabrication of actuators based on surface-tension.

III.I. Shape Memory Polymer Actuators

Recently, Lendlein and coworkers reported very interesting reversible shape memory actuation (105). These actuators consisted of two different structural units in the form of interpenetrating network (IPN). The two separate structural units are crystallizable domains and show different functions (Figure 14). The domains with higher $T_{m,SGD}$ determine the shape shifting geometry (SGD) of the material, while the domains with lower $T_{m,\ AD}$ takes charge of the actuating performance of the shape memory polymer. By orientation of the chain conformation within the domains, the actuation capability of the polymer can be achieved, showing reversible directional length changes of the actuator domains (AD) during crystallization and melting. The same group has also reported another reversible shape memory actuator based on covalently cross-linked copolymers with a broad melting temperature range, which displays a long-term temperature-memory allowing more than 250 cycles of thermally-triggered actuations without changing the performance of the material (106).

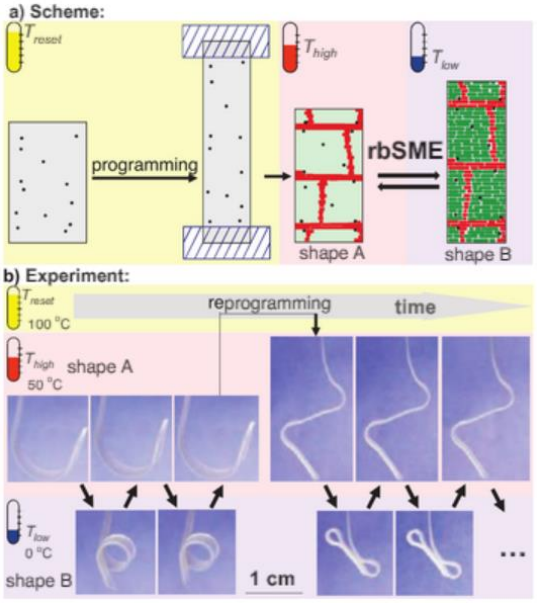

Figure 14. Scheme of reversible actuation behavior of SHPs (a): After deformation at T_{reset}, the skeleton domains (red), which determine the shape-changing geometry can undergo crystallization upon cooling (programming). The SHPs are controlled by the reversible crystallization and melting

of oriented actuating domains (green). (b) A serie of images showing SM behavior of a polymer ribbon from polypentadecalactone-polycaprolactone. The programmable bow shape was achieved through deformation of a helical sample at T_{reset}, then cooling to T_{low}, and subsequent heating to T_{high}. The shape memory process took place as a reversible transformation between shape A (bow) at T_{high} and shape B (helix) at T_{low}. The specimen was reprogrammed at T_{reset} into a new shape A that could be reversibly transformed to a tightly folded shape. [105]

III.II. Liquid-crystalline Actuators

Liquid-crystalline elastomers (LCEs) are another interesting class of stimuli-responsive actuators that are able to convert external energy into macroscopic mechanical work. LCEs are synthesized by polymerization of reactive liquid-crystalline (LC) monomers whose orientation can be controlled through utilizing alignment layers and fixed by photoreactions, leading to the formation of hierarchical materials with well defined molecular architectures. Such materials display a combined properties of polymeric elastomers (entropy elasticity) and liquid crystals (self-organization).

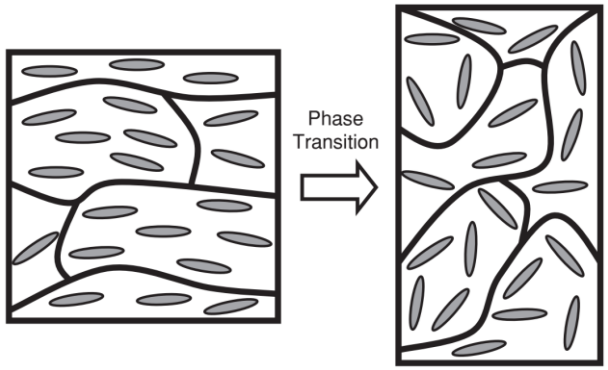

Figure 15. Scheme of the liquid-crystalline actuator. In the LC phase, the polymer adopts an extended chain conformation due to the anisotropic liquid crystal orientation. Upon heating to the isotropic phase, the polymer regains its coiled conformation, resulting in a macroscopic shape change. [92]

The basic mechanism for the shape shifting of LCEs is schematically shown in Figure 15 (92). Upon orientation of the mesogenic units (either as side groups or in the chain backbone) along a certain direaction (LC director), the polymer chains experience an anisotropic circumstance and stray from the isotropic random coil conformation, result in differences between the radius of gyration R_G that parallel and perpendicular to the LC director. When the LCE is heated into the isotropic phase, the loss of orientation of the LC mesogens brings the polymer chain conformation back to the isotropic random coil, which leads to macroscopic shape change of the whole sample. The actuation is reversible since the LC-isotropic phase transition is reversible.

III.II.I. Preparation Methods of LCE Actuators

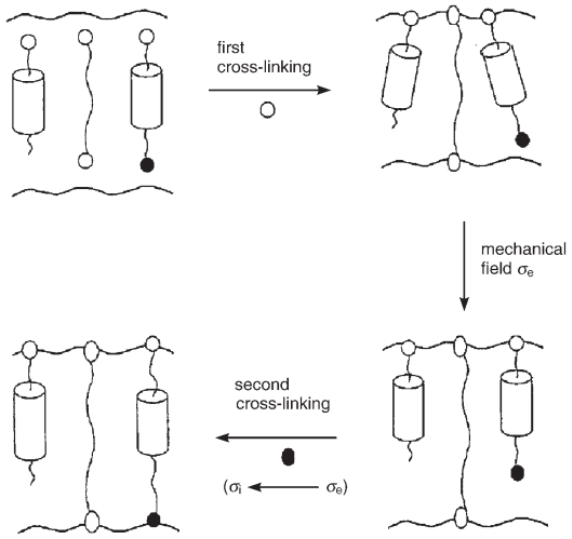

Figure 16. Preparation of LCEs using the two-step method. [91]

The prerequisite for achieving actuating properties will be the orientation of the mesogenic units to form a LC monodomain (91). For this, generally a slightly crosslinked LCE is synthesized and stretched uniaxially to a certain strain, leading to the monodomain and extension of the polymer chains. In the LC phase, the mesogenic units in the material align themselves either parallel or perpendicular (lying on the feature of the coupling) to the macromolecular chains, resulting in a monodomain structure. Then the polymer is crosslinked in the LC phase to fix the anisotropic conformation of the polymer chains. The original concept of LCE actuator was proposed by de

Gennes and the first LCE sample was synthesized by Finkelmann and coworkers (107). From then on, many LCEs with different architectures of polymer chains and various kinds of LC mesogenic units have been synthesized. There are two general approaches for preparation of LCEs: the two-step method (108-110) and the one-step method (111). For the two-step method (Figure 16), slightly cross-linked polymers are synthesized in the first step. Then a constant force is applied to deform the cross-linked polymer to induce anisotropy of the mesogens and the polymer network. In the second step, cross-linking reaction is used to fix the anisotropy of the mesogens and the polymer network. The superiority of this approach is that the formation of anisotropic property of the mesogens and the polymer network in the first step is reproducible, thereby well aligned molecular architectures of LCEs are achieved (108-110). As shown in Figure 16, LC monomers or prepolymers with reactive moieties align uniformly in the load direction. These aligned LC mesogenic monomers and prepolymers can undergo photopolymerization or thermal polymerization or chemically cross-linked reaction upon exposure to a certain stimulus or input of reactive crosslinking agents, leading to the formation of anisotropic LC networks with various cross-linked densities and macroscopically well aligned LCEs (112). For the one-step method (111), the orientation of LC monomers is firstly established in a glass cell, and then the anisotropy of the mesogens and the polymer network is fixed by in-situ photopolymerization in the LC cell. It is very easy to prepare LCEs but difficul to synthesize LCEs at macroscopic level using this method. Broer and coworkers employed the one-step method to synthesize well aligned side-chain LCEs by in situ photo-polymerization of macroscopically oriented mesogenic monomers (111).

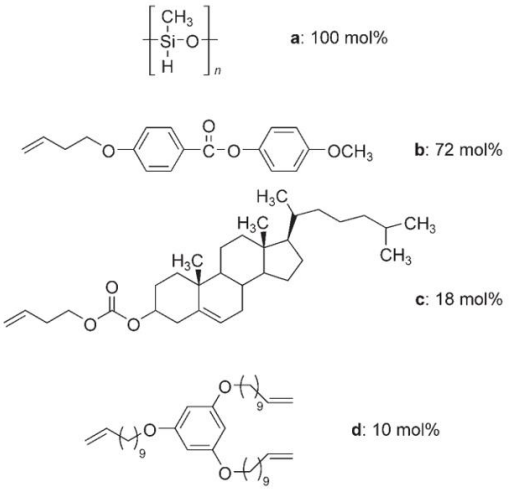

Figure 17. Chemical structure of the monomers for synthesis of a cholesteric LCE. [91,115]

LCEs with different LC phases, e.g. nematic (113,114), cholesteric (115-117), smectic (118-126), and discotic (127), were synthesized by polymerization of different mesogenic monomers using these two methods. For example, Muhoray and coworkers reported a cholesteric LCE (monomers a–d, Figure 17) with an autonomous and uniform alignment in the form of a spiral architecture (91,115).

III.II.II. Thermo-responsive LCE Actuators

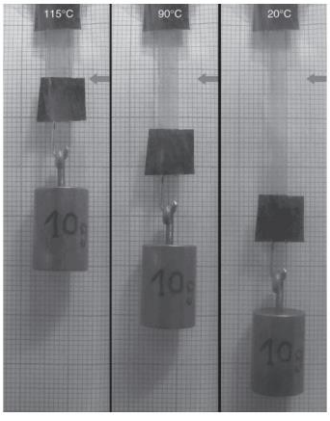

Figure 18. A 10 gram object is attached to the end of a polysiloxane LCE monodomain specimen. Upon heating the LCE contracts and lifts up the object. [92,131]

The first demonstration of anisotropic actuation of monodomain LCEs by a thermal phase transition between the LC state and isotropic state was reported by Finkelmann and coworkers (108). A nematic LCE sample was prepared through using the two-step method, which shows a contraction of ~26% due to the change of mesogenic alignment (108). This anisotropic actuation of LCEs has attracted widespread attention both in experimental and theoretical studies (128-130). Figure 18 illustratively demonstrate the length change behavior of a muscle-like LCE sample prepared by Finkelmann's group (92,131). A 10 gram object was attached to the end of a LCE sample. Upon heating by the surrounding air, the film contracted and lifted up the object. When cooled, the LCE sample extended and the object went back to its original position. These features strongly depend on the nature of the coupling between the polymer chain conformation and the director of the mesogenic units.

Recent efforts have been made to extend the preparation methods to programmable LCEs. White and coworkers (132) prepared photoalignment-sensitive LCE materials by using LC cells, which showed very large conical deformations that could produce as much as 2.5 J kg^{-1} of useful work (Figure 19). Moreover, a self-folding Miura-ori origami sample was prepared by spatially patterning (voxelating) in local areas of a LCE sample.

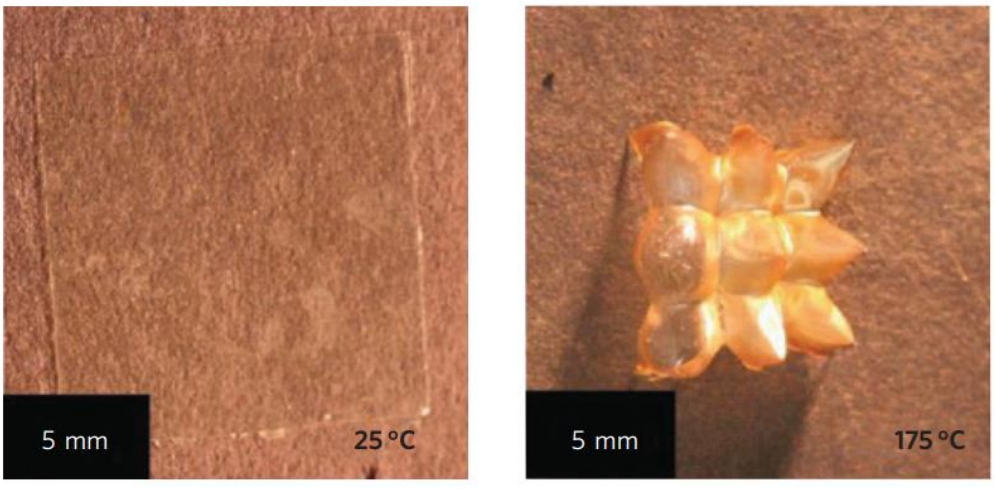

Figure 19. LCE films were prepared with a 3 × 3 array of +1 radial defects and showed very large conical deformations upon heating.[132]

III.II.III. Chemical Stimuli-responsive LCE Actuators

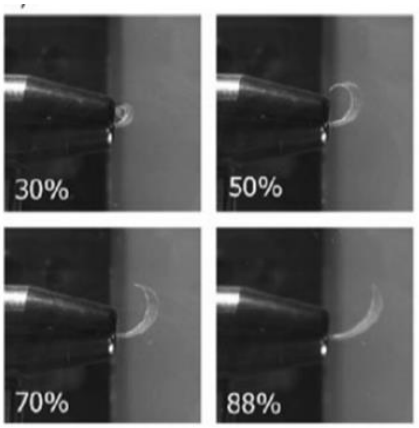

Figure 20. Digital images of the twisted films under different humidity conditions. [133]

Broer et al. (133) reported pH- or water-responsive actuators, which exhibited rapid, large-amplitude, reversible deformations (Figure 20). The LCE actuator responded equally to humidity or pH changes in all areas of the film due to the uniaxial alignment and only slightly elongated upon exposure to a uniform stimulus. A large bending amplitude of the actuator was achieved by changing the pH value or humidity of the top and bottom surfaces. Environmental gradients were not necessary for the twisted and splayed configurations to generate macroscopic actuation. For both stimuli, the preferred expansion directions on the opposite sides of the sample were offset by 90°.

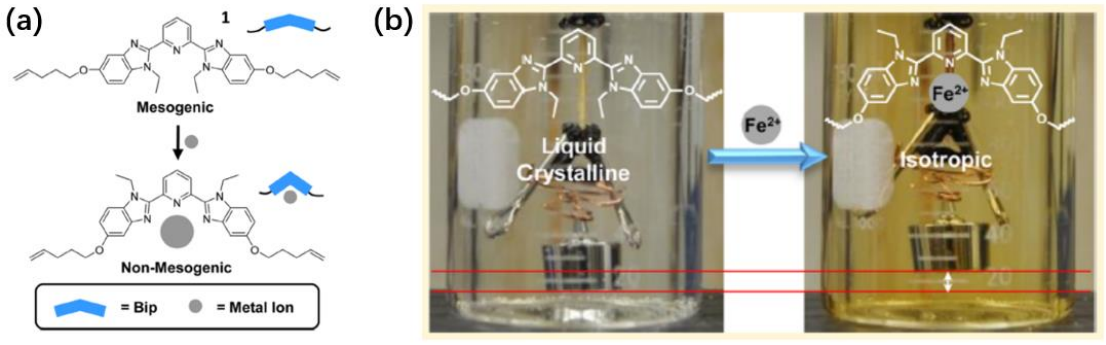

Figure 21. (a) Bip mesogens (1) display a conformational change upon binding a metal ion resulting in a change from mesogenic to nonmesogenic behavior. (b) A film of the LCE that had

been previously heated, stretched to 100% strain, and then cooled in the stretched state holds a 10 g mass in a beaker of 1:1 water:THF. $Fe(OTf)_2$ is added and stirred to produce a 1 mM solution. After 20 min the sample had noticeably lifted the mass. [134]

Recently, Rowan and coworkers (134) synthesized a liquid crystalline elastomer by incorporating liquid crystalline metal-binding Bip (2,6-bisbenzimidazolylpyridine) monomers into polymeric networks via thiol−ene chemistry, which exhibited liquid crystalline behavior that can be harnessed to access soft shape memory with excellent thermal fixity and recovery. They found that the permanent shape of these multidomain LCEs could be recovered by exposure to metal ions solution at room temperature, presumably due to a LC-isotropic transition induced by the metal ion binding. The original properties of the material could be recovered by removal of the metal ions from the film with diethylenetriamine. Furthermore, long-range alignment of the mesogens could be obtained through physical stretching above the LC-isotropic transition temperature. Upon exposure to a thermo-, photo-, or metallostimulus, the stretched aligned state converted to contracted isotropic state, resulting in a contractile force in the sample that can be as high as 0.254 N (Figure 21).

III.II.IV. Light-responsive LCE Actuators

Photo-responsive LCE actuators have attracted a considerable amount of attention, because light as a clean energy source can provide rapid precise and remote manipulation. As described above, LCEs exhibit thermoelastic features: upon heating above or cooling below the nematic-isotropic phase transition temperature, they undergo contraction or extension along the aligned direction of mesogenic units. If this feature of LCEs is incorperated with the photochemical phase transition (photochemically induced decrease of mesogens alignment order) or controlled by photothermal effect, it is expected that actuation of LCE actuators can be controlled by light (135-139).

Ikeda and co-workers developed photoresponsive azobenzene LCE actuators (138-140). The three-dimensional bending mode can be used to construct artificial hands and microrobots for particular manipulations. As shown in Figure 22, the film underwent bending and unbending upon exposure to UV and visible light respectively. Under UV light irradiation, the monodomain LCE actuator

bent along the direction of mesogens toward the incident light, and the bent film recovered to the original flat shape upon exposure to visible light. These photo-actuations were reversible and could be readily controlled through changing the wavelength of light. They found that the bending was again observed along the direction of mesogens even when the film was rotated by 90°, showing that the bending behavior is anisotropic and determined only by the rubbing direction of the LC cell.

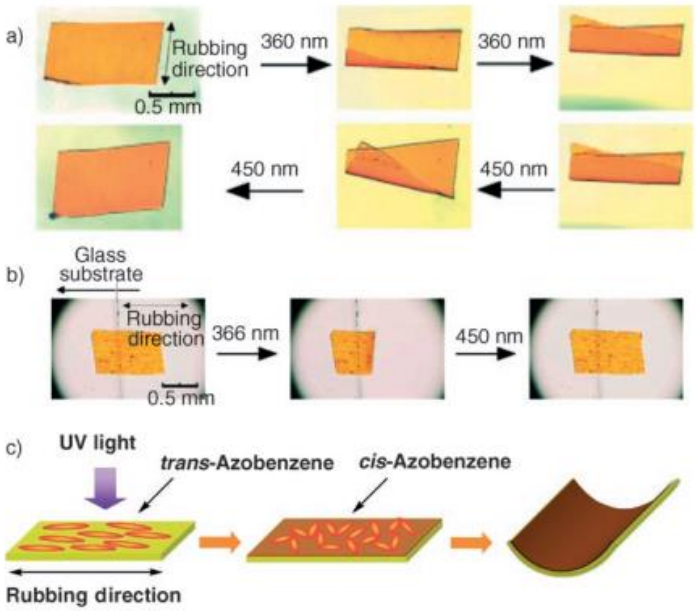

Figure 22. Photocontrolled Bending and unbending actuation of (a) an LC gel in toluene and (b) an LCE film in air. (c) The proposed mechanism for the photoactuation of LCE films. [91]

Upon exposure to UV light, the azobenzene mesogenic units undergo the *trans-cis* isomerization and thus destabilize of the nematic phase (decrease in alignment order) or even induce the nematic-isotropic phase transition of the LCE. However, the extinction coefficient of the azobenzene groups at around 360 nm is large (2.6×10^4 L mol^{-1} cm^{-1}) and thus more than 99% of the incident photons are absorbed by a surface with a thickness less than 1 micrometer (138-140). Since the thickness of the film was about 20 μm, the decrease of aligned order of the mesogens takes place only in the surface area towards the light source, but in most part of the film the azobenzene mesogens remain their *trans*-state. Therefore, the volume contraction takes place only in the film

surface, thus result in the film bending towards the incident light. Moreover, the azobenzene mesogens prefer to align along the rubbing direction of the LC cells, therefore, the decrease of the aligned order of the mesogens is induced only along this direction, leading to the anisotropic actuation. Ikeda and co-workers (139) also discovered that repeated and precise bending along any direction on demand could be achieved by exposing polydomain azobenzene LCE films to linearly polarized light (Figure 23). The actuator bent towards the incident light in a direction parallel to the polarized direction of the light.

Recently, Katsonis and coworkers developed spring-like LCEs that converted light energy into mechanical work at the macroscopic scale (Figure 24). They employed azobenzene as molecular switches by embedding them in liquid-crystalline polymer springs to convert and amplify the molecular movements into controllable and reversible twisting motions, such as winding, unwinding and helix inversion. Furthermore, the spring-like LCEs could produce work in the form of moving a macroscopic object and mimicking mechanical motions, similar to plant tendrils helping the plant access sunlight.

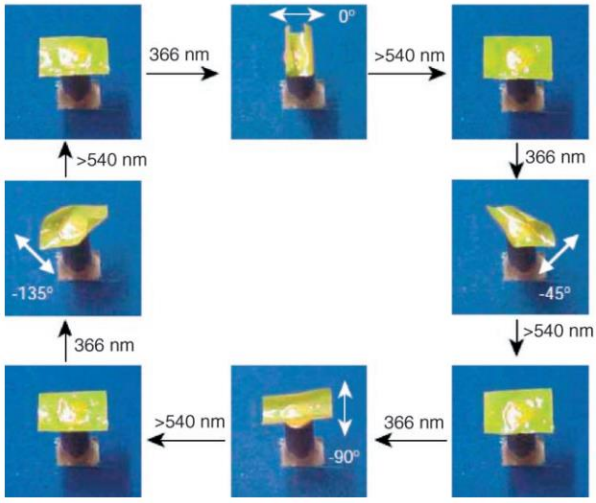

Figure 23. Precise control of the bending direction of a LCE actuator using linearly polarized light. Digital images of the film bending towards the linearly polarized light at different angles of polarization (white arrows) at λ=366 nm; the bent films are flattened upon exposure to visible light at λ>540 nm. [139]

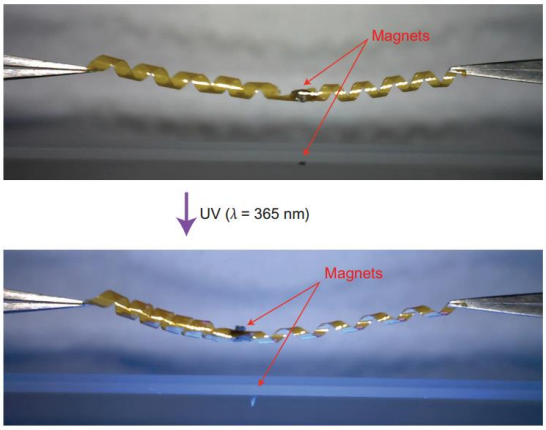

Figure 24. A magnet (m≈2 mg) attached to the knot of a helical ribbon underwent a push-pull shuttling motion upon exposure to UV light at λ=366 nm. The motion could be transmitted to another magnet (m≈0.5 mg) placed 10 mm below. [141]

III.III. Actuators Based on Volume Changes

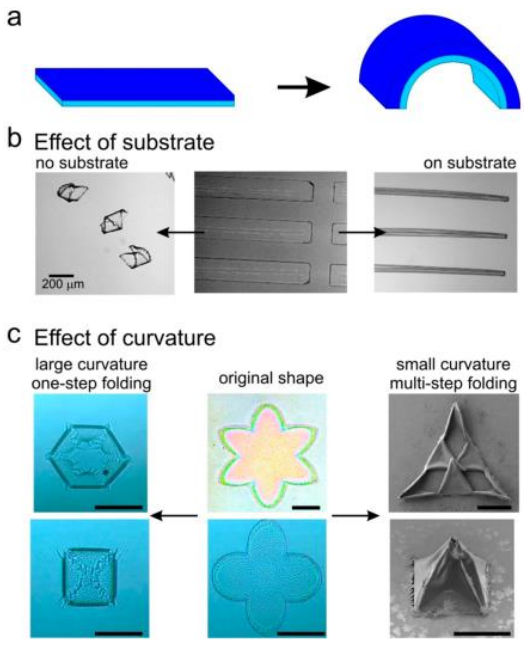

Figure 25. Different scenes of bilayer acuation based on (a) a poly(N-isopropylacrylamide) hydrogel: lying on the introdution of (b) a substrate [145] and (c) the shape of the actuator. Scale bars are 200 µm [100,146].

The actuators based on volume changes are usually hydrogels, which are capable of swelling and shrinkage either in an aqueous environment or in humid air. The swelling degree of hydrogels is determined by the balance of crosslinking density, the molar free energy of mixing, as well as the mixing entropy (90). The cross-linking density of a hydrogel is constant, while the energy and entropy components strongly rely on temperature, pH and solvent quality. Therefore, the swelling degree of hydrogels can be tuned by changing the temperature or pH. It was reported that complex deformations of thermo-responsive hydrogels could be achieved by employment of a gradient of stimuli (temperature, pH, light, etc.) (142-144).

Inhomogeneous hydrogels are also a very interesting topic in the field of hydrogel actuators. It was reported that inhomogeneous hydrogels not only can move in a variety of complex mode but also can form complex 3D shapes. Ionov and coworkers developed a type of stimuli-responsive hydrogel with bilayers structure (Figure 25a). They are not only able to form simple shapes such as tubes and scrolls (145) (Figure 25b) but also can convert themselves into sophisticated structures. The same authors also developed a hydrogel that can form capsules when the bending curvature is large (Figure 25c, left photographs) (100). Later, they reported a similar bilayer that displayed a more complex bending with a smaller bending curvature in a multistep manner (Figure 25c, right photographs) (146). Furthermore, different 3D shapes with sharp hinges such as a pyramid could be achieved through sequential steps. The step-by-step folding of self-folding films can also be obtained through local activation of their selected regions using light.

III.IV. Surface-Tension-Driven Actuators

Generally, the internal properties of polymers are usually employed to produce motions because the contribution of surface tension remains negligible on the macroscale. However, when the dimension of the actuators is reduced to the microscale and nanoscale, the effect of surface tension becomes large enough to enable the design of surface-tension actuators. Gracias and coworkers (101) reported the design of self-folding polymer containers by utilizing surface-tension-driven shape changes (Figure 26). In the unfolded state, the self-folding containers are made from six squares of SU-8 photoresists that are connected to each other by patches of polycaprolcatone (PCL).

The self-folding behavior was driven by a minimization of surface tension of the liquefying PCL hinges. It was observed that at temperatures above 58 °C, the PCL hinges transitioned from a white, opaque solid state to a transparent melting state, and the panels underwent an upward rotation due to a torque generated by the phase transition (Figure 26c).

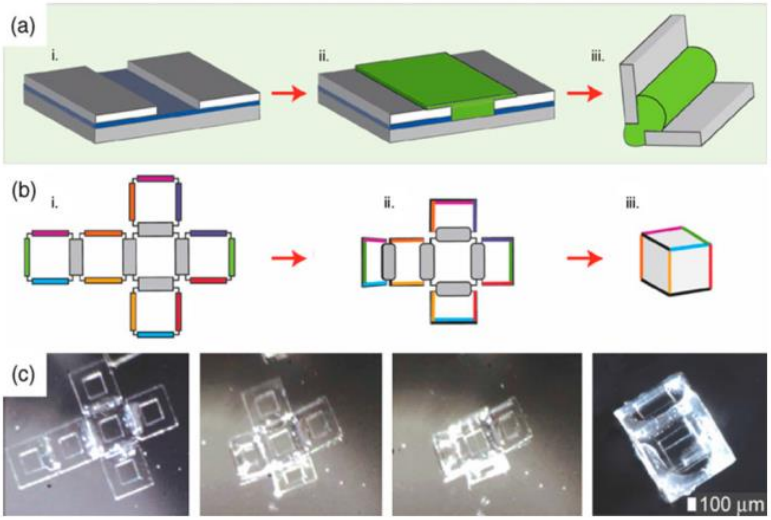

Figure 26. Preparation procedure and self-folding mechanism for polymer actuators based on surface tension. (a) (i–iii) Schematic illustration of fabrication procedures. (b) (i–iii) Schematic demonstrating the self-folding of a cubic container. (c) Series of photograph showing a 1-mm-dimension, six windowed polymer container self-folding at 60 ℃ . [101]

IV. Dynamic Covalent Bonds

Dynamic bonds can be defined as any class of bonds that can selectively undergo reversible breaking and reformation when external stimuli break their equilibrium conditions (3). Generally, dynamic bonds can be categorized into two broad kinds, including supramolecular interactions and dynamic covalent chemistry. The dynamic process can either be automatic or triggered by external stimuli, such as temperature, light, pH, electric field, ultrasound, magnetic field and mechanical force. Therefore, dynamic bonds can endow the polymers with stimuli-responsive properties if they are incorporated into the polymeric architectures. The non-covalent dynamic bonds include a wide range of interactions such as hydrogen bonding (147,148), π-π stacking (148-150), host-guest

interaction (151,152) and metal-ligand bonding (151), and are widely used in the field of dynamic combinatorial libraries, supramolecular polymers, hydrogels, organic semiconductors, and so on. However, the polymers based on non-covalent chemistry are usually soft materials owing to the relatively weak molecular interactions. The dynamic covalent bonds, such as Diels-Alder (DA) reaction (73), radical-exchange (64,65,78,80,84,153,154) and transesterification (155-157), can undergo breaking and reformation under suitable conditions without detrimental side reactions, allowing the formation of robust covalent molecules while sustaining dynamic properties that can only be accessed upon exposure to particular external stimuli. Recently, many approaches have been developed by combining the ideal features of traditional thermosets with the dynamic properties of controllably reversible bonds to yield stimuli-responsive polymer networks (3,158). The combination of these two polymer properties have broadly enriched the functions of thermosets, such as self-healing (63), triggered shape changes (153) or stress relaxation (84), remolding (156) and reversible motions (159).

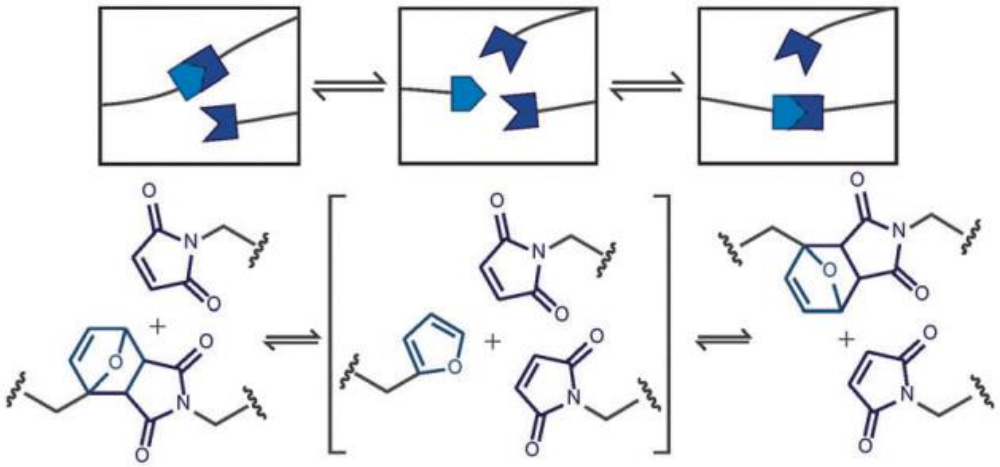

Figure 27. Reversible addition reactions of Diels–Alder cycloaddition, result in de-crosslinking and reformation of the polymer network. [158]

As one class of covalent dynamic bonds, the thermally reversible DA reaction, a [4π + 2π] cycloaddition between an alkene and diene, can undergo a retro-DA reaction on heating and re-bonding upon cooling, enabling the rearrangement of the starting materials (Figure 27). Wudl and

coworkers made use of this reaction to develop a self-healing material with mechanical properties equaling commercial epoxy resins (63).

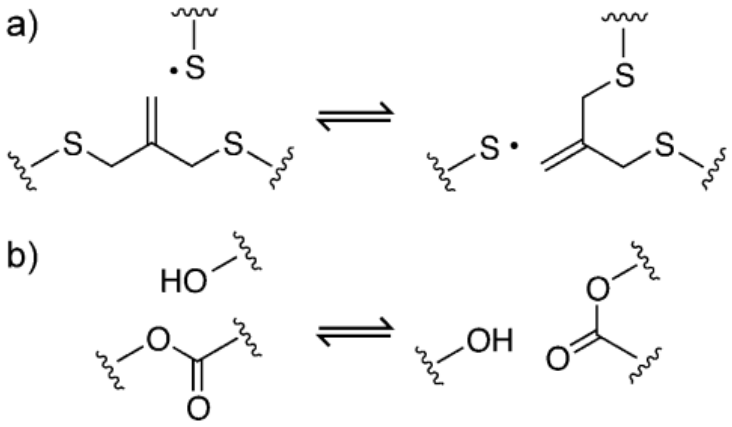

Figure 28. Two typical examples of bond exchangeable reactions. (a) Thiyl radical-mediated addition–fragmentation of an allyl sulfide; (b) catalytic transesterification reaction between hydroxy and ester groups. Both the reactions undergo rearrangement of the polymer network by simply exchange of bond connectivity with no change in the reactants and products. The total number of links and the network integrity keep constant. [161]

Figure 28 illustrates the dynamic mechanisms of two kinds of exchangeable bonds in the polymer networks. Functional groups capable of addition-fragmentation chain transfer (AFT), such as allyl sulfides and trithiocarbonates (TTC), were recently introduced in the crosslinked polymers. Radical generation and the succedent bond exchange reactions take place under irradiation with light in the presence of a radical-generated photoinitiator, enabling the achievements of photoinduced plasticity (84), photo lithographically defined features (153), and even light-triggered self-healing (80,160).

V. Objective of the Thesis

The overall objective of this thesis is to learn from nature to design, fabricate and investigate covalent dynamic polymers that display the smart features or functions of stimuli-controlled shape memory, self-healing and motions.

More specifically, on one hand, we studied the use of ultrasound to heal polymers, with the purpose of developing a new external stimulus that affords remote activation and spatiotemporal control, yet has distinct advantages over the much studied stimulus of light. As reported in Chapter 1, we show that ultrasound (HIFU) is effective using our proposed concept of ultrasound-triggered, shape memory-assisted self-healing of covalently cross-linked dynamic polymers. Our designed covalently cross-linked, microphase-separated polyurethane provides high mechanical strength and toughness, while the dynamic motifs embedded in the polymer structure can respond to HIFU to undergo bond breaking and reformation leading to the self-healing. The localized and directed repairing can be achieved in a remote and controlled manner. This novel modality, combining ultrasound stimulation, dynamic polymer, shape memory and self-healing, has the potential applications for long-term load-bearing engineering components anti-fatigue medical devices like pacemakers as well as artificial hip and knee used in the biomedical engineering.

On the other hand, the research conducted in this thesis aimed at developing new startegies in designing optical polymer actuators that are more robust for light-controlled motions than the actuators known to date. As reported in Chapter 2, we described the design and synthesis of malleable azobenzene liquid crystalline elastomers (ALCEs) based on transesterification. We show that by pre-storing mechanical strain energy in ALCE films, unprecedented contraction force can be generated by light as a result of the phototriggered release of the stored strain energy in addition to the direct optical to mechanical energy conversion from the trans-cis photoisomerization of azobenzene mesogens. Furthermore, we made use of the energy-storing actuator to fabricate rolling structures, such as wheels and spring-like motors, which can be driven by light to undergo continuous motions with tunable rolling speed and controllable moving directions at the macroscopic scale.

On the basis of the second research project, in order to further enhance the light-controlled motions of liquid crystal polymers, we simultaneously imparted NIR light and UV-Vis light responsiveness to the azobenzene liquid crystal dynamic polymer network by doping AuNRs to the polymer matrix (namely AuNR-ALCNs). In addition, we also took advantages of bilayer structures to enhance the light-controlled motions of the liquid crystal nanocomposites, and successfully

controlled the motion directions of the actuator. Furthermore, we control the local motion of the actuator by locally encoding the liquid crystal molecular alignments in different regions of the bilayer films. Finally, the photo-triggered molecular level motions (i.e., the LC sematic-isotropic phase transition and photoisomerization of azobenzene) were synergistically added up and converted into complex robot-like combinatorial macroscopic motions, in the form of a light-driven polymer “crane” grabbing, lifting, lowering, and releasing a tubular object.

In the last chapter of the thesis, Chapter 4, we present an overall discussion on the accomplishment and significance of the conducted research. We also propose some future works that are worth being pursued.

CHAPITRE 1. ULTRASOUND HEALABLE SHAPE MEMORY DYNAMIC POLYMERS

1.1. About the Project

Self-healing polymers represent a class of smart materials which can perform self-diagnosis and self-healing after suffering injuries to improve to improve the safety, lifetime, energy efficiency and environmental impact of man-made materials. Despite the many progresses made in recent years, it is still very challenging to integrate a number of desirable features and properties into one single material, such as good mechanical properties, high healing efficiency, rapid stimuli-responsiveness, excellent performance of shape memory-assisted crack closure, remote and spatially controllable healing process. Using rationally designed polymer structure, we developed a material that possesses high mechanical strength and toughness, and exhibits high healing efficiency upon exposure to high-intensity focused ultrasound (HIFU) owing to bond breaking and reformation of the dynamic motifs (Diels-Alder bonds) incorporated in the chain and crack closure assisted by the shape-memory function. High-intensity focused ultrasound (HIFU), which is utilized as an extracorporeal tool for the treatment of tumors owing to its thermal effect, can trigger self-healing of polymers in both spatial and temporal manner by selecting the time and location of ultrasound application. In the previous researches, the commonly used methods for triggering self-healing are limited to a number of stimuli such as temperature change by direct heating, light, pH and electric field. However, each stimulus has some advantages and disadvantages and may not be convenient in certain application circumstances. HIFU, can provide unique advantages in some situations, especially in the field of biomedical engineering. For example, if the polymer implants in the minimally invasive surgical techniques are made of self-healing polymers, the use of focused ultrasound beams allows the healing process to be activated remotely, to occur deep in the materials in a non-invasive and non-radioactive way, and to be controlled in localized region without detriment to the undamaged parts of the materials and impacting the overall performance.

This work was published in *Journal of Materials Chemistry A*, **2014**, 2, 16051-16060 by Xili Lu, Guoxia Fei, Hesheng Xia and Yue Zhao. This research work was conducted in the Sichuan University under the supervision of Prof. Xia and co-supervision of Prof. Zhao. I designed and performed the experiments reported in the paper. Guoxia Fei gave me a lot of useful suggestions about this project and helped me with the SAXS experiments. I wrote the first draft of the manuscript. Prof. Zhao finalized the manuscript with revision contributions from Prof. Xia.

1.2. Paper Published in Journal of Materials Chemistry A, 2014, 2, 16051.

Ultrasound healable shape memory dynamic polymers

Xili Lu,[a] Guoxia Fei,[a] Hesheng Xia*[a] and Yue Zhao*[b]

[a]State Key Laboratory of Polymer Materials Engineering, Polymer Research Institute, Sichuan University, Chengdu 610065, China. E-mail: xiahs@scu.edu.cn

[b]Département de chimie, Université de Sherbrooke, Sherbrooke, Québec, J1K 2R1, Canada. Email: yue.zhao@usherbrooke.ca.

1.2.1 Abstract

The concept of using ultrasound to trigger shape memory assisted healing of covalently cross-linked dynamic polymers is demonstrated. The well-designed dynamically crosslinked poly(3-caprolactone)-based polyurethane bearing Diels–Alder bonds not only possesses high mechanical strength and toughness, but also exhibits shape memory assisted crack-closure and healing upon exposure to highintensity focused ultrasound owing to breaking and reformation of dynamic bonds. The use of focused ultrasound allows the healing process to be activated remotely and to be controlled locally by depositing the acoustic energy only in the damaged region without detriment to the undamaged parts of the material. The healable polyurethane materials have potential applications such as long-term load-bearing engineering components and anti-fatigue medical devices.

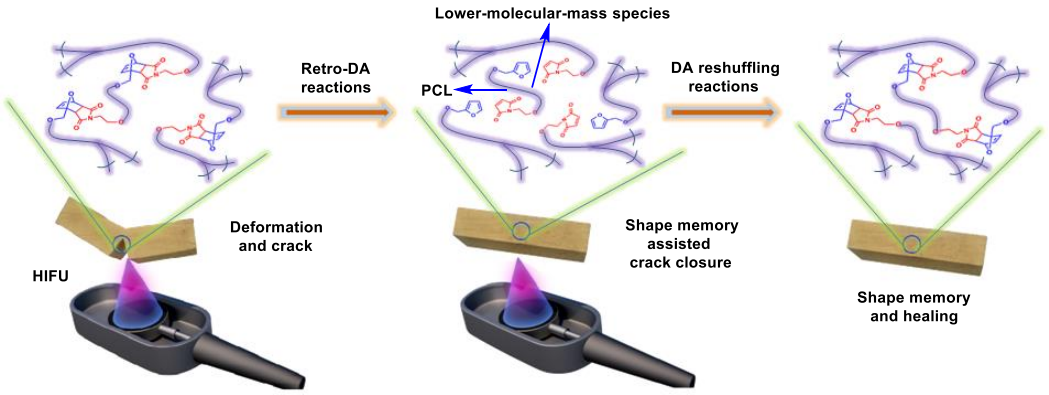

1.2.2. Introduction

Self-healing materials have attracted great attention because of their potential applications in the fields of transportation, aerospace, electronics and biomedical engineering, by improving the safety, lifetime, energy efficiency and environmental impact of the materials.[1-3] Two different approaches have been developed to prepare intrinsic self-healing materials. The first approach uses noncovalent chemistry, such as hydrogen bonding,[4-8] π-π stacking,[9] host-guest interaction[10,11] and metal-ligand bond.[12,13] The second approach uses dynamic covalent chemistry including dynamic urea bond,[14] Diels-Alder reaction,[15-17] radical-exchange[18-23] and transesterification[24] reaction and so on. For the latter one, most healable materials possess better mechanical properties comparing to those self-healing polymers based on noncovalent dynamic chemistry, but the healing needs the input of external energy such as heat[15,16,20] or light.[18,21,22] The conventional heating raises the temperature of the entire material, which is detrimental to the undamaged parts of the material and impacts its overall performance. Light can be focused precisely onto damaged spots to locally heal polymers, but it only works when the plastic is thin or transparent. Therefore, developing new stimulus responsive healable polymers with good mechanical properties remains a key challenge.

High-intensity focused ultrasound (HIFU) is widely used as an extracorporeal tool for the treatment of tumors,[25,26] as well as a stimulus to control drug delivery,[27-30] and trigger shape memory[31] of smart material systems due to its non-invasiveness and non-radiativity. The HIFU beam can be brought to a tight focal spot with a small area at a distance from its source. Moreover, ultrasound can effectively penetrate much deeper than light with minimum side effects. Generally, materials with strong mechanical properties often require high temperature and strong stimulus to repair, which may be harmful for the properties. HIFU can resolve these problems by depositing the acoustic energy just in the damaged area in a non-invasive and non-radiative way.

In most situations, damage in polymers often occurs in company with macroscopic deformation. Generally, the crack surfaces cannot autonomously close proximity for healing without manual intervention. In some real applications, the damaged and deformed parts cannot even be taken out for repairing. In order to address this challenge, shape memory function was introduced into self-

healing materials to recover the shape and close the crack. For example, one strategy is to embed shape memory alloy wires[32-34] or shape memory polymer fibers[35,36] into polymer matrix to improve the healing performance. Another strategy reported by Mather and co-workers is to make thermoplastic linear poly(ε-caprolactone) (PCL) blended with crosslinked PCL network[37] or PCL fibers randomly distributed in a shape memory epoxy matrix.[38] Recently, Rowan et al synthesized a single-component polymer that inherently exhibits shape memory assisted self-healing property under UV light irradiation.[39] Despite those well-designed systems, there still remains some challenges. The novel shape memory and healable material systems with improved mechanical strength, as well as novel stimulus means instead of UV light, should be developed.

In this project, we present ultrasound-healable shape-memory dynamic polymers to address the above challenges. The specially designed polymers can integrate good mechanical properties, ultrasound responsiveness, shape memory and healing ability into one structure. The novel polymers, hereafter designated as PU−FM (Fig. 1-1a), are PCL-based polyurethane (PU) networks with Diels−Alder (DA) bonds, i.e. furan-maleimide (FM) adducts, alternately located in the backbone of polymer chains between adjacent crosslinking points. The crosslinked PU network can provide the dynamic polymers with excellent mechanical properties and solvent resistance. The PCL chain segments can fix a temporary deformation when cooling below Tm and the permanent shape can be recovered when the sample is heated above T_m due to the presence of covalent cross-link network. DA motifs in the chain backbone can undergo reversible bond breaking and reformation under HIFU treatment to provide the healing property. The important molecular structure feature for PU−FM is specially designed for better ultrasound responsiveness by manipulating the location of the ultrasound-sensitive dynamic bonds in the polymer chain structure, allowing lower-molecular-mass species with good mobility to be produced under ultrasound.

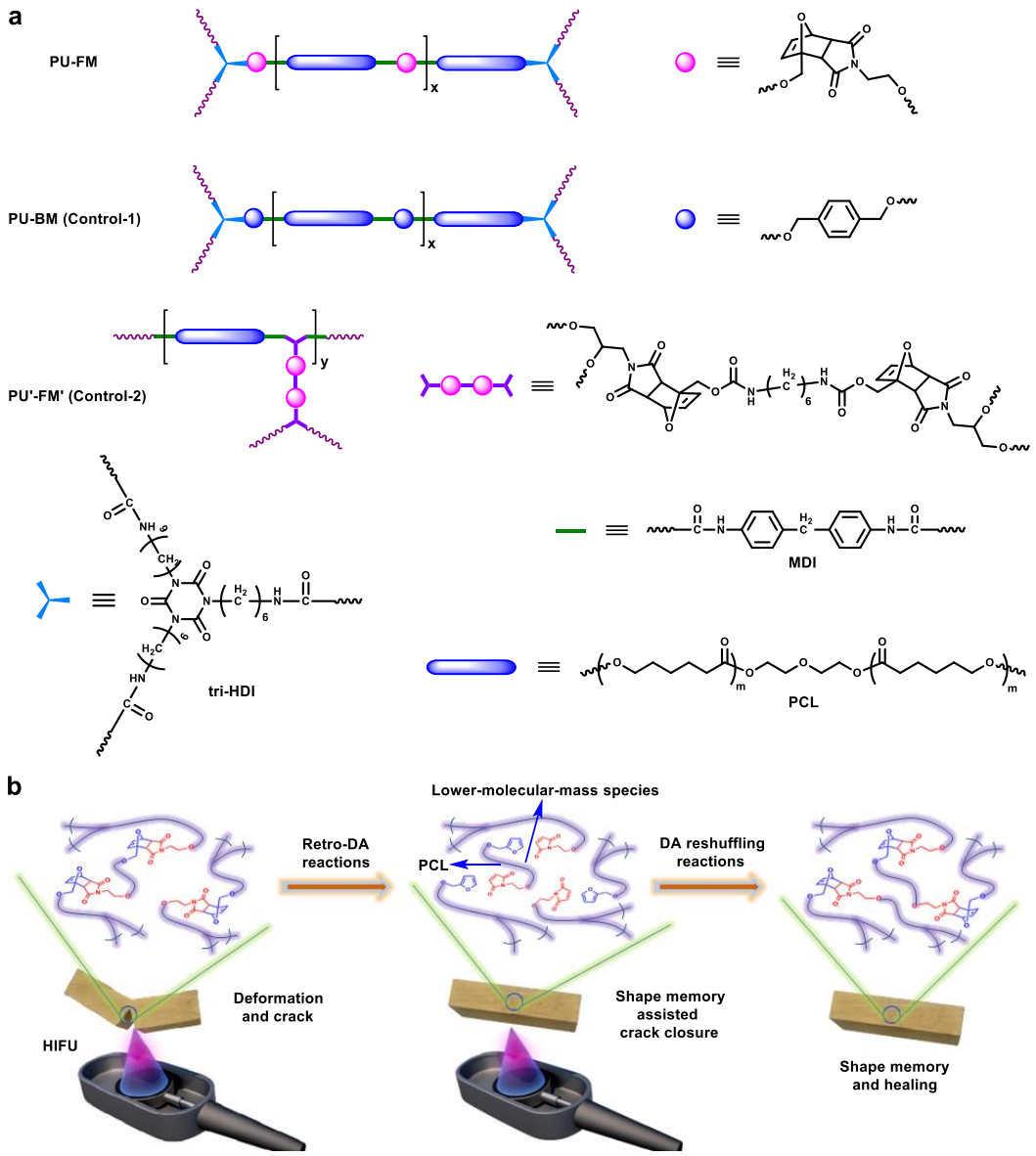

Figure 1-1. (a) Structures characteristic of the dynamic polymer PU−FM and the control samples. (b) Schematic illustration of the concept for HIFU-triggered shape memory assisted healing of PU−FM.

Fig. 1-1b illustrates the concept of the HIFU triggered shape recovery and healing. When the damaged area with deformation and crack in the polymer sample is exposed to the focus of HIFU, the temperature of the selected area rises rapidly due to the significant acoustic energy deposition as well as viscous shearing and relaxation of polymer chains induced by focused HIFU mechanical

waves, which allows the shape recovery and crack closure to be achieved. Meanwhile, under HIFU treatment, as the temperature rises, the DA motifs in the main chain of polymer are acoustically activated and will absorb energy to undergo a retro-DA reaction, which causes a concomitant reversible degradation of the polymer network, followed by wetting, diffusion and entanglement of the temporary lower-molecular-mass species across the crack surfaces. The dissociated furan and maleimide moieties will experience rebonding or reshuffling reactions to form cycloaddition adducts upon cooling after the HIFU is switched off. The novel modality for HIFU-triggered shape memory assisted healing of covalently cross-linked dynamic polymers is proposed for the first time and its distinct advantages include: 1) HIFU can repair materials with high mechanical strength, avoiding the input of high temperature and other strong stimulus; 2) localized and directed repair can be easily achieved by HIFU via depositing the acoustic energy only in the damaged area in a non-invasive and non-radiative way; 3) ultrasound can effectively penetrate much deeper into the materials than light to repair the interior cracks or defeats in a remote and controlled way; and 4) shape memory effect can be used to close the cracks for efficient repairing of large defects or damage and repair the macroscopic deformation.

In order to confirm and understand the roles of the dynamic DA bonds on ultrasound-responsiveness and healing, two control samples were also prepared. We used 1,4-benzenedimethanol instead of DA-bonds to prepare parallel polymers PU−BM (Control-1, Fig. 1a) having a similar molecular structure as PU−FM. Furthermore, in order to demonstrate the importance of DA bond location and amounts, another sample PU′−FM′ (Control-2, Fig. 1-1a) with DA bonds only located at cross-link points instead of in the polymer chain were synthesized.

1.2.3. Results and Discussion

1.2.3.1 Materials Synthesis and Structure Characterization

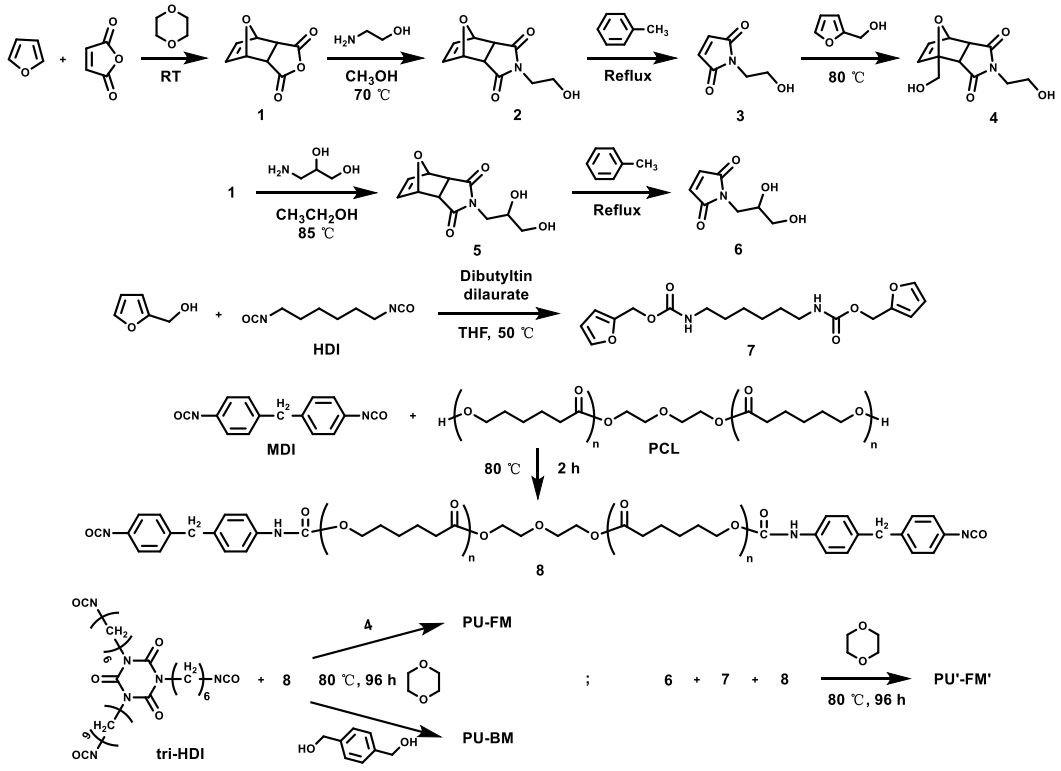

Scheme 1-1. Synthetic routes for the covalently cross-linked dynamic polymer PU−FM and the control polymers.

The synthetic routes for PU-FM as shown in Scheme 1-1 can be simply described as follows: The small molecule containing DA bonds and two reactive hydroxyl (compound **4**) were synthesized by four step reactions[40] (see Supporting Information). The NCO-terminated PCL prepolymer (precursor **8**) was synthesized by the reaction of 4, 4'-methylene diphenyl diisocyanate (MDI) and polycaprolactone diol (Mn=4,000 g mol^{-1}) with a molar ratio of 2:1 at 80 °C. Then compound **4**, precursor **8** and hexamethylene diisocyanate trimer (tri-HDI) were mixed and reacted to obtain a pale yellow and non-transparent solid. In order to study the effects of crosslink degree on the mechanical properties and ultrasound healing ability of PU−FM, several cross-linked polymers with different crosslinking index (ρ, 20−50%, the definition shown in Supporting Information)

were prepared. The control samples of PU−BM$_{20}$ without DA bond and PU′−FM′$_{20}$ with DA bonds in the crosslinking sites were prepared through the similar procedures but using different small molecular diol as shown in Scheme 1-1. Both PU−BM$_{20}$ and PU′−FM′$_{20}$ have a crosslink index of 20%. Based on the molecular structures shown in Scheme 1, we can calculate the amount of DA bonds in the polyurethane network. For the sample PU−FM$_{20}$, the calculated amount of DA bonds is ~51.7 mole%, while for PU′−FM′$_{20}$ sample, it is ~16.6 mole%.

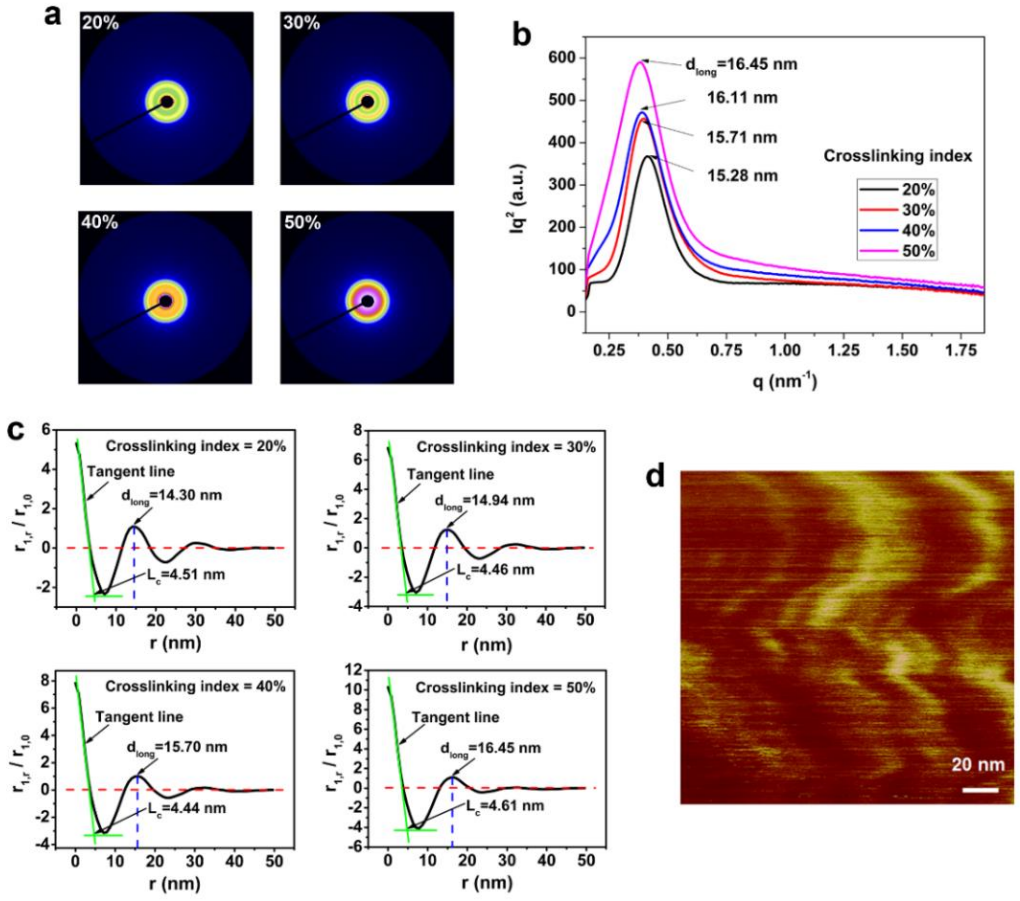

Figure 1-2. (a) 2D SAXS patterns of PU−FM with different crosslinking index (20-50%). (b) The Lorentz corrected SAXS plots of PU−FM. (c) The normalized correlation functions of all the PU−FM samples, the long period can be estimated as the corresponding r value at the first peak from the correlation function. The lamellar thickness can be estimated as the corresponding r value

at the intersection point of the two tangent lines. (d) AFM (tapping mode) phase image of PU−FM_{20}.

The microstructures of PU−FM were characterized by SAXS (Fig. 1-2). The 2D SAXS patterns (Fig. 1-2a) reveal the presence of microphase-separated structure in PU−FM, which is a common and well known property of polyurethane. The Lorentz corrected SAXS plots show an intense peak at low q for all samples, indicating the presence of microdomain periodicity and microphase separation in the material (Fig. 1-2b). The presence of these microphase-separated structures can provide better mechanical properties for polyurethane. It can be deduced that flexible polyether PCL forms the soft domain, whereas the other components, including the DA adducts, 4, 4′-diphenylmethane diisocyanate (MDI) and hexamethylene diisocyanate trimer (tri-HDI), form the hard domain. With increasing the crosslinking index, the long period increases from 15.28 nm to 16.45 nm. The correlation function analysis also shows a similar increase in the long period from 14.30 nm to 16.45 nm (Fig. 1-2c). Interestingly, the estimated lamellar thicknesses are almost the same (4.44−4.61 nm), indicating that the lamellar thickness only depends on the components of hard domain but not the crosslinking index. Furthermore, Atomic Force Microscope (AFM) was used to detect the morphology of the microphase-separated structure. The worm-like hard domains (bright) and soft domains (dark) can be observed for PU−FM with a crosslink index of 20% (PU−FM_{20}) as a representative example (Fig. 1-2d).

Table 1-1. Mechanical properties of PU−FM with different crosslink index.

Sample*	molar ratio [tri-HDI] : [**8**] : [**4**]	crosslink index (ρ)	Young's modulus (MPa)	Yield Strength (MPa)	Stress at Break (MPa)	Strain at Break (%)
PU- FM_{20}	8 : 48 : 60	20%	208 ± 3	22.0 ± 0.5	23.6 ± 1.2	1925 ± 137
PU- FM_{30}	12 : 42 : 60	30%	239 ± 4	23.1 ± 0.5	24.6 ± 1.2	1878 ± 148
PU- FM_{40}	16 : 36 : 60	40%	258 ± 4	24.2 ± 0.6	25.9 ± 1.8	1768 ± 125
PU- FM_{50}	20 : 30 : 60	50%	292 ± 4	24.7 ± 0.7	28.0 ± 2.3	1637 ± 133

*PU−FM_{20}, PU−FM_{30}, PU−FM_{40} and PU−FM_{50}, means that the crosslink index of the polymer is 20%, 30%, 40%, 50% respectively. Strain rate: 500 mm min^{-1}.

The mechanical properties are summarized in Table 1-1. The typical stress-strain curves of the PU−FM (Fig. 1-5a) follow the shape of those of typical crystalline polymers including three distinct regions. Our prepared dynamic polymers are stiff solids with mechanical properties comparable to the commercial polyester-type polyurethane. A significant increase in Young's modulus is observed with increasing the crosslinking index (Table 1-1). The presence of a yield region with a long plateau in the stress-strain curves can be ascribed to the progressive rearrangement and reorientation of polymer chains along the direction of stretching. In the final stretching stage, the stress again increases with strain, showing a big upturn in the slope of the stress-strain curves, due to the strain-hardening phenomenon. In addition, it is noteworthy that the stress at break increases with the cross-link degree while the strain at break shows an opposite trend, which is not surprising, as more cross-links will restrain the mobility of polymer segments.

1.2.3.2 HIFU-triggered Shape Memory Assisted Crack Closure and Healing

The shape memory transition temperature (T_{trans}), here as the melting point of the PCL segments of PU−FM, was determined by DSC and DMA (Fig. 1-S3 and 1-S4, Supporting Information). DSC reveals that the PU−FM have a melting transition of ~58 °C, and DMA shows a dramatic drop in the storage modulus at ~65 °C. The DMA curve of PU-FM is similar with the normal polyurethane without DA bonds we synthesized using the same PCL diol.[41] The absence of a plateau before 60 °C in the DMA curve is related to the PCL segment.[42] The shape memory properties of the obtained dynamic polymers under thermal stimulus were studied by cyclic thermomechanical tensile tests (Fig. 1-3a). The PU−FM samples were equilibrated at 65 °C for 30 min before deformation. One cycle consists of four steps: (1) elongated to 100% strain corresponding to the maximum strain (ε_m) at a constant rate of 2 mm min^{-1}, (2) cooled to 0 °C at a rate of 3 °C min^{-1} to fix the deformation under a constant stress, (3) held for 10 min at 0 °C to obtain a fixed strain (ε_u) upon unloading of the stress and (4) reheated to 65 °C at a rate of 10 °C min^{-1} and held for 10 min, allowing the shape recovery to complete to a recovery strain (ε_p). In a thermomechanical cycle, the shape fixity ratio (R_f) and shape recovery ratio (R_r) are defined as below:

$$R_f = \frac{\varepsilon_u}{\varepsilon_m} \times 100\% \qquad (1)$$

$$R_r = \frac{\varepsilon_m - \varepsilon_p}{\varepsilon_m} \times 100\% \qquad (2)$$

The results in Fig. 1-3a show that PU−FM samples exhibit excellent shape memory behaviors, with a shape fixity ratio (R_f) of ~99% and a shape recovery ratio (R_r) of ~99%. The shape memory characteristic of PU-FM is similar with the normal PCL-based polyurethane without DA bonds we synthesized previously.[41] It is noteworthy that the crosslinking index nearly has no significant effect on the shape memory property of PU−FM.

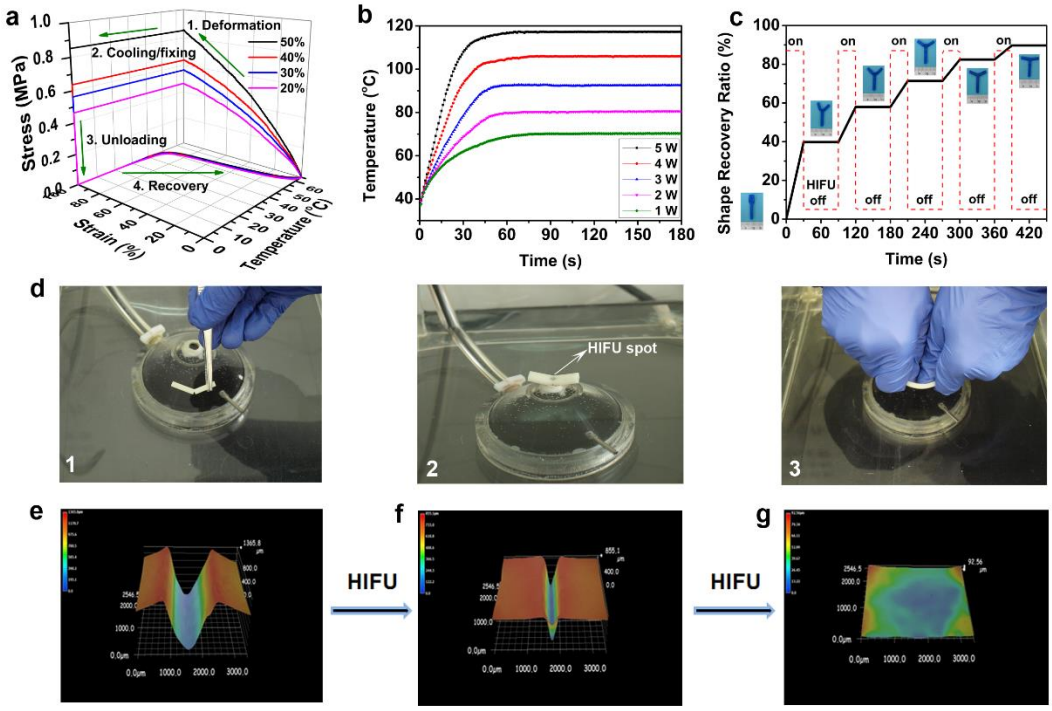

Figure 1-3. (a) Shape-memory thermomechanical cycle tests for PU−FM. (b) The HIFU induced temperature rise of PU−FM$_{20}$ at different HIFU powers output. (c) HIFU controlled shape memory behaviors of PU−FM. (d) Photos of (1) the sample with crack and deformation, (2) the partial shape recovery sample under HIFU treatment and (3) the crack closed and healed sample after HIFU treatment. 3D images of a deformed and damaged PU−FM$_{20}$ sheet (e) with deformation and

crack, (f) after shape recovery assisted partial crack closure and (g) after complete crack closure and healing under HIFU.

The use of HIFU for controlling shape memory of the covalently cross-linked dynamic polymers was investigated. HIFU induced thermal effect is the intrinsic reason for HIFU-triggered shape memory and thus we firstly investigated the temperature rise of PU−FM_{20} with time under different HIFU powers output (Fig. 1-3b). In this experiment, a piece of the polymer sample (35 mm in length, 8 mm in width and 3.0 mm in thickness) was placed on the HIFU focal spot and the temperature rise was recorded with a thermal infrared camera (Fig. 1-S1, Supporting Information). The temperature of PU−FM rises quickly until it reaches a thermal equilibrium value, which is proportional to the HIFU power output. For example, at a HIFU power output of 3 W, the temperature rises rapidly from 37 °C to ~90 °C in ~50 s, and then remains unchanged. The prominent temperature rise of the polymer matrix is due to the absorption of acoustic energy caused by viscous shearing and relaxation of polymer chains induced by focused HIFU mechanical waves.[43] Since the HIFU can focus its acoustic energy on a spot area, it can localize the heating in a small area and hence activate the shape recovery process only in a selected part of the polymer.[31]

Fig. 1-3c shows the temporal control of the shape recovery in a selected area by using HIFU. A sample of cross-linked PU−FM_{20} with a permanent shape ‘‘T’’ was processed into a temporary shape ‘‘I’’ (folded at $T > T_{trans}$ followed by cooling to $T < T_{trans}$). The focus of the HIFU beam was directed to the folding area of the sample, then HIFU was switched on for 30 s, the shape recovery (unfolding) started. Once HIFU was off, the shape recovery halted immediately retaining the temporal shape. Thus the shape of the polymer sample can change from temporary shape ‘‘I’’ to intermediate shape ‘‘Y’’ and to permanent shape ‘‘T’’ by switching on/off the HIFU. All the intermediate shapes were stable in the absence of HIFU.

Furthermore, HIFU-triggered shape memory assisted crack closure and healing was investigated. The process was demonstrated in Movie 1-S1 (Supporting Information) and some captured photos during the process were shown in Fig. 1-3d. Also this process was observed by using a digital microscope with large depth-of-field (Fig. 1-3e). For the experiment, a polymer sheet sample of

PU−FM$_{20}$ (length ~ 35 mm, width ~ 5 mm, thickness ~ 3 mm) was cut and bent to obtain a crack with a depth of ~50% of the sheet thickness and an angle of ~45° between the two cut surfaces (Fig. 1-3d and e), the deformation and large crack were then retained. Then the sample was moved to the HIFU focal area and subject to HIFU treatment, the crack immediately closed from ~45° to ~0° (Fig. 1-3d, f and g) due to the shape memory effect and started to heal after the crack closure (Movie 1-S1, Supporting Information). The above results demonstrate that under HIFU treatment, PU−FM$_{20}$ exhibits excellent shape memory property, which has the ability to bring the crack surfaces back together in spatial proximity and provides the prerequisite for the bond formation between the damage surfaces to realize the healing.

1.2.3.3 HIFU Healing Mechanism

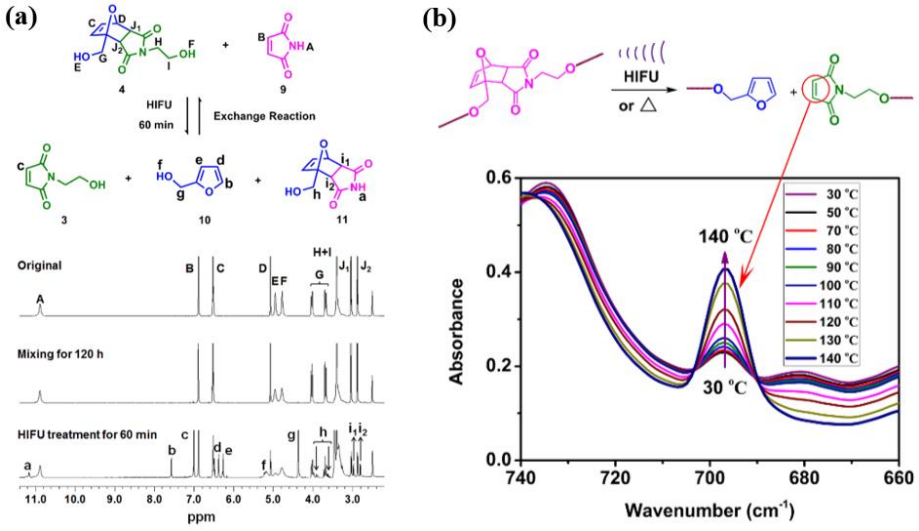

Figure 1-4. (a) ^{1}H NMR spectra of the exchange Diels-Alder reaction before and after HIFU treatment. (b) Temperature-dependent FTIR spectra of PU−FM$_{20}$, recording the variations of absorbance intensity of C=C (maleimide) with increasing temperature from 30 to 150 °C at a heating rate of 5 °C min^{-1}.

In order to further confirm the proposed molecular mechanism based on the DA bonding for HIFU healing, we adopted a model reaction using two low-molecular-weight compounds, DA adducts **4** and maleimide **9**, to investigate the ultrasound-responsive reshuffling or dynamic exchange

capacity of DA units. Previous research[44] has demonstrated that DA bond as one class of mechanophores can respond to ultrasound to undergo retro [4 + 2] cycloadditions. We suppose that, on exposure to HIFU, the furan-maleimide adducts can undergo retro-DA reactions and exchange reaction due to the thermal and mechanical effects of HIFU, enabling the network reorganization and successful healing of damaged polymers. A 0.1 mol L^{-1} solution of furan-maleimide adduct **4** and maleimide **9** (1:1) in d_6-DMSO was prepared in a screw-top NMR tube and exposed to the HIFU focal spot (Movie 1-S2, Supporting Information). After HIFU treatment for 60 min, some DA adducts **4** indeed undergo retro-DA reactions and generate compound **10** and **3**, which can be confirmed by the appearance of the new ^{1}H NMR peaks b–f (Fig. 1-4a). Also the maleimide **9** reacts with the liberated furfuryl alcohol **10** to form a new DA adduct **11**, which shows new ^{1}H NMR peaks a, h and i (Fig. 4a). Owing to the dissociation of DA adducts **4** and consumption of maleimide **9**, the ^{1}H NMR peaks A−J of the original samples decrease significantly. As a control experiment, the mixture of compound **4** and **9** shows no change in ^{1}H NMR spectrum even after mixing them for 120 h at room temperature without HIFU treatment. Thus, the exchange reactions of DA units by HIFU treatment are confirmed.

Temperature-dependent FTIR was also employed to investigate the dissociation temperature of DA motifs in bulk materials. Fig. 1-4b shows the variations of the intensity of imide peak near 700 cm^{-1} which is assigned to C=C of maleimide[45,46] with temperature. The intensities of imide peak remain nearly unchanged when the temperature is below 80 °C and start to increase at ~80 °C due to the dissociation of DA adducts, being consistent with the previously reported work.[47,48] The HIFU responsiveness and relatively low dissociation temperature of DA units here allows the use of HIFU to trigger the healing of the dynamic polymer PU−FM.

1.2.3.4 HIFU Healing Performance of Polymer

HIFU healing efficiency of PU−FM was measured. The PU−FM_{20} samples were cut and bent to obtain a crack with ~50% of the sheet width and an angle of ~10° between two cut surfaces (Fig. S2, Supporting Information). These samples were subsequently healed by exposure to HIFU treatment. Unless otherwise stated, HIFU power output was set at 3 W. Fig. 1-5a shows stress-

strain curves for the original, damaged and HIFU healed samples at different HIFU treatment time. The damaged sample after cutting has an ultimate elongation of only ~66% compared to ~1788% of the original one. And the toughness of the damaged sample is only ~2% of that of the original sample. When the sample is healed by HIFU treatment, the strain and stress increases significantly with HIFU exposure time. After HIFU treatment for 60 min, the sample exhibits almost the same stress and strain at break as the original material, showing a healing efficiency of ~92% (Fig. 1-5d).

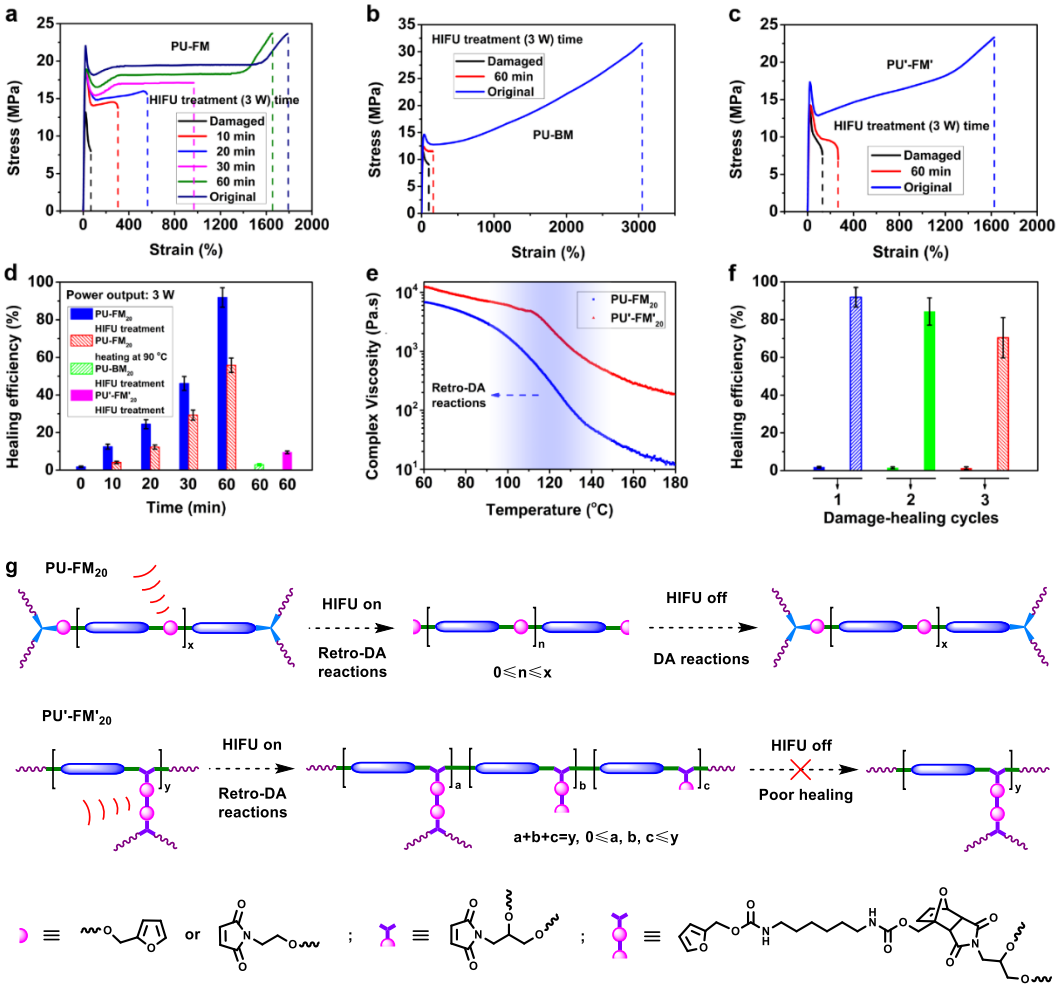

Figure 1-5. Stress-strain behavior of damaged and healed PU−FM_{20} (a) and control samples PU−BM_{20} (b) and PU′−FM′$_{20}$ (c). (d) Healing efficiency of PU−FM_{20}, PU−BM_{20} and PU′−FM′$_{20}$ by HIFU treatment or conventional heating. (e) The complex viscosity of PU−FM_{20} and

PU′−FM′$_{20}$ measured from 60 to 180 °C. (f) Healing efficiency of PU−FM$_{20}$ after multiple "damage-healing" cycles. (g) The proposed HIFU healing mechanism of PU−FM$_{20}$ and PU′−FM′$_{20}$. The healing efficiency is defined as the ratio of the toughness after healing over the original toughness of the undamaged sample, i.e. healing efficiency=100% (toughness$_{healed}$/toughness$_{original}$), where toughness is the energy corresponding to the integral area under the stress–strain curve. All errors are standard deviations.

In contrast, after HIFU treatment for 60 min, the control sample PU−BM$_{20}$ (Control-1) without DA bonds shows a very weak recovery, ~5% of the original elongation at break (Fig. 1-5b) and a very low healing efficiency of ~3% (Fig. 1-5d). This result indicates that the HIFU-triggered healing of PU−FM$_{20}$ is owing to the reversible DA reaction. For the sample PU−BM$_{20}$, no retro-DA reaction occurs and the polymer crosslinking network restrains the chain diffusion and re-entanglement, and thus the healing occurs at a very low level.

In order to highlight the unique molecular architecture of PU−FM and gain further insight into the relationship between the dynamic bond locations and HIFU healing efficiency of dynamic polymers, another control sample PU′−FM′$_{20}$ (Control-2) with DA bonds located at cross-link points was investigated. Surprisingly, PU′−FM′$_{20}$ has a very low healing efficiency of only ~10% (Fig. 1-5c and d) after HIFU treatment for 60 min. This can be attributed to the different molecular architecture for the two kinds of polymer. A molecular mechanism was proposed to explain this interesting phenomenon (Fig. 1-5g). On one hand, the amount of DA bonds for the sample PU−FM$_{20}$ is ~51.7 mole%, much higher than that for PU′−FM′$_{20}$ (~16.6 mole%), which indicates that the PU−FM$_{20}$ is more dynamically responsive than PU′−FM′$_{20}$. On the other hand, under HIFU treatment, the DA motifs in PU−FM$_{20}$ are acoustically activated and PU−FM$_{20}$ undergoes a retro-DA reaction to produce linear lower-molecular-mass oligomers, which can provide good mobility for better healing efficiency. However, for PU′−FM′$_{20}$ sample, under the same conditions it can only produce partially de-crosslinked polymer networks and/or high molecular weight linear PU because DA bonds in PU′−FM′$_{20}$ are only located at the crosslink points and also the amounts of DA bonds in PU′−FM′$_{20}$ (~16.6 mole%) is much less than that in PU−FM$_{20}$ (~51.7 mole%). This assumption was confirmed by comparing the dynamic rheological behaviors of PU−FM$_{20}$ and

PU′−FM′$_{20}$, measured in a parallel-plate rheometer from 60 to 180 °C. As shown in Fig. 1-5e, the complex viscosity of PU−FM$_{20}$ starts to decline at ~80 °C and experiences a sharp decrease during 110 to 130 °C due to the dissociation of furan-maleimide adducts. This is attributed to the formation of linear lower molecular weight oligomers resulted from the dissociation of DA bonds. While PU′−FM′$_{20}$ shows a much less decrease in the viscosity, indicating that only partially de-crosslinked polymer networks and the formation of high molecular weight linear PU. These results are also confirmed by the decreases in the complex modulus G′ and G″ with temperature at a fixed frequency of 1 Hz (Fig. 1-S5). Therefore, PU−FM$_{20}$ has a much better healing efficiency owing to the lower molecular weight oligomers with better mobility and ability of wetting, diffusion and re-entanglement that enhance the reshuffling DA reactions between crack surfaces. More importantly, these results suggest that ultrasound responsiveness can be adjusted by controlling the location and amounts of DA bonds in the molecular chain.

For comparison, the PU−FM$_{20}$ samples were also healed by conventional heating at 90 °C (the equilibrium temperature of PU−FM$_{20}$ under HIFU treatment at a power output of 3 W, see Fig. 1-3b). As shown in Fig. 1-5d, HIFU treatment has a better healing effect than conventional heating. For example, the healing efficiency of PU−FM$_{20}$ after conventional heating for 60 min is ~56%, far lower than that by HIFU treatment (~92%). This control experiment reflects the unique feature of HIFU triggered healing, different from the conventional thermal treatment. Not only HIFU induces thermal effect, but also the mechanical vibration of ultrasound wave can facilitate the retro-DA reaction, diffusion of the temporary lower molecular weight species between two crack surfaces, as well as the disentanglement of polymer chains.

We also applied multiple “damage-healing” cycles (cutting and healing for 60 min with 3 W HIFU as one cycle, and one day as the cycle time interval) for PU−FM$_{20}$ to probe the repetitive healing ability of the dynamic polymers. The healing efficiency of the first, second and third “damage-healing” cycle are ~92%, ~84% and ~70% respectively (Fig. 1-5f), suggesting the materials can be healed multiple times. The decrease in the healing efficiency may be attributed to the breaking of permanent chemical bonds by cutting and physical damage by the long-time HIFU treatment.

We further investigated the effect of HIFU intensity on the healing ability of PU−FM. As shown in Fig. 1-6a, a medium HIFU intensity (3 W) can achieve the best healing efficiency. Low HIFU intensity (1 W) fails to effectively activate the DA reshuffling reactions, leading to a low healing efficiency of ~33% even after HIFU treatment for 60 min. Although a better healing efficiency, ~57%, can be achieved by high HIFU intensity (5 W) in early stage (HIFU treatment for 20 min), however the healing efficiency decreases significantly to ~16% after HIFU treatment for 60 min. This is due to physical damage caused by strong thermal and mechanical effects of ultrasound wave at a high HIFU power for a longer time. The ultrasound healing efficiency of polymer samples with different crosslinking index was also investigated. Fig. 1-6b shows the change of healing efficiency of PU−FM with different crosslinking index under HIFU treatment (3 W) for different time. It is noteworthy that the dynamic polymers with low crosslinking index heal fast and have higher healing efficiency than those with high crosslinking index. This observation can be explained by the fact that low crosslinking density can endow the polymer chains with better mobility to facilitate the DA reshuffling reactions, while high crosslinking density will restrict the chain mobility.

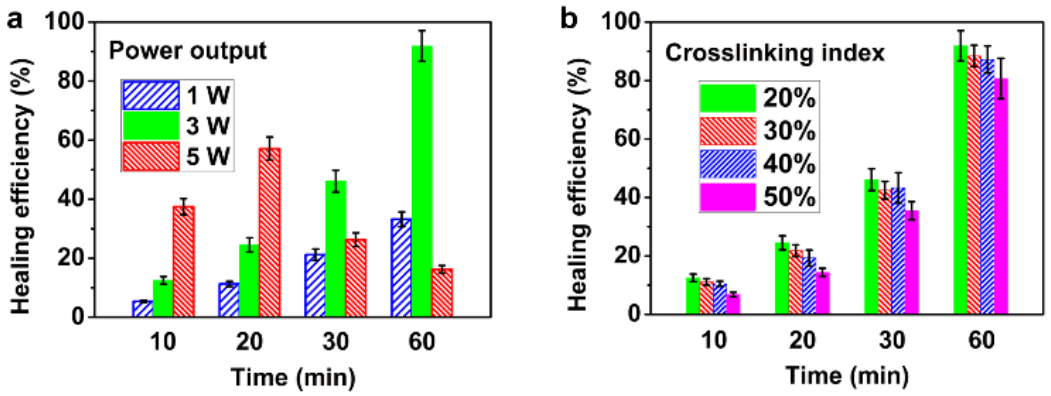

Figure 1-6. (a) Healing efficiency of PU−FM$_{20}$ under HIFU treatment with various power outputs for different time. (b) Healing efficiency of PU−FM with different crosslinking index ρ under HIFU treatment (3 W) for different time. All errors are standard deviations.

1.2.4. Conclusions

In conclusion, we have proposed and demonstrated a novel concept for HIFU-triggered shape memory assisted crack closure and healing of polymers for the first time. The unique molecular architecture can endow the dynamic polymers with good mechanical properties, ultrasound responsiveness, good healing and shape memory ability. The shape memory actions triggered by HIFU can close the crack, which provides the prerequisite for the bond formation between the damage surfaces during the healing process. HIFU triggered retro-DA reactions and DA reshuffling reactions are the main reasons for the effective healing of covalently cross-linked dynamic polymers. The localized, on-demand repairing can be easily achieved by HIFU via depositing the acoustic energy only in the damaged area with pinpoint accuracy and minimum side effects in a remote and controlled way. The modality, i.e., HIFU-triggered shape memory assisted healing of polymers based on reversible Diels−Alder reaction, as well as the unique molecular architecture design strategy, can be extended to a wide range of dynamic materials.

Acknowledgements

H. X. acknowledges financial support from major project of Chinese Ministry of Education (313036), the Programme of Introducing Talents of Discipline to Universities (B13040), and National Natural Science Foundation of China (51203102, 51010004); and Y. Z. acknowledges financial support from the Natural Sciences and Engineering Research Council of Canada (NSERC) and le Fonds de recherche du Québec: Nature et technologies (FRQNT).

Notes and references

1 B. J. Blaiszik, S. L. B. Kramer, S. C. Olugebefola, J. S. Moore, N. R. Sottos and S. R. White, *Annu. Rev. Mater. Res.*, **2010**, 40, 179.

2 S. Burattini, B. W. Greenland, D. Chappell, H. M. Colquhoun and W. Hayes, *Chem. Soc. Rev.*, **2010**, 39, 1973.

3 E. B. Murphy and F. Wudl, *Prog. Polym. Sci.*, **2010**, 35, 223.

4 P. Cordier, F. Tournilhac, C. Soulie-Ziakovic and L. Leibler, *Nature*, **2008**, 451, 977.

5 Y. Chen, A. M. Kushner, G. A. Williams and Z. Guan, *Nat. Chem.*, **2012**, 4, 467.

6 A. Phadke, C. Zhang, B. Arman, C.-C. Hsu, R. A. Mashelkar, A. K. Lele, M. J. Tauber, G. Arya and S. Varghese, *Proc. Natl. Acad. Sci. USA*, **2012**, 109, 4383.

7 G. M. L. van Gemert, J. W. Peeters, S. H. M. Söntjens, H. M. Janssen and A. W. Bosman, *Macromol. Chem. Phys.*, **2012**, 213, 234.

8 M. V. Biyani, E. J. Foster and C. Weder, *ACS Macro Lett.*, **2013**, 2, 236.

9 J. Fox, J. J. Wie, B. W. Greenland, S. Burattini, W. Hayes, H. M. Colquhoun, M. E. Mackay and S. J. Rowan, *J. Am. Chem. Soc.*, **2012**, 134, 5362.

10 M. Zhang, D. Xu, X. Yan, J. Chen, S. Dong, B. Zheng and F. Huang, *Angew. Chem. Int. Ed.*, **2012**, 51, 7011.

11 T. Kakuta, Y. Takashima, M. Nakahata, M. Otsubo, H. Yamaguchi and A. Harada, *Adv. Mater.*, **2013**, 25, 2849.

12 M. Burnworth, L. Tang, J. R. Kumpfer, A. J. Duncan, F. L. Beyer, G. L. Fiore, S. J. Rowan and C. Weder, *Nature*, **2011**, 472, 334.

13 S. Coulibaly, A. Roulin, S. Balog, M. V. Biyani, E. J. Foster, S. J. Rowan, G. L. Fiore and C. Weder, *Macromolecules*, **2014**, 47, 152.

14 H. Ying, Y. Zhang and J. Cheng, *Nat. Commun.*, **2014**, 5, 3218.

15 X. Chen, M. A. Dam, K. Ono, A. Mal, H. Shen, S. R. Nutt, K. Sheran and F. Wudl, *Science*, **2002**, 295, 1698.

16 X. Chen, F. Wudl, A. K. Mal, H. Shen and S. R. Nutt, *Macromolecules*, **2003**, 36, 1802.

17 B. J. Adzima, C. J. Kloxin and C. N. Bowman, *Adv. Mater.*, **2010**, 22, 2784.

18 B. Ghosh and M. W. Urban, *Science*, **2009**, 323, 1458.

19 B. Ghosh, K. V. Chellappan and M. W. Urban, *J. Mater. Chem.*, **2011**, 21, 14473.

20 C. E. Yuan, M. Z. Rong, M. Q. Zhang, Z. P. Zhang and Y. C. Yuan, *Chem. Mater.*, **2011**, 23, 5076.

21 Y. Amamoto, J. Kamada, H. Otsuka, A. Takahara and K. Matyjaszewski, *Angew. Chem. Int. Ed.*, **2011**, 50, 1660.

22 Y. Amamoto, H. Otsuka, A. Takahara and K. Matyjaszewski, *Adv. Mater.*, **2012**, 24, 3975.

23 K. Imato, M. Nishihara, T. Kanehara, Y. Amamoto, A. Takahara and H. Otsuka, *Angew. Chem. Int. Ed.*, **2012**, 51, 1138.

24 M. Capelot, D. Montarnal, F. Tournilhac and L. Leibler, *J. Am. Chem. Soc.*, **2012**, 134, 7664.

25 J. E. Kennedy, G. R. ter Haar and D. Cranston, *Br. J. Radiol.*, **2003**, 76, 590.

26 J. E. Kennedy, *Nat. Rev. Cancer*, **2005**, 5, 321.

27 H. Zhang, H. Xia, J. Wang and Y. Li, *J. Control. Release*, **2009**, 139, 31.

28 G. D. Moon, S.-W. Choi, X. Cai, W. Li, E. C. Cho, U. Jeong, L. V. Wang and Y. Xia, *J. Am. Chem. Soc.*, **2011**, 133, 4762.

29 C.-Y. Wang, C.-H. Yang, Y.-S. Lin, C.-H. Chen and K.-S. Huang, *Biomaterials*, **2012**, 33, 1547.

30 H.-Y. Huang, S.-H. Hu, S.-Y. Hung, C.-S. Chiang, H.-L. Liu, T.-L. Chiu, H.-Y. Lai, Y.-Y. Chen and S.-Y. Chen, *J. Control. Release*, **2013**, 172, 118.

31 G. Li, G. Fei, H. Xia, J. Han and Y. Zhao, *J. Mater. Chem.*, **2012**, 22, 7692.

32 E. L. Kirkby, J. D. Rule, V. J. Michaud, N. R. Sottos, S. R. White and J.-A. E. Månson, *Adv. Funct. Mater.*, **2008**, 18, 2253.

33 E. L. Kirkby, V. J. Michaud, J. A. E. Månson, N. R. Sottos and S. R. White, *Polymer*, **2009**, 50, 5533.

34 S. Neuser, V. Michaud and S. R. White, *Polymer*, **2012**, 53, 370.

35 G. Li, H. Meng and J. Hu, *J. R. Soc. Interface*, **2012**, 9, 3279.

36 G. Li, O. Ajisafe and H. Meng, *Polymer*, **2013**, 54, 920.

37 E. D. Rodriguez, X. Luo and P. T. Mather, *ACS Appl. Mater. Interfaces*, **2011**, 3, 152.

38 X. Luo and P. T. Mather, *ACS Macro Lett.*, **2013**, 2, 152.

39 39 B. T. Michal, C. A. Jaye, E. J. Spencer and S. J. Rowan, ACS Macro Lett., 2013, 2, 694.

40 W. H. Heath, F. Palmieri, J. R. Adams, B. K. Long, J. Chute, T. W. Holcombe, S. Zieren, M. J. Truitt, J. L. White and C. G. Willson, *Macromolecules*, **2008**, 41, 719.

41 J. Han, G. Fei, G. Li and H. Xia, *Macromol. Chem. Phys.*, **2013**, 214, 1195.

42 Q. Meng, J. Hu, Y. Zhu, J. Lu and Y. Liu, *J. Appl. Polym. Sci.*, **2007**, 106, 2515.

43 B. Liu, H. Xia, G. Fei, G. Li and W. Fan, *Macromol. Chem. Phys.*, **2013**, 214, 2519.

44 K. M. Wiggins, J. A. Syrett, D. M. Haddleton and C. W. Bielawski, *J. Am. Chem. Soc.*, **2011**, 133, 7180.

45 L. Wu, R. Mincheva, Y. Xu, J.-M. Raquez and P. Dubois, *Biomacromolecules*, **2012**, 13, 2973.

46 C. Zeng, H. Seino, J. Ren, K. Hatanaka and N. Yoshie, *Macromolecules*, **2013**, 46, 1794.

47 Y. Chujo, K. Sada and T. Saegusa, *Macromolecules*, **1990**, 23, 2636.

48 R. C. Boutelle and B. H. Northrop, *J. Org. Chem.*, **2011**, 76, 7994.

1.2.5. Supporting Information

1.2.5.1. Materials

Unless otherwise stated, all solvents and reagents were obtained from commercial suppliers with the highest purity available and used without further purification. Polycaprolactone diol (Perstorp, Capa2402, Mn=4,000 g mol^{-1}) was dried under vacuum at 110 ℃ for 12 h prior to use. Anhydrous tetrahydrofuran (THF) and 1,4-dioxane were obtained by distillation over sodium benzophenone. Compound **4**, **6** and **7** were synthesized using reported procedures[1,2] with some modifications. All reactions were carried out under an inert atmosphere of oxygen-free N_2 unless otherwise stated.

1.2.5.2 General characterizations

The ^{1}H NMR and ^{13}C NMR spectra were recorded on a Bruker 400 (400 MHz) spectrometer. All chemical shifts were reported in parts per million (ppm) downfield from TMS using the residual protonated solvent as an internal standard (d_6-DMSO, ^{1}H 2.50 ppm and ^{13}C 39.7 ppm). DSC experiments were carried out under nitrogen atmosphere on TA Instruments DSCQ2000 at a heating rate of 5 °C min^{-1}. Dynamic Mechanical Thermal Analysis (DMTA) experiments were performed on a TA Instruments Q-800 instrument system in the dual cantilever mode. The storage modulus (G′), loss modulus (G″) and loss factor (tanδ) were measured from −100 to 100 °C under a nitrogen atmosphere at a heating rate of 3 °C min^{-1}. The strain amplitude used was 50 μm and the test frequency was 1 Hz. Surface temperatures were determined with a FLIR Systems infrared camera (Thermovision A20, Sweden). Dynamic rheological measurements were carried out in a dynamic rheometer (Bohlin Gemini 2000, Malvern, Britain) in constant-strain mode by controlling the strain at 1%. The diameter of the plate was 25 mm, and the gap was about 1 mm. All of the samples were tested from 60 to 180 °C at a heating rate of 3 ℃ min^{-1} at a frequency of 1 Hz.

1.2.5.3. Experimental setup

The general apparatus was assembled as shown in Figure 1-S1.

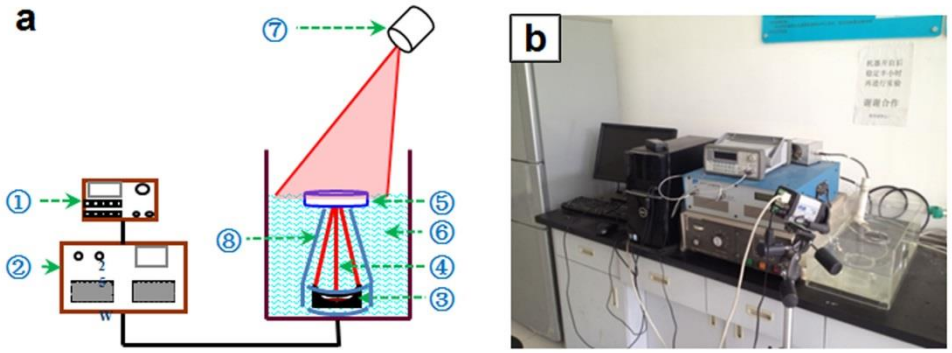

Figure 1-S1. Schematic illustration for experimental setup (a) and photo of the used high intensity focused ultrasound (HIFU) apparatus (b). ①: Arbitrary waveform generator, ②: RF power amplifier, ③: Acoustic lens transducer, ④: Ultrasound beams, ⑤: Polymer sample, ⑥: Water bath, ⑦: Infrared camera, ⑧: Transducer shell.

The high intensity focused ultrasound (HIFU) apparatus comprises three main components: an arbitrary waveform generator (Agilent 33220A Function Generator), a RF power amplifier (A150, Electronics & innovation) and an acoustic lens transducer (H-101, Sonic Concept, USA). The acoustic lens transducer with a high acoustic focal pressure within a long focal volume of Φ1.26 mm × 11 mm and a geometric focal length of 62.6 mm was mounted at the bottom of a tank filled with water and the beams of ultrasound were pointed upwards and focused on a specified spot. The ultrasound power output can be adjusted in the range of 0~150 W and the frequency of ultrasound is 1.1 MHz.

1.2.5.4. Synthetic Procedures

Synthesis of 4,10-Dioxatricyclo[5.2.1.$0^{2,6}$]dec-8-ene-3,5-dione (**compound 1**). A solution of maleic anhydride (20 g, 204 mmol) in 50 mL anhydrous dioxane was charged to a flame dried 100 mL round-bottom flask with a magnetic stir bar. Furan (15 mL) was added via syringe and the solution was allowed to stir at room temperature for 30 min. The flask was sealed with a rubber

plug and the mixture was kept still overnight. The product precipitated out of solution and was collected via vacuum filtration and washed with diethyl ether. The colorless crystals were 100% exo-addition product by NMR analysis and used without further purification. Yield 93.7%; mp 114–116 °C; ^{1}H NMR (400 MHz, d$_6$-DMSO, 298 K) δ (ppm) 6.580 (s, 2H), 5.349 (s, 2H), 3.311 (s, 2H); ^{13}C NMR (100 MHz, d$_6$-DMSO, 298 K) δ (ppm) 171.83, 137.11, 81.938, 49.356; FT-IR (KBr) ν=3095.3, 3033.4, 2997.2, 1860.8, 1790.4, 1226.9 cm^{-1}.

Synthesis of 4-(2-Hydroxyethyl)-10-oxa-4-azatricyclo[5.2.1.0^{2,6}]dec-8-ene-3,5-dione (**compound 2**). The anhydride **1** (5.00 g, 30.1 mmol) was suspended in MeOH (7 mL) in a flame dried 50 mL three-neck round-bottom flask with a magnetic stir bar and reflux condenser. The solution was purged with nitrogen for 10 minutes in an ice bath, after which ethanolamine (1.84 g, 30.1 mmol) in 3 mL MeOH was added dropwise via a dropping funnel. The resulting solution was allowed to stir for 5 min at 0 °C, then turned dark orange and was refluxed for 24 h. The flask was cooled to room temperature, and after 2 h the product began to crystallize. The mixture was stored in a freezer overnight, and the precipitate was collected by vacuum filtration. The resulting white crystals were washed with 2-propanol and used without further purification. Yield 70.5%; mp 134–137 °C; ^{1}H NMR (400 MHz, d$_6$-DMSO, 298 K) δ (ppm) 6.552 (s, 2H), 5.123 (s, 2H), 4.799 (s, 1H), 3.417 (s, 4H), 2.928 (s, 2H); ^{13}C NMR (100 MHz, d$_6$-DMSO, 298 K) δ (ppm) 176.72, 136.67, 80.518, 57.489, 47.349, 40.828; FT-IR (KBr) ν=3477.3, 3095.2, 2971.7, 2936.0, 2894.6, 1768.3, 1696.0 cm^{-1}.

Synthesis of 1-(2-Hydroxyethyl)-1*H*-pyrrole-2,5-dione (**compound 3**). To a flame dried 100 mL round-bottom flask equipped with a stir bar and vigreaux condenser was charged with compound **2** (4.18g, 20.0 mmol) and toluene (50 mL). The reaction was refluxed overnight. The resulting mixture was hot filtered, and the product crystallized from solution upon cooling. The colorless solid was collected via vacuum filtration, washed with diethyl ether and used without further purification. Yield 92.4%; mp 70–72 °C; ^{1}H NMR (400 MHz, d$_6$-DMSO, 298 K) δ (ppm) 7.014 (s, 2H), 4.793 (s, 1H), 3.456 (s, 4H); ^{13}C NMR (100 MHz, d$_6$-DMSO, 298 K) δ (ppm) 171.31, 134.65, 58.145, 40.147; FT-IR (KBr) ν=3445.9, 3275.4, 3108.4, 2964.1, 2932.9, 2880.2, 1711.9, 1406.3, 1158.7 cm^{-1}.

Synthesis of 1-(Hydroxymethyl)-10-oxatricyclo[5.2.1.$0^{2,6}$]dec-8-ene-3,5-dione-2-aminoethanol (**compound 4**). Compound **3** (1.41g, 10.0 mmol), high purity benzene (20 mL) and freshly distilled furfuryl alcohol (0.99g, 10.1 mmol) were added to a 100 mL round-bottom flask equipped with a magnetic stir bar and reflux condenser. The reaction was refluxed for 24 h, during which the product precipitated. The resulting mixture was cooled to room temperature. The product was collected via vacuum filtration and washed with diethyl ether. Yield 88.0%; mp 110–115 °C; ^{1}H NMR (400 MHz, d_6-DMSO, 298 K) δ (ppm) 6.504 (br, 2H), 5.076 (s, 1H), 4.956 (t, 1H), 4.792 (t, 1H), 4.020 (dd, 1H), 3.670 (dd, 1H), 3.402 (br, 4H), 3.032 (d, 1H), 2.869 (d, 1H); ^{13}C NMR (100 MHz, d_6-DMSO, 298 K) δ (ppm) 176.71, 175.28, 138.39, 136.76, 91.930, 80.461, 59.209, 57.581, 50.219, 48.036, 40.851; FT-IR (KBr) ν=3434.0, 3083.2, 2948.6, 1696.0, 1404.1, 1188.7, 1037.9 cm^{-1}.

Synthesis of N-(2,3-dihydroxy-propyl)-10-oxa-4-aza-tricyclo[5.2.1.$0^{2,6}$]-dec-8-ene-3,5-dione (**compound 5**). The anhydride **1** (5.00 g, 30.1 mmol) was suspended in EtOH (7.5 mL) in a flame dried 50 mL three-neck round-bottom flask with a magnetic stir bar and reflux condenser. A solution of 3-amino-1,2-propanediol (2.74 g, 30.1 mmol) in EtOH (2 mL) was added drop wise to the reaction system via a dropping funnel. The resulting mixture was refluxed at 85 °C for 12 hours, during which the solution turned orange and then the product began to precipitate. After the reaction, the mixture was stored in a freezer overnight, and the crystal was collected by vacuum filtration and washed with diethyl ether. The product was dried under vacuum and used without further purification. Yield 54.5%; ^{1}H NMR (400 MHz, d_6-DMSO, 298 K) δ (ppm) 6.550 (s, 2H), 5.126 (s, 2H), 4.805 (s, 1H), 4.586 (s, 1H), 3.672 (m, 1H), 3.349 (d, 2H), 3.277 (d, 2H), 2.928 (s, 2H); ^{13}C NMR (100 MHz, d_6-DMSO, 298 K) δ (ppm) 176.60, 136.46, 80.312, 68.054, 63.882, 47.151, 41.753; FT-IR (KBr) ν=3396.7, 2999.2, 2935.1, 2894.5, 1768.7, 1696.2, 1436.5, 1404.8, 1339.8, 1189.1, 1062.9, 883.1 cm^{-1}.

Synthesis of N-(2,3-dihydroxypropyl)maleimide (**compound 6**). To a flame dried 100 mL round-bottom flask equipped with a stir bar and vigreaux condenser was charged with compound **5** (4.78g, 20.0 mmol) and toluene (50 mL). The reaction was refluxed overnight. The resulting mixture was hot filtered, and the product crystallized from solution upon cooling. The colorless solid was

collected via vacuum filtration, washed with petroleum ether and used without further purification. Yield 83.6%; ^{1}H NMR (400 MHz, d_6-DMSO, 298 K) δ (ppm) 7.000 (s, 2H), 4.873 (d, 1H), 4.645 (t, 1H), 3.682 (m, 1H), 3.422 (d, 2H), 3.345 (m, 2H); ^{13}C NMR (100 MHz, d_6-DMSO, 298 K) δ (ppm) 171.64, 134.89, 68.922, 64.504, 41.612; FT-IR (KBr) ν=3500.2, 3411.0, 3102.8, 2942.9, 2892.1, 1702.3, 1444.2, 1412.7, 1330.1, 1166.8, 1101.4, 1050.4 cm^{-1}.

Synthesis of 1,6-hexamethylene-bis(2-furanylmethylcarbamate) (**compound 7**). A flame dried 100 mL three-necked flask equipped with magnetic stirrer, thermometer, and condenser was charged with furfuryl alcohol (9.80 g, 0.10 mol), anhydrous THF (50mL) and dibutyltin dilaurate (0.50 g). The solution was purged with dry nitrogen for 10 minutes and 1,6-hexamethylene diisocyanate (HDI, 8.40 g, 0.05 mol) was added dropwise via a dropping funnel under vigorous stirring. The reaction mixture was maintained for 30 min at room temperature and stirred for 4 h at 50 °C. Then the resulting white product was recrystallized from methanol. Yield 88.4%; mp 101–103 °C; ^{1}H NMR (400 MHz, d_6-DMSO, 298 K) δ (ppm) 7.654 (d, 2H), 7.225 (m, 2H), 6.444 (d, 4H), 4.983 (s, 4H), 2.957 (m, 4H), 1.356 (s, 4H), 1.214 (s, 4H); ^{13}C NMR (100 MHz, d_6-DMSO, 298 K) δ (ppm) 155.92, 150.49, 143.53, 110.82, 110.38, 57.431, 40.404, 29.605, 26.130; FT-IR (KBr) ν=3327.9, 3048.2, 2940.2, 2864.2, 1687.1, 1534.4, 1469.3, 1338.8, 1262.2 cm^{-1}.

Synthesis of polymers. The PU−FM and the control polymers were synthesized according to Scheme 1-1. Typically, the synthesis of PU−FM_{20} is as follows. Firstly, a precursor **8** was synthesized by the reaction of PCL and MDI (1:2) at 80 °C under nitrogen atmosphere for 2 h. The precursor **8** (13.50 g, 3.00 mmol), compound **4** (0.8960 g, 3.75 mmol) and hexamethylene diisocyanate trimer (tri-HDI) (0.2520 g, 0.50 mmol) were dissolved in anhydrous 1,4-dioxane (15 mL). The mixture was degassed under reduced pressure and then cast into Teflon molds. Polymerization reaction and evaporation of the solvent took place at 80 °C under nitrogen atmosphere for 96 h. The polymer was further dried under vacuum to obtain a pale yellow non-transparent solid. The samples of PU−BM_{20} and PU′−FM'_{20} were prepared through the similar procedures by using the following monomer molar ratios respectively: (1) [tri-HDI]:[compound **8**]:[1,4-benzenedimethanol (BM)]=8:48:60; (2) [compound **6**]:[compound **7**]:[compound **8**]=5:1:5. After demolding, all the polymers were kept in a desiccator to avoid moisture.

Table 1-S1. The component of PU−FM with different crosslinking index.

Sample	$PU-FM_{20}$	$PU-FM_{30}$	$PU-FM_{40}$	$PU-FM_{50}$
[tri-HDI] : [**8**] : [**4**]	8 : 48 : 60	12 : 42 : 60	16 : 36 : 60	20 : 30 : 60
ρ	20%	30%	40%	50%

The crosslinking index represents the content of crosslinkers. For PU-FM, the cross-linking index is defined as the molar ratio between isocyanate groups of tri-HDI and the total isocyanate groups. The crosslinking index ρ (for PU−FM) and ρ' (for PU′−FM′), are given as:

$$\rho = 100\% \frac{3N_{\text{tri-HDI}}}{2N_4} \qquad \rho' = 100\% \frac{4N_7}{2N_{\text{MDI}}} = 100\% \frac{4N_7}{2(2N_8)}$$

where $N_{\text{tri-HDI}}$, N_4 , N_7, N_{MDI} and N_8 are the mole number of tri-HDI, compound **4**, compound **7**, MDI, and compound **8** respectively. Note that: for PU′−FM′, (1) the mole number of hydroxyl groups which serve as cross-linkages is equal to $4N_7$; (2) according to the synthesis procedures, N_{MDI} is equal to $2N_8$.

For $PU-FM_{20}$, tri-HDI : compound 8 : compound 4 = 8 : 48 : 60, the DA bonds content is molar ratio of **compound 4**: 60/(8+48+60)=51.7%; for PU'-FM'20, Compound 6 : compound 7 : compound 8 = 5:1:5, the DA bonds content is **twice** molar ratio of compound 7 (compound 7 has **two** DA bonds): 1*2/(5+2+5)=16.6%.

1.2.5.5. Morphology characterization

Small-angle X-ray scattering (SAXS) experiments were performed at the beamline BL16B1 at Shanghai Synchrotron Radiation Facility (SSRF), China, using the third generation of synchrotron radiation light sources. The energy of the X-ray radiation was 10 keV and the wavelength of the radiation source is 0.124 nm. The scattering patterns were collected by a Mar165 CCD detector (Diamond Light Source, Oxfordshire, UK), which had a resolution of 2048×2048 pixels (pixel size=80×80 μm^2). The image acquisition time was 200 s and the sample-to-detector distance was

2030 mm. All the images were corrected for background scattering, air scattering and beam fluctuations. The two-dimensional data sets were azimuthally averaged to give intensity as a function of the magnitude of the scattering vector, q, where $q=4\pi\sin(\theta)/\lambda$ and 2θ is the scattering angle. The long period (d_{long}) was calculated with the Bragg equation: $d_{long}=2\pi/q_{max}$ (nm), in which q_{max} corresponds to the peak position in the scattering curves (i.e., $I(q)q^2$ vs. q). Sections for AFM were prepared by ultramicrotomy using a Leica UCT ultracryomicrotome and the AFM data were collected on a Nano Scope MultiMode IIIa AFM (Veeco Instruments, USA) in a tapping mode. 3D images in Figure 3 were collected with a VHX-1000C Digital Microscope (Keyence, Japan).

1.2.5.6. Mechanical Testing

The mechanical properties of PU−FM and the control polymers were measured using an Instron 5567 machine (USA) with a 500 mm min^{-1} strain rate at 25 °C. In order to clearly show the process of HIFU-triggered crack closure assisted healing of PU−FM and obtain a better healing efficiency, the test samples were tailored using a gauge dimension: 35 mm × 8 mm, thickness of 3.0-3.2 mm measured for each sample with a digital vernier caliper. Each measurement was repeated at least three times. Young's modulus was determined from the initial slope of the stress–strain curves.

1.2.5.7. HIFU-triggered Shape Memory Assisted Healing

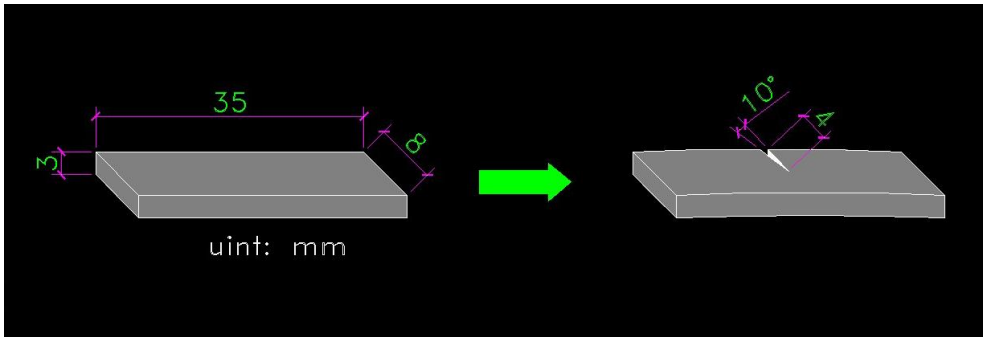

Figure 1-S2. Schematic illustration of the dimensions of the sample plates used for stress-strain experiments and of the damaged samples for HIFU-triggered shape memory assisted healing experiments.

As shown in Figure 1-S2, samples of PU−FM and the control polymers were cut and bent to obtain a crack with ~50% of the sheet width and an angle of ~10° between two cut scars. Using the HIFU apparatus setup shown in Figure 1-S1, the localized and directed control of shape memory assisted healing of the damaged samples were investigated by exposure of samples to the HIFU focus.

1.2.5.8. HIFU-triggered Dynamic Exchange Reactions of Low Molecular Weight Model Compounds

Ultrasound-responsive dynamic exchange reactions were carried out directly in screw-cap NMR tubes equipped into the HIFU apparatus. The ^{1}H NMR spectra were recorded on a Bruker 400 (400 MHz) spectrometer, and chemical shifts were recorded in parts per million (ppm) downfield from TMS using the residual protonated solvent as an internal standard (d_6-DMSO, ^{1}H 2.50 ppm). Equimolar amounts of furan-maleimide Diels-Alder adduct **4** and maleimide **9** were dissolved in 0.5 mL of d_6-DMSO in a screw-cap NMR tube to give a 0.1 mol L^{-1} solution. The top of the NMR tube was then wrapped tightly in Teflon tape. An initial ^{1}H NMR spectrum was obtained at 25 ℃ immediately after sample preparation and taken as time = 0 h. The second ^{1}H NMR spectrum was obtained after the sample had been kept at 25 °C for 120 h. The NMR tube was then exposed to the HIFU focal spot, and the third ^{1}H NMR spectrum was obtained after the sample exposing to HIFU treatment for 60 min.

1.2.5.9. Temperature-dependent FTIR Characterization of the Dynamic Polymers

The temperature-dependent absorbance FTIR spectra of PU−FM_{20} were recorded with a 4 cm^{-1} spectral resolution on a Nicolet-IS10 (Thermo Electron Co., USA) spectrometer by signal averaging 20 scans. Two pieces of microscope KBr windows, which have no absorption bands in the MIR region, were used to prepare a transmission cell. Variable-temperature spectra, controlled by a temperature control instrument including programmed heating cell and circulating water jacket cooling system, were collected between 30 and 150 °C with a heating rate of 5 °C min^{-1}.

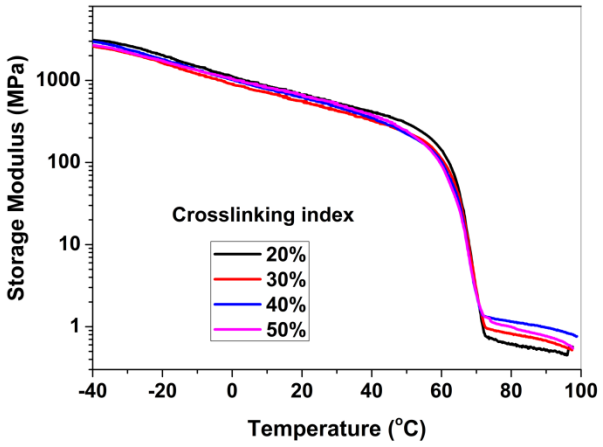

Figure 1-S3. Dynamic Mechanical Thermal Analysis (DMTA) traces of PU−FM. Experiments were conducted under N_2 at a heating rate of 3 °C min^{-1} and a frequency of 1 Hz.

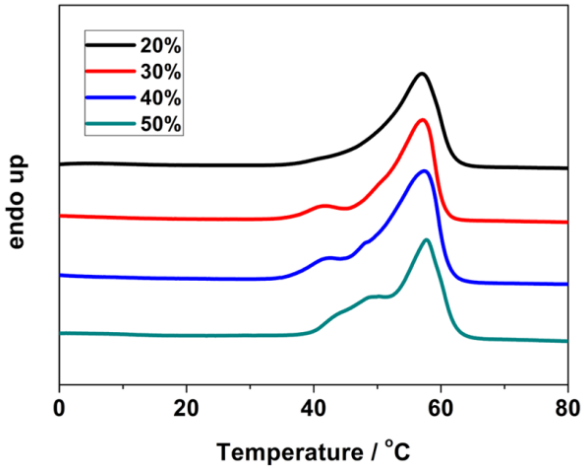

Figure 1-S4. Differential scanning calorimetry (DSC) traces of PU−FM, showing the T_m of PCL segments in PU−FM ranging from 57 to 60 ℃ . Experiments were conducted at a heating rate of 5 °C min^{-1} under nitrogen atmosphere.

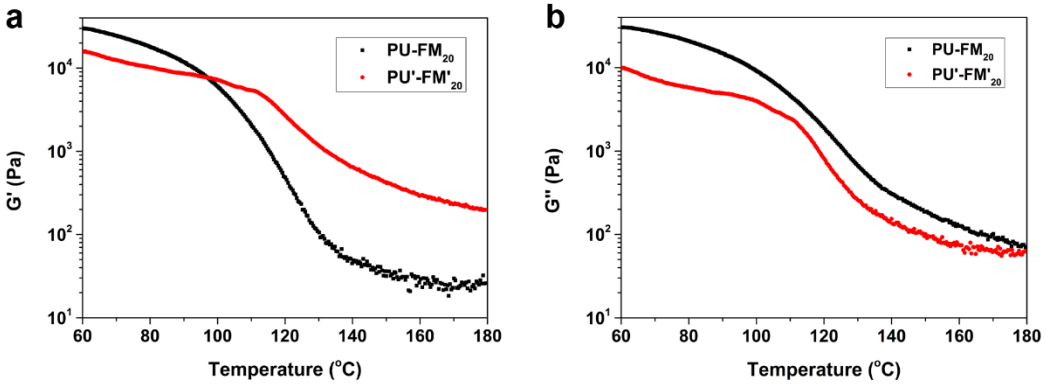

Figure 1-S5. (a) Elastic modulus (storage modulus G′) and (b) viscous modulus (loss modulus G″) versus temperature at a fixed frequency of 1 Hz.

1.2.5.10. ^{1}H and ^{13}C NMR spectra

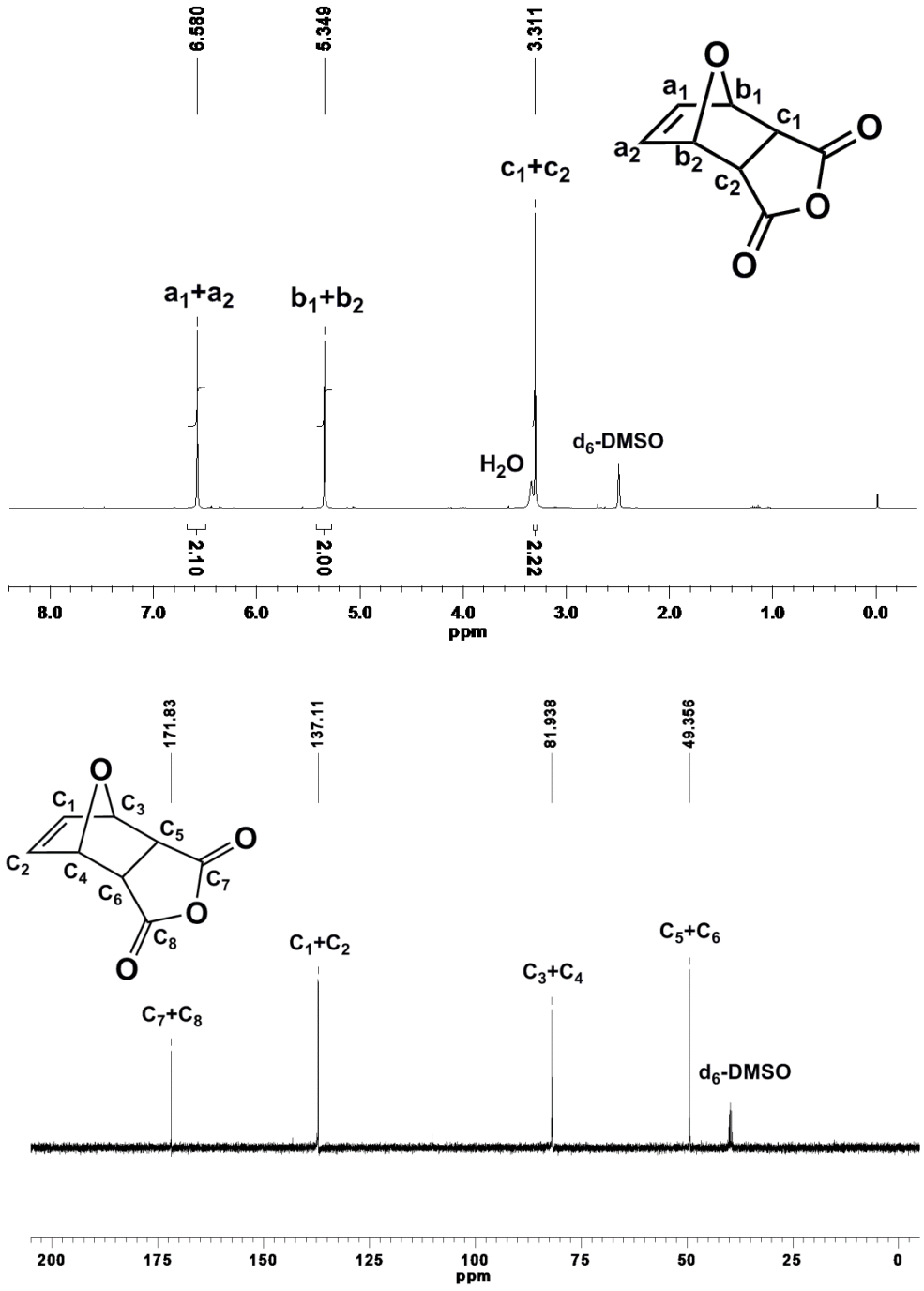

Figure 1-S6. ^{1}H (top) and ^{13}C (bottom) NMR spectra of 4,10-dioxatricyclo[5.2.1.$0^{2,6}$]dec-8-ene-3,5- dione.

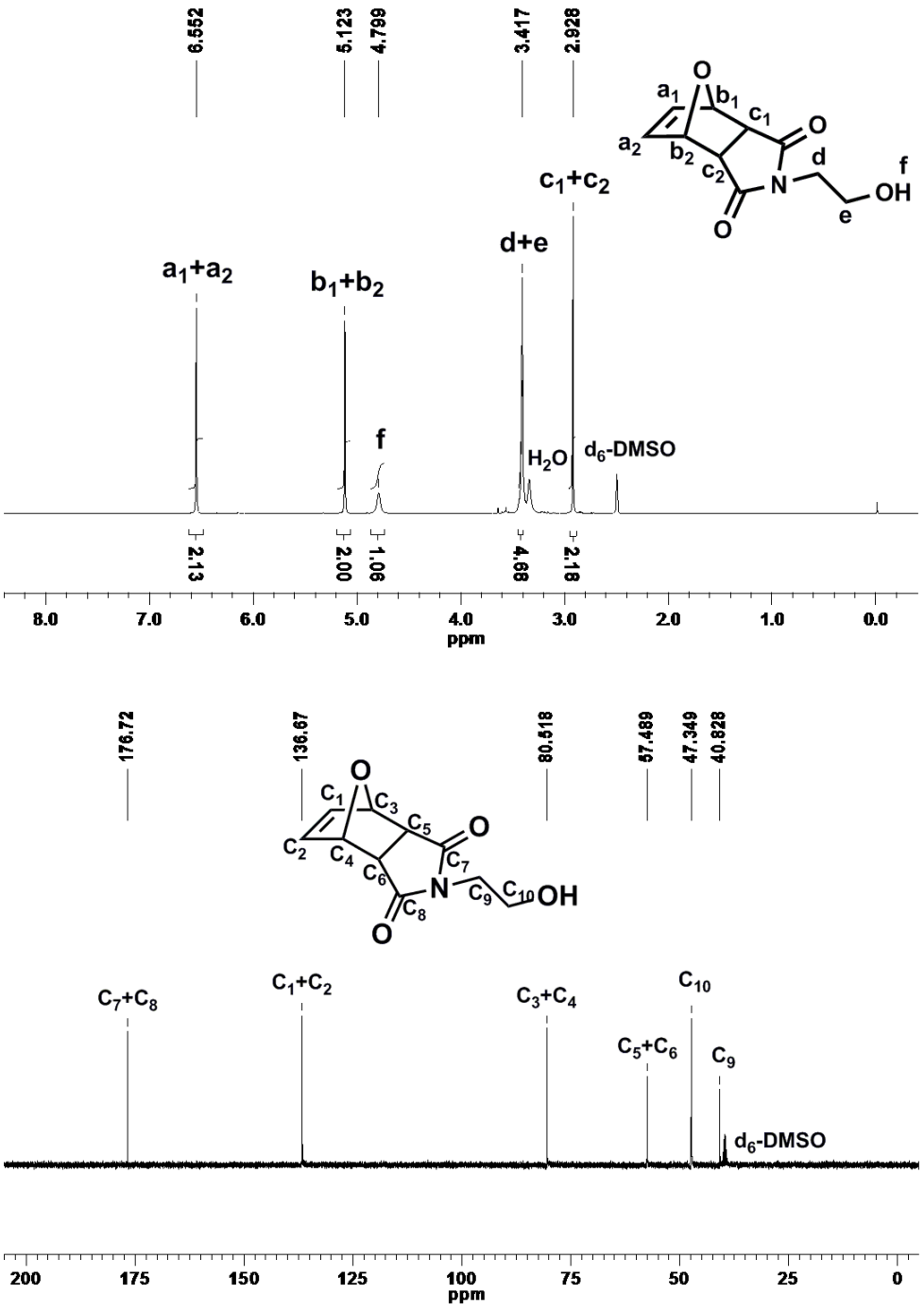

Figure 1-S7. ^{1}H (top) and ^{13}C (bottom) NMR spectra of 4-(2-hydroxyethyl)-10-oxa-4-azatricyclo [5.2.1.$0^{2,6}$]dec-8-ene-3,5-dione.

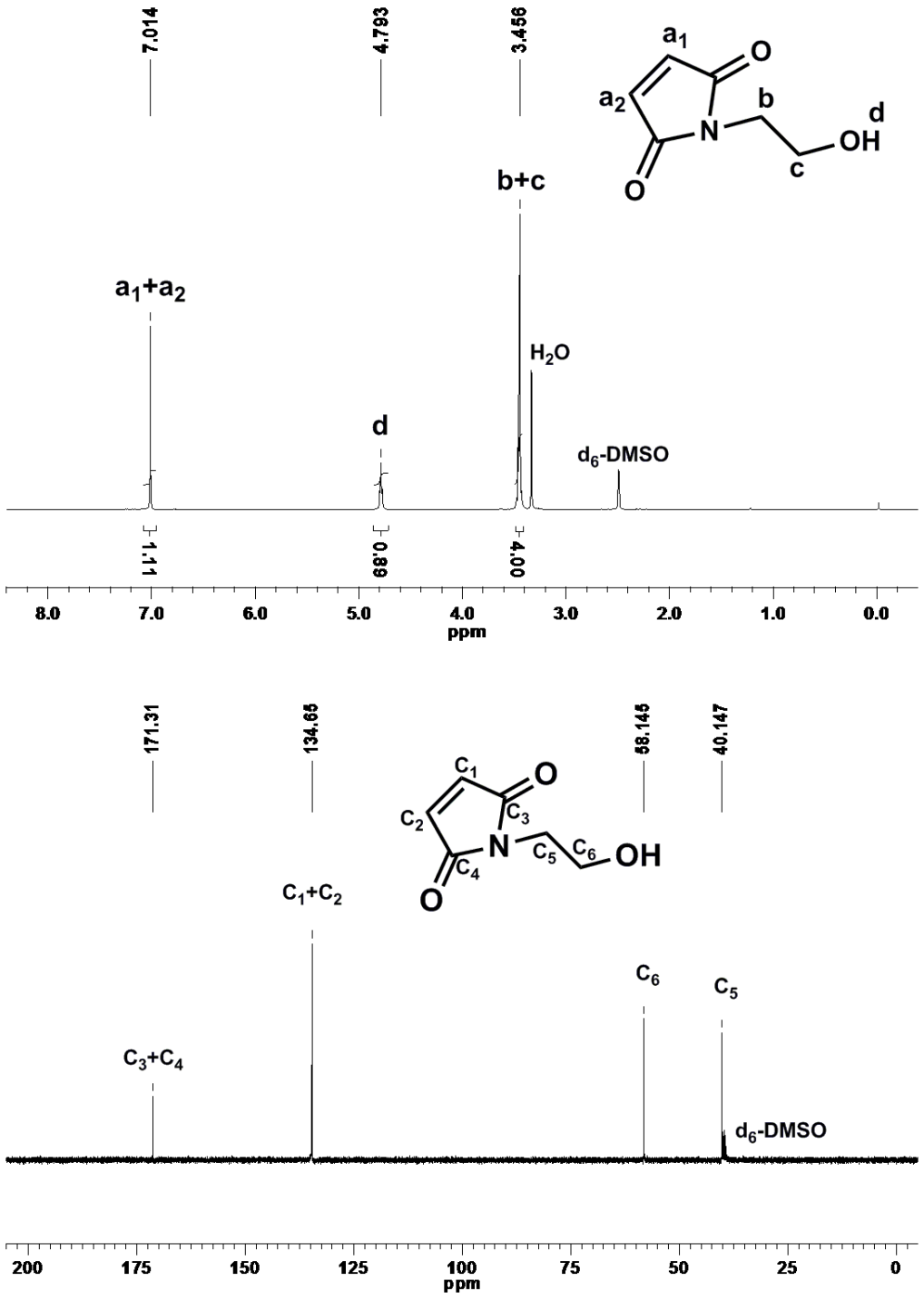

Figure 1-S8. ^{1}H (top) and ^{13}C (bottom) NMR spectra of 1-(2-hydroxyethyl)-1*H*-pyrrole-2,5-dione.

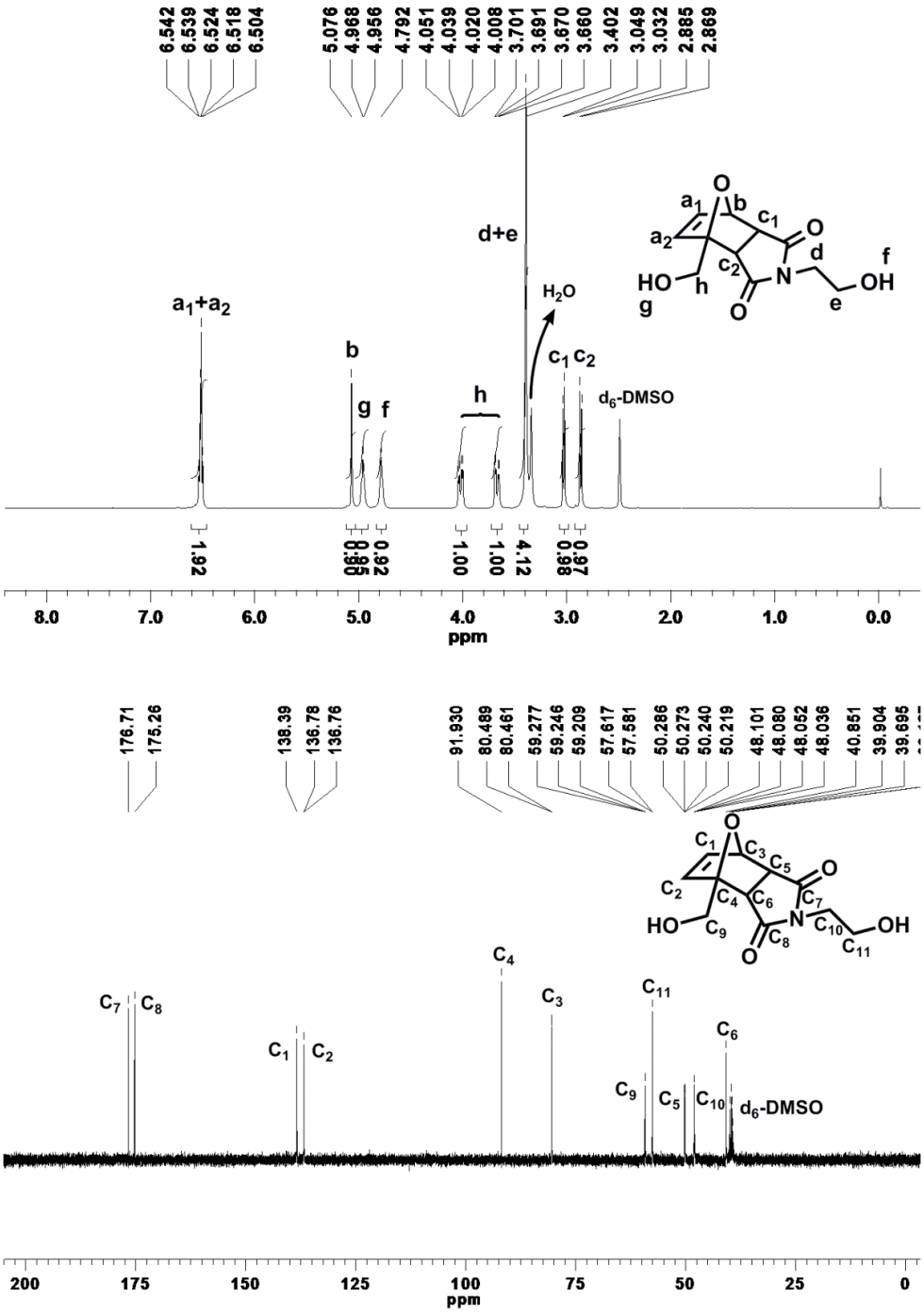

Figure 1-S9. ^{1}H (top) and ^{13}C (bottom) NMR spectra of 1-(hydroxymethyl)-10-oxatricyclo [5.2.1.$0^{2,6}$]dec-8-ene-3,5-dione-2-aminoethanol.

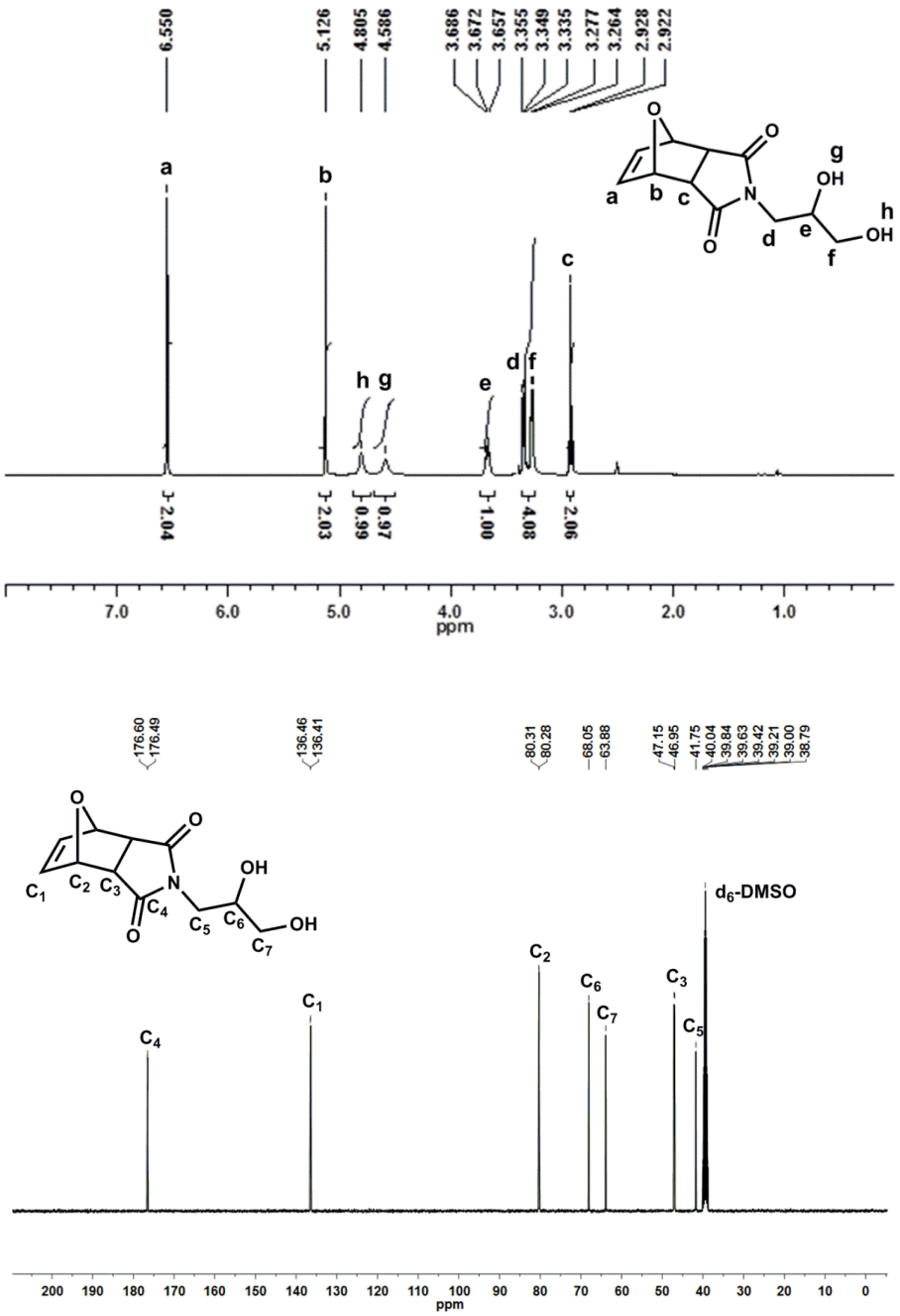

Figure 1-S10. ^{1}H (top) and ^{13}C (bottom) NMR spectra of N-(2,3-dihydroxy-propyl)-10-oxa-4- aza-tricyclo[5.2.1.$0^{2,6}$]-dec-8-ene-3,5-dione.

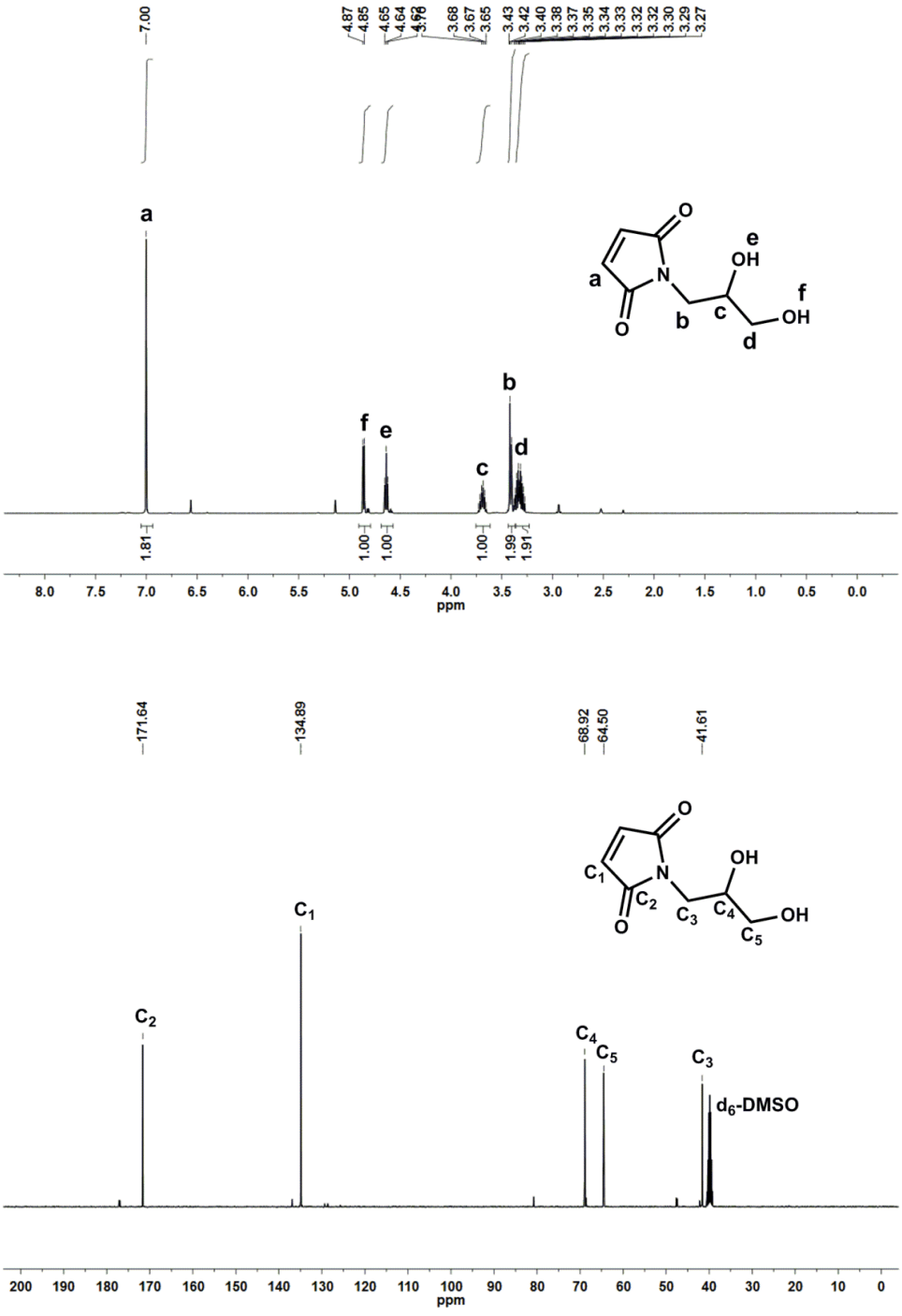

Figure 1-S11. ^{1}H (top) and ^{13}C (bottom) NMR spectra of N-(2,3-dihydroxypropyl)maleimide.

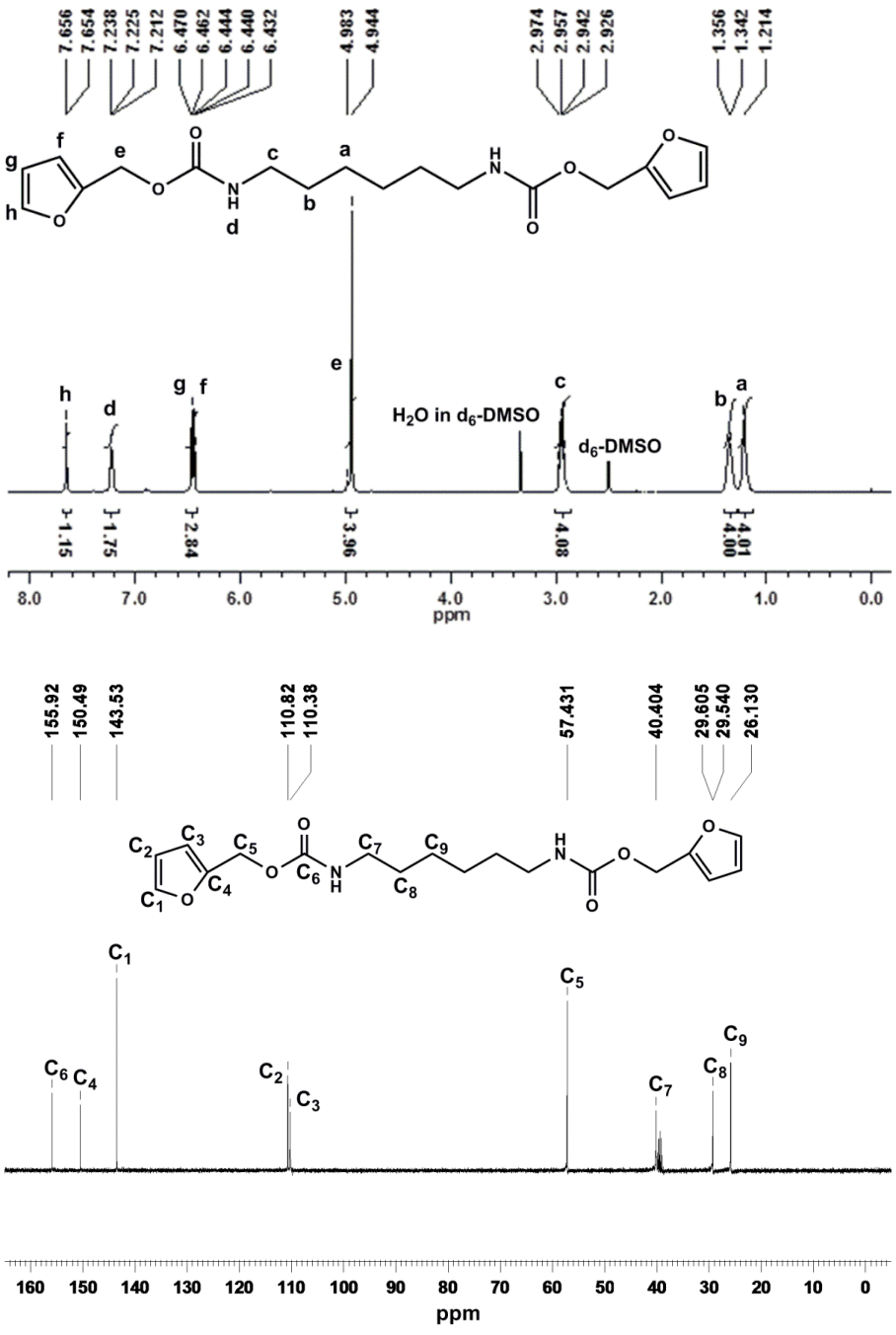

Figure 1-S12. ^{1}H (top) and ^{13}C (bottom) NMR spectra of 1,6-hexamethylene-bis (2-furanylmethylcarbamate).

1.2.5.11. Supporting Movie Legend

Movie 1-S1 records the process of HIFU-triggered shape memory assisted healing of PU−FM. The damaged samples were prepared as shown in Figure 1-S2 and then exposed to the HIFU focal spot for a period of time under a given HIFU power output.

Movie 1-S2 shows the experiment for HIFU-triggered reshuffling or dynamic exchange reaction of the low molecular weight DA model compounds.

References

1 Heath, W. H.; Palmieri, F.; Adams, J. R.; Long, B. K.; Chute, J.; Holcombe, T. W.; Zieren, S.; Truitt, M. J.; White, J. L.; Willson, C. G. *Macromolecules*, 2008, **41**, 719.

2 Gaina, V.; Gaina, C. *Polym. -Plas. Technol. and Eng.*, 2002, **41**, 523.

1.3. Summary of the Project

In this project, we have proposed a novel concept for HIFU-triggered shape memory assisted self-healing of polymers for the first time. The shape memory actions triggered by HIFU can close the crack, which provides the prerequisite for the bond formation between the damage surfaces during the healing process. HIFU triggering retro-DA reactions and DA reshuffling reactions is the main reason for the effective healing of covalently cross-linked dynamic polymers. In contrast to previous self-healing polymers, our covalently cross-linked dynamic polymer system simultaneously integrates very good mechanical properties, ultrasound responsiveness, excellent shape memory (shape fixity ratio and shape recovery ratio both close to 99%) and self-healing ability (self-healing efficiency ~92%) into one structure via a precise molecular architectures design. The localized, on-demand repair can be easily achieved by HIFU via depositing the acoustic energy only in the damaged area with pinpoint accuracy and minimum side effects in a remote and controlled way. This approach, i.e., HIFU-triggered shape memory assisted self-healing of polymers based on reversible Diels-Alder reaction, can be extended to a wide range of other dynamic materials.

CHAPITRE 2. TUNABLE PHOTOCONTROLLED MOTIONS USING STORED STRAIN ENERGY IN MALLEABLE AZOBENZENE LIQUID CRYSTALLINE POLYMER ACTUATORS

2.1. About the Project

Light-driven polymer actuators have gained much interest in recent years. Most successful materials are azobenzene-based liquid crystal elastomers (LCEs) or networks (LCNs). In those materials, the reversible *trans-cis* photoisomerization of the chromophore combines the cooperative motion of liquid crystal molecules to generate reversible deformation or motion of the polymers. Although it works well in many cases as reported in the literature, how to convert a change in molecular geometry (e.g., azobenzene after photoisomerization) into an efficient macroscopic motion remains challenging. Any light-driven motion requires a photoinduced mechanical force. This force in azobenzene LCEs or LCNs is small, partly due to the very low achievable efficiency of the optical to mechanical energy conversion. Therefore, the photoinduced force arising from direct optical to mechanical energy conversion may not be strong enough to allow robust (fast and continuous) motion of large-size polymer actuators, which needs large forces. In the present work, we show that by pre-storing mechanical strain energy in reprocessable azobenzene LCN films, unprecedented contraction force can be generated by UV light irradiation as a result of the phototriggered release of the stored energy in addition to the direct optical to mechanical energy conversion stemming from the trans-cis photoisomerization of azobenzene. The strong mechanical force enables motions of large-size polymer actuators in the form of wheels or spring-like “motors” that can be either pushed forward or pulled backward by the actinic UV light, with tunable rolling speed determined by the amount of pre-stored strain energy in the ALCE. This approach to amplifying the photoinduced mechanical force is general for azobenzene-containing liquid crystal elastomers or networks and should help their exploitation for applications.

This work was published in *Advanced Materials,* **2017**, 29, 1606467 by Xili Lu, Shengwei Guo, Xia Tong, Hesheng Xia and Yue Zhao. This research work was conducted in the Université de Sherbrooke under the supervision of Prof. Zhao and co-supervision of Prof. Xia. I prepared all the polymer samples and performed the experiments described in this publication. Shengwei Guo assisted me with some experiments for light-driven motions and Xia Tong assisted me with some characterizations. I wrote the first draft of the manuscript. Prof. Zhao finalized the manuscript with revision contributions from Prof. Xia.

2.2. Paper Published in Advanced Materials, 2017, 29, 1606467.

Tunable Photocontrolled Motions Using Stored Strain Energy in Malleable Azobenzene Liquid Crystalline Polymer Actuators

Xili Lu[a,b], Shengwei Guo[b,c], Xia Tong[b], Hesheng Xia[*a] and Yue Zhao[*b]

[a]State Key Laboratory of Polymer Materials Engineering, Polymer Research Institute, Sichuan University, Chengdu 610065, China. E-mail: xiahs@scu.edu.cn

[b]Département de chimie, Université de Sherbrooke, Sherbrooke, Québec, J1K 2R1, Canada. Email: yue.zhao@usherbrooke.ca.

[c]School of Material Science & Engineering, Beifang University of Nationalities, Yinchuan 750021, China.

Keywords: photocontrolled motion, polymer actuators, azobenzene, liquid crystal polymers, reprocessable polymer networks

2.2.1. Abstract

A new strategy for enhancing the photoinduced mechanical force is demonstrated using a reprocessable azobenzene-containing liquid crystalline network (LCN). The basic idea is to store mechanical strain energy in the polymer beforehand so that UV light can then be used to generate a mechanical force not only from the direct light to mechanical energy conversion upon the *trans–cis* photoisomerization of azobenzene mesogens but also from the light-triggered release of the prestored strain energy. It is shown that the two mechanisms can add up to result in unprecedented photoindued mechanical force. Together with the malleability of the polymer stemming from the use of dynamic covalent bonds for chain crosslinking, large-size polymer photoactuators in the form of wheels or spring-like "motors" can be constructed, and, by adjusting the amount of prestored strain energy in the polymer, a variety of robust, light-driven motions with tunable rolling or moving direction and speed can be achieved. The approach of prestoring a controllable amount of strain energy to obtain a strong and tunable photoinduced mechanical force in azobenzene LCN can be further explored for applications of light-driven polymer actuators.

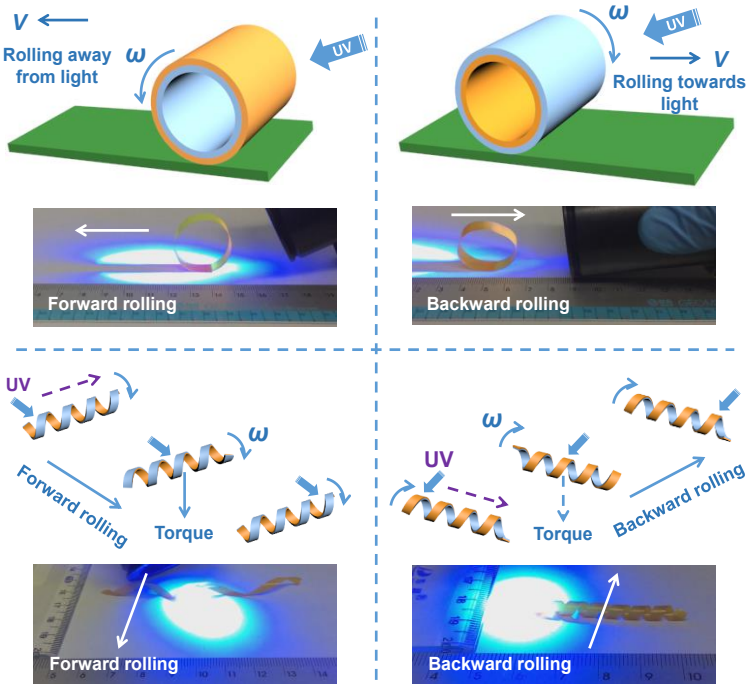

2.2.2. Introduction

In biological systems, sensing environmental changes and converting environmental stimuli (e.g., humidity, light or touch) into motions is an essential function for many living organisms, such as hygroscopic seed dispersal,[1] tendril curling of climbing plants[2] and trap closure of carnivorous plants.[3] These nastic plant motions, which are mainly derived from the well-defined hierarchically ordered architectures and their interactions with the environment,[4] have been a source of inspiration for materials scientists to design and fabricate stimuli-movable or deformable materials for envisioned applications in a wide range of areas such as motors,[5] artificial muscles,[6] soft robots,[7] photocontrolled fluid slugs,[8] oscillations,[9] energy generators[10] and reconfigurable devices.[11] Among those biomimetic smart materials, liquid crystalline elastomers (LCEs)[11,12] have been attracting broad and growing interest in recent years because of their versatility in creating material motions, such as bending,[13] rolling,[5a,14] walking,[15] swimming,[7a,16] oscillating,[9] twisting[17] and push–pull shuttling motions.[17] Particularly, LCEs incorporating azobenzene mesogens (hereafter referred to as ALCEs) capable of reversible trans-cis photoisomerization represent arguably the most promising candidate for realizing envisioned practical applications. On the other hand, to address the issue of processability of crosslinked polymers, exchangeable bonds[18] that can undergo fast breaking and reforming without changing the total number of bonds upon changes in environmental conditions have been applied to LCEs[6a,19] and ALCEs[20] to impart them with reversible or dynamic crosslinking and thus to afford reprocessability, reshaping and reconfiguration of the materials.

However, stimuli-responsive LCE- or ALCE-based actuators that are able to exhibit robust, self-propelling (continuous), macroscopic motions with tunable moving speed and controllable moving direction remain to be a challenge and largely unexplored; and rational material design and processing methodology need to be developed to improve the performance of light-driven actuators. In this project, we demonstrate a strategy to address the challenge using photoresponsive malleable ALCE actuators, in the form of wheels and spring-like “motors”. Our assumption is that the light-driven motion or deformation speed of an actuator would be mainly determined by the magnitude of the photoinduced stress,

while the moving direction and mode have an important relationship with the three-dimensional (3D) architecture of the actuator. We show that the photoinduced stress in ALCEs can be greatly amplified by storing strain energy in highly stretched ALCE films, and that the motion speed can be tuned by adjusting the stored energy. As for the motion direction (pulled towards or pushed away from the actinic light), it can be controlled by properly designed architectures of the actuator. Moreover, we show a light-driven vehicle configured with a spring-like "motor" as one example of envisioned applications.

2.2.3. Results and Discussion

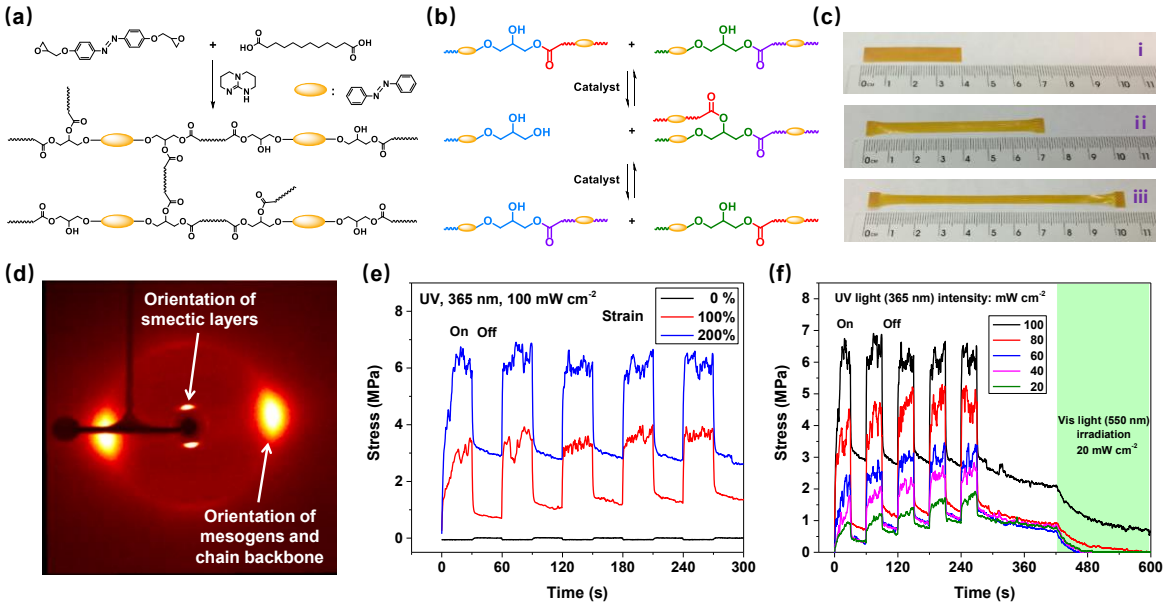

Figure 2-1. (a) Synthesis route to the azobenzene liquid-crystalline elastomer. (b) Schematic illustration of the reversible transesterification reaction. (c) Photographs of the (i) unstretched film (40 mm×6 mm×25 μm) and the stretched films with 100% (ii) and 200% (iii) strain. (d) Wide-angle X-ray scattering image of a stretched ALCE film (200% strain). (e) Actuation stress as a function of time as UV light (365 nm, 100 mW cm^{-2}) is periodically turned on (time, 30 s) and off (time, 30 s) on the film. (f) Actuation stress as a function of time as UV light is periodically turned on (time, 30 s) and off (time, 30 s) on the film (200% strain) for different UV light intensities. The subsequent visible light (550 nm, 20 mW cm^{-2}) irradiation time period is indicated.

The cross-linked liquid crystalline polymer network was synthesized through the reaction between 4,4'-diglycidyloxy-azobenzene and dodecanedioic acid (1:1) using a method reported in the literature[6a,18,19] (**Figure 2-1**a; and Figure 2-S1, Supporting Information). At high temperatures, the catalytic transesterification reaction takes place and allows for rearrangements of the epoxy-acid derived network without modification of the numbers of links and average functionality, thus affording malleable and easy processing properties (Figure 2-1b). On heating, the polymer displays a glass transition temperature (T_g) at ~55 ℃ and a smectic-isotropic phase transition (T_{si}) at ~122 ℃ (Figure 2-S2, Supporting Information). Thin film can easily be obtained by hot-compressing the polymer granules at 180 ℃, followed by cooling to room temperature (Figure 2-S3, Supporting Information); then the film can be stretched at a temperature (100 °C for this study) between T_g and T_{si} (Figure 2-S4, Supporting Information), i.e., in the liquid crystal (LC) state, to different strains (Figure 2-1c). According to the wide-angle X-ray scattering (WAXS) measurements carried out on a stretched film (200% strain), the stretching leads to the formation of monodomain structure with azobenzene mesogens and chain backbones oriented along the strain direction (Figure 2-1d; Figure 2-S5, Supporting Information). It is seen that the smectic order remains in the stretched film, with the normal of the smectic layers aligned along the strain direction. To prove the point that the amount of stored strain energy and thus the photo-deliverable force can be controlled by the stretching, we carried out the isostrain measurements at room temperature for the unstretched and stretched films (100% and 200% strains). By applying UV light (365 nm) to a stripe-shaped sample (20 mm×3.5 mm×13 μm, cut from the films in Figure 2-1c) held under constant strain in the sample holder of a tensile tester (Instron 5965, experimental setup in Figure 2-S6, Supporting Information), any contractile force generated in the film can be sensed and measured. As can be seen from the results (Figure 2-1e), upon exposure to the UV light, while almost no stress was generated in the unstretched film, the stretched film generated a large stress that increases with the strain, reaching ~4 MPa for the film at 100% strain and close to 7 MPa for the film at 200% strain, which is much higher than the photoinduced forces usually found in ALCEs.[21] On turning off the UV light, the force dropped, but not to the original level, as a significant amount of force remained at the UV-off state. The cycle of force up and down under UV light on and off, respectively, can be repeated for

many times. On the other hand, as expected, higher UV light intensity can also generate larger contraction force for a given strain of the film (Figure 2-1f). In the latter experiments, after 5 cycles of UV light on and off, the remaining force decreased slightly over time. However, upon exposure of visible light (550 nm, 20 mW cm^{-2}), the force started to drop again to approach zero.

On the basis of the above results from the isostrain light-generated contraction force measurements, the following points can be made. (1) The films with different strains mainly differ in the orientation degree of the azobenzene mesogens and chain backbone along the stretching direction. The fact that a larger film strain results in a greater force suggests that polymer chain relaxation induced by UV light irradiation had a major contribution. This is similar to stretched conventional shape memory polymer (SMP) under the isostrain test and exposure to light for photothermal effect induced heating above T_g or melting temperature T_m of the polymer.[22] (2) The fact that after turning off the UV light, the contraction force drops only partly (Figure 2-1e, f), and the remaining force further diminishes only upon visible light irradiation (Figure 2-1f) implies that the photoinduced contraction force originates from both *trans-cis* photoisomerization of azobenzene mesogens and a photothermal effect. This is possible given that ALCE films were obtained by stretching at a high temperature $T_{stretching}$ ($T_g<T_{stretching}<T_{si}$) and the extensional states of polymer chains and networks were fixed by both the oriented azobenzene mesogens in the smectic phase and T_g upon cooling to room temperature. On exposure to UV light, the azobenzene mesogens use part of the absorbed optical energy to undergo the *trans–cis* photoisomerization and the resulting order-disorder phase transition and meanwhile convert the other part of optical energy into heat to provide chain mobility. In such a case, it can be pictured that under UV irradiation of the stretched film, a combination of the order-disorder phase transition arising from the *trans-cis* photoisomerization of azobenzene mesogens with a heating effect, which could bring the polymer above T_g, will allow polymer chain backbone to relax, while under the isostrain state the stopped chain relaxation is translated into the measured contraction force. We will argue further on in the paper that unlike normal SMPs, at least a significant part of the photoinduced stress in

ALCE is recoverable after turning off the UV light, which accounts for the light-driven, continuous motion of large-size 3D rolling structures to be shown below.

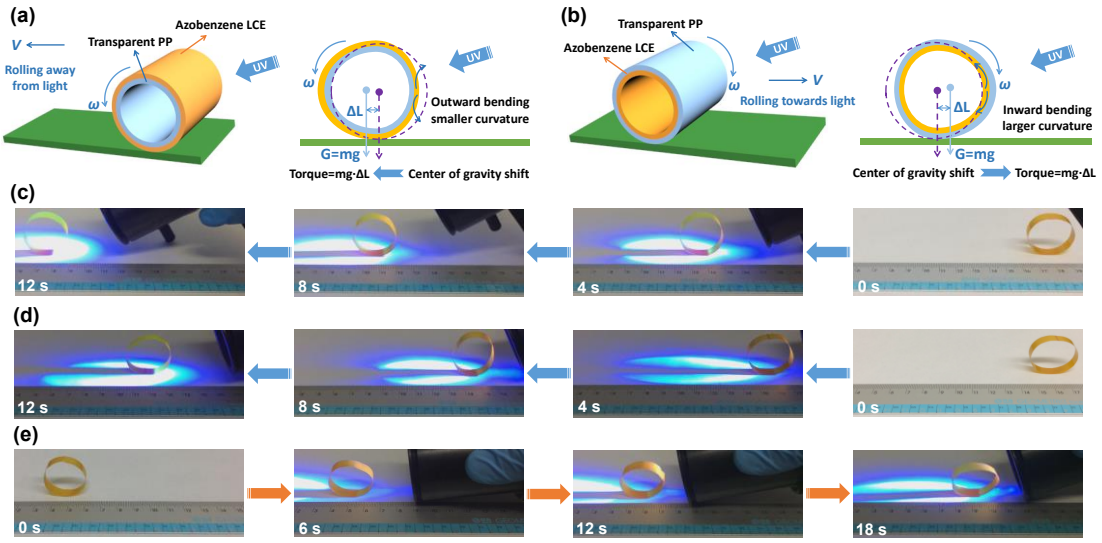

Figure 2-2. Schematic showing (a) leftward and (b) rightward shift of the center of gravity in the wheel due to the UV-light-induced asymmetric deformation. The induced torque drives the wheel (a) rolling away from or (b) rolling towards the light source. Photograph series showing continuous light-driven forward-rolling or backward-rolling of different wheels: the wheels in (c) and (d) were fabricated with ALCE films stretched to 200% and 100% strain, respectively, and set as the outer layer, while the wheel in (e) was assembled with a ALCE film (200% strain) as the inner layer.

Knowing that the strain energy stored in our stretched ALCE films can amplify photoinduced contraction force and that this force can be tuned by adjusting the film strain degree, we expected that actuators fabricated by using a stretched ALCE film could display light-driven motion at the macroscopic scale with an enhanced photocontrol. A number of experiments have been realized in order to demonstrate this feature. Unless otherwise stated, all actuators or devices were fabricated using stretched ALCE films with a thickness of ~20 μm and driven by UV light with intensity of 100 mW cm^{-2}. It is known that on exposure to UV light most incident photons (up to 99%) are absorbed within 1 μm of the surface layer due to the high extinction coefficient of azobenzene moieties (about 2.0×10^4 L mol^{-1} cm^{-1} at 365 nm).[21] Therefore, change in orientation of the azobenzene mesogens

induced by the *trans–cis* photoisomerization and the photothermal effect should take place only in the film surface region. As a result, an uneven distribution of the anisotropic deformation is formed and the bending motion can be achieved in the film. Such UV-induced bending and visible light-induced unbending was indeed observed (in the form of closing and blooming of an ALCE flower, Figure 2-S7, Movie 2-S1, Supporting Information).

With elongated ALCE films in hand, light-driving wheels that could undergo fast and continuous motions with tunable rolling speed and controllable rolling direction were fabricated. To this end, ALCE film was stretched to either 100% or 200% strain before being laminated with a flexible transparent polypropylene film (biaxially oriented polypropylene, hereafter referred to as BOPP, ~45 μm in thickness, commercial transparent scotch-tape). From the bilayer film, a rectangular stripe (85 mm × 8.5 mm) was cut and then rolled around a glass tube (πd_1=85 mm, d_1=27.07 mm) and end-to-end joined to form a wheel at 65 ℃ followed by cooling to fix the closed tubular shape, with the ALCE film either as the inner or outer layer. The comparisons in **Figure 2-2** were made under the same UV irradiation conditions and with wheels of similar size (prepared by rolling the films around a same glass tube). As schematized (Figure 2-2a), upon UV light irradiation, the non-uniform bending of the ALCE outer layer causes the curvature of the bilayer to decrease on the light-facing side, that is, the right side receiving illumination has the tendency to flatten while the unexposed left side remains unchanged. This asymmetric deformation causes a shift of the center of mass to the left side, which results in a torque that drives the wheel rolling away from the light beam on a flat surface (Figure 2-2c; Movie 2-S2, Supporting Information). Because the UV light induced contraction (photoisomerization of the azobenzene moieties) only occurs in the surface region of the ALCE film, a recoverable stress leading to an expansion force, with the help of the elastic deformation of the BOPP layer, may allow the bilayer to recover the initial curvature when the deformed part rolls and departs from the light beam. Therefore, the light-driven rolling is cycled under the continuous light irradiation. To demonstrate the control of the rolling speed, the wheels in Figure 2-2c,d were fabricated with ALCE films stretched to 200% and 100% strain respectively, and set as the outer layer facing directly the UV light beam

coming from the right side. Indeed, under the same UV irradiation intensity, the wheel with more strain energy stored in the film and thus greater light-induced contraction force, rolls at a faster speed (about 1 cm s^{-1}, calculation from Movie 2-S2, Supporting Information) than the wheel with the less stretched film (about 0.33 cm s^{-1}, calculation from Movie 2-S3, Supporting Information). Besides, the rolling speed can be adjusted by changing other parameters such as the light intensity and the radius of the wheel motor (wheels with smaller diameter of 16.68 mm, Movie 2-S5, Supporting Information: forward rolling at ~0.13 cm s^{-1}; Movie 2-S6, Supporting Information: backward rolling at ~0.14 cm s^{-1}).

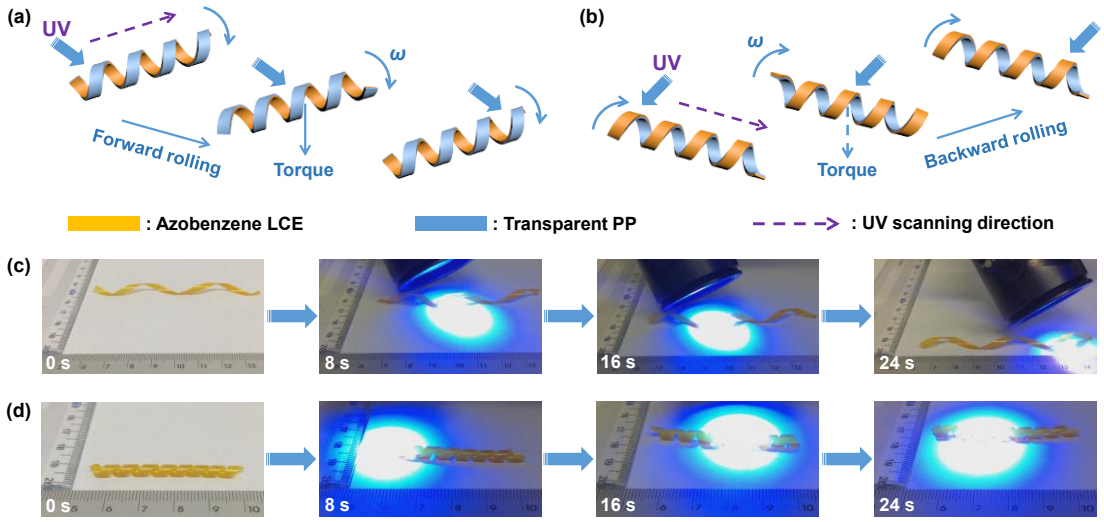

Figure 2-3. Schematic showing (a) light-pushing-forward rolling and (b) light-pulling-backward rolling of the helical ribbons due to UV-light-induced torque. Photograph series as showing light-driven (c) forward-rolling and (d) backward-rolling motions of spring-like "motors": the helical ribbons in (c) and (d) were fabricated with ALCE films set as the inner layer and the outer layer respectively.

To reverse the wheel rolling direction, i. e., towards the light beam, the stretched ALCE film only needs to be set as the inner layer. In this case (Figure 2-2b), upon receiving the UV light passed through the BOPP outer layer, the bending of the inner ALCE layer can no longer flatten the outer layer but bend further the bilayer to increase the curvature instead, while the left part of the wheel remains unchanged. This asymmetric deformation causes a shift of the wheel's center of mass to the right side, thereby resulting in a torque

that drives the wheel rolling towards the light at a speed of ~0.23 cm s^{-1} (Figure 2-2e, calculation from Movie 2-S4, Supporting Information). The results in Figure 2-2 demonstrates that the wheel rolling speed can be controlled by the amount of strain energy stored in the ALCE film, which can be adjusted by the ALEC film strain. Moreover, the wheel rolling direction, either away from or towards the excitation light beam, can readily be controlled by setting the ALCE film as the inner or the outer layer of the bilayer wheel, respectively.

The robust light-driven motion can also be realized using stretched bilayer film in the form of a spring. The spring was readily fabricated by twisting the film (around a cylindrical metal rod) into either left-handed or right-handed helical ribbon at 65 ℃ followed by cooling to fix the helical shape. Likewise, the ALCE could be set as either the inward or outward layer of the spring. The orientation of the polymer chain backbone and azobenzene mesogens follows the helical path. First, we mention that the deformation or motion behavior of the spring under UV light irradiation was found to be determined by the location of the ALCE film (inward or outward) but not related to the handedness of the helical spring (Movie 2-S7~S9, Supporting Information). When UV light was applied to the top of the spring (vertical irradiation), the spring-like ribbon with inward ALCE layer underwent a rapid winding transformation (Movie 2-S10, Supporting Information), while the spring with outward ALCE layer displayed a rapid unwinding motion (Movie 2-S11, Supporting Information). In both cases, upon removal of the vertical UV light, the photoinduced motion was reversed to recover the original helical state. Furthermore, UV light could be applied through an oblique angle to manipulate the motion of the spring-like structure. As shown in **Figure 2-3**, both light-pushing-forward rolling and light-pulling-backward rolling of the spring were achieved. On one hand, with the stretched ALCE film as the inward layer, scanning the UV light from the left end to the right end along the axis of the spring resulted in its forward rolling (Figure 2-3a,c; Movie 2-S7, Supporting Information). By contrast, with the ALCE film as the outward layer, the UV light scanning along the helical axis gave rise to backward rolling of the spring. A possible interpretation is proposed as follows (Figure 2-3b,d; Movie 2-S8, Supporting Information). For the spring with inward ALCE layer (Figure 2-3a), with the UV light spot moving continuously along

the axis of the spring at an oblique angle, the illuminated area of the ALCE ribbon executes a rapid winding motion, which is followed by an unwinding motion as the UV light leaves the area. Somehow, the winding (helix-tightening) to unwinding (helix-loosening) transition generates a torque leading to forward rolling. Since different parts of the spring are subjected to the same winding-unwinding motion successively, an apparent continuous rolling motion is obtained. In the case of the spring with outward ALCE layer (Figure 2-3b), the opposite unwinding to winding transition is induced by the UV light; and the resulting torque appears to act in the opposite direction too, resulting in light-pulling backward rolling. Same as the wheels (Figure 2-2), the stretched ALCE film with stored energy is key to the light-driven motion. Furthermore, as demonstrated in Figure 2-4, the rolling of the helical ribbon can deliver a motoring force. By linking the two ends of a helical ribbon with two wheels made with polyurethane foam, the light-driven forward rolling results in rotation of the two wheels (Movie 2-S12, Supporting Information).

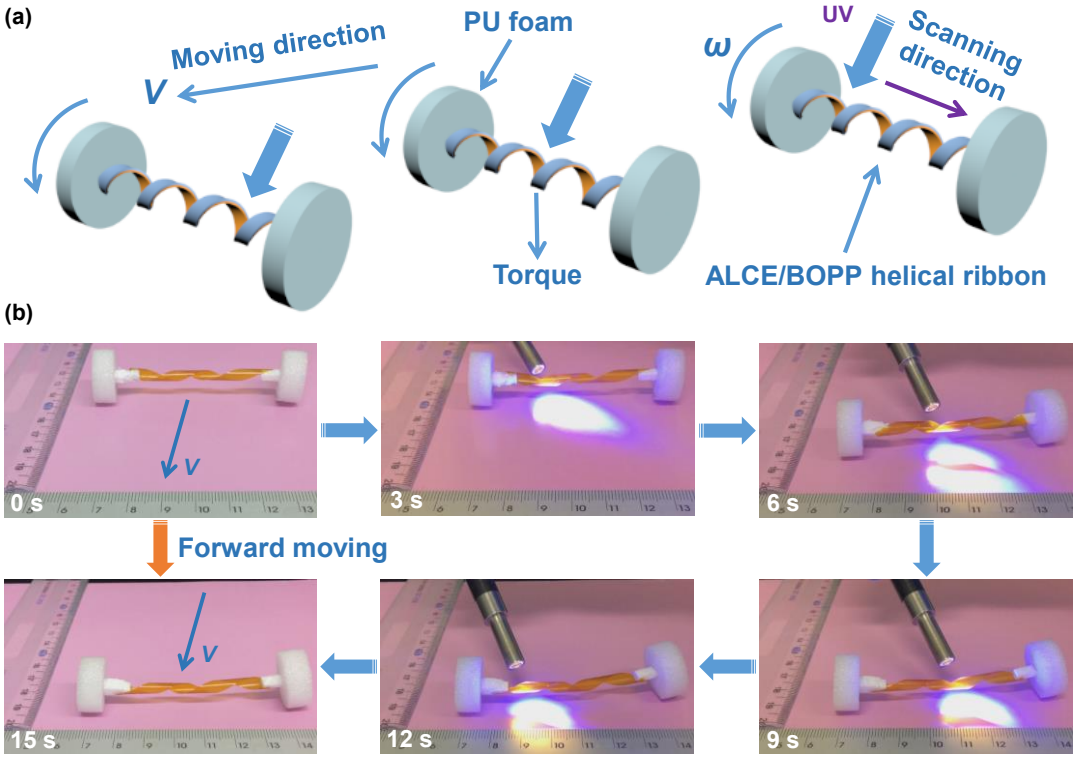

Figure 2-4. (a) Schematic and (b) photograph series showing light-driven forward moving of a "vehicle" configured with a spring-like "motor".

The wheel in Figure 2-2c was used to test how far the light-driven motion could go. Even after 100 rotations, the wheel showed no sign of decreased speed or sensitivity. This continuous rolling, together with the winding/unwinding (or vice versa) motion of the helical ribbons under on/off of vertical UV light exposure, implies that the photoisomerization and photothermal effect in this ALCE could work synergistically to provide stability for stored strain energy and produce recoverable stress. In normal SMPs, thermally- or photothermally-induced stress comes from chain relaxation releasing entropy elastic strain energy, and once released, the stress cannot be recovered without reprogramming the temporary shape. In elongated ALCE films, aligned azobenzene mesogens are part of stretched chain backbone and form smectic layers that can act as physical crosslinks interconnecting flexible chain segments. Upon UV irradiation, the *trans*-*cis* photoisomerization of azobenzene, from rod-like trans to bent cis isomer, not only induces an order-to-disorder transition but also disassembles the crosslinks, which leads to chain relaxation. In the LC phase, if a complete reconversion from *cis* to *trans* isomer occurs, azobenzene moieties on chain backbone can be realigned and smectic layer crosslinks restored, resulting in stretching of flexible chain segments and recover of the stress. Under UV irradiation, the inevitable photothermal effect helps chain relaxation, but can also thermally activate the reverse *cis*-*trans* isomerization. Consequently, with UV light turned off or removed from the sample, a significant content of *trans* azobenzene could be formed, which restores partly the order and recovers part of the stress. In the isostrain experiment, such a recovery of stress means a drop of the contraction force. The results of contraction force measurement in Figure 2-1 indicate that the stress recovery in ALCE is possible but not complete. This is understandable because a significant portion of *cis* azobenzene remain. Only with subsequent *cis*-*trans* photoisomerization under visible light irradiation, aligned structure can be further rebuilt leading to more stress recovery, as revealed by a further decrease of the contraction force (Figure 2-1f). At the highest UV intensity used (100 mW/cm^2), the visible light irradiation could not erase completely the contraction force. This residual force is likely indication of an irrecoverable stress in the sample, which should be no surprise, because greater photothermal effect under higher UV intensity could inflict some irreversible chain relaxation or restructuring in the material. However, to enable photocontrolled motion or rolling of 3D objects using pre-stored strain

energy, even part of photoinduced stress is irrecoverable, the recoverable force could still do the work. For light-driven continuous motion, it is desirable to minimize the irrecoverable stress, which is an important issue to address in future research.

Before concluding, we wish to briefly explain what distinguishes or differentiates the present study from some related works. First, Ikeda's group already reported a study on photoinduced motions of an azobenzene-containing LCE with dynamic crosslinks using transesterification reaction.[20a] While their LCE has azobenzene moieties as side-chain crosslinkers, our ALCE has an epoxy-acid derived rearrangeable network with azobenzene moieties positioned in the chain backbone to achieve large contraction force upon photoinduced release of stored strain energy. Secondly, White and coworkers studied a glassy, amorphous, azobenzene-functionalized polyimide, and reported the finding that pre-strain of the material could increase photoinduced contractile stress (1.2 MPa) and enhance the deflection of thin cantilevers.[23] In the present study, we proposed and validated the strategy of using pre-stored strain energy to achieve large and tunable photoinduced contractile stress (up to 7 MPa) for azobenzene LCEs. The liquid crystalline nature of the material results in a recoverable photomechanical force that enables continuous motions of large rolling objects. Thirdly, photoinduced rolling of a spiral ribbon was reported by Wie et al.[14] Their used sample is an azobenzene-containing liquid crystalline network (azo-LCN) prepared by in situ polymerization of a reactive LC monomer mixture in the twisted nematic conformation. By contrast, our spiral ribbons were fabricated from stretched, reprocessable ALCE strips. The robust reshaping capability of ALCE, combined with the adjustable stored strain energy and bilayer construction, means that a variety of 3D objects can readily be fabricated for photocontrolled fast and continuous actuation.

2.2.4. Conclusions

In summary, we have demonstrated the use of exchangeable chemical bonds to enable the processability of LECs bearing azobenzene moieties in the chain backbone. The synthesized ALCE could readily be compressed into thin films, reshaped or stretched to yield high orientation of azobenzene mesogens and chain backbone. We have investigated

the photoinduced deformation and motion by exploring the combined effect of the *trans-cis* photoisomerization of azobenzene, which is the basis for most ALCEs, and the strain energy stored in highly extended polymer chains, which is the basis of the shape memory effect. From the isostrain experiments, it was found that both the photoisomerization of the azobenzene mesogens located in the chain backbone and a photothermal effect could contribute synergistically to a recoverable contraction force generated by the stretched film exposed to UV light, and that the contraction can be easily controlled by the film strain. Using stretched ALCE films laminated to a transparent BOPP film, light-driven moving 3D objects, such as wheels and spring-like ribbons were fabricated. We show that light could be converted into mechanical energy to execute a variety of robust, tunable and continuous motions at the macroscopic scale. Both wheels and spring-like ribbons can roll away from or towards the UV light by setting the stretched ALCE film as the inner or outer layer respectively. In addition to the controllable rolling direction, the rolling speed could be controlled by adjusting the amount of stored energy in the ALCE film that is proportional to the elongation degree. Our demonstrated strategy has the potential to be the basis of a platform technology, where the design of malleable ALCEs can be extended to a broad range of dynamic chemistries[24] (for example, Diels–Alder reaction[25] and radical-exchange reaction[26]) and chromophores (such as, spiropyrans[27] and diarylethenes[28]). We anticipate that the use of stored strain energy to amplify the magnitude of photoinduced mechanical force opens new avenues of studies and represents one step forward towards applications of optical polymer actuators.

Acknowledgements

Y. Zhao acknowledges the financial support from the Natural Sciences and Engineering Research Council of Canada (NSERC) and le Fonds québécois de la recherche sur la nature et les technologies of Québec (FQRNT). X. Lu and S. Guo thank China Scholarship Council (CSC) for scholarship allowing them to study in Canada. H. Xia acknowledges the financial support of National Natural Science Foundation of China (51433006) and The Young Talent Team Science and Technology Innovation Project of Sichuan Province (2016TD0010). Y. Zhao is a member of the FQRNT-funded Center for Self-Assembled Chemical Structures (CSACS) and the Centre québécois sur les matériaux fonctionnels

(CQMF). The authors thank Dr. Daniel Fortin (Université de Sherbrooke) for helping the X-ray diffraction measurements.

Reference

[1] a) S. Armon, E. Efrati, R. Kupferman, E. Sharon, *Science* **2011**, 333, 1726; b) R. Elbaum, L. Zaltzman, I. Burgert, P. Fratzl, *Science* **2007**, 316, 884.

[2] S. J. Gerbode, J. R. Puzey, A. G. McCormick, L. Mahadevan, *Science* **2012**, 337, 1087.

[3] a) Y. Forterre, J. M. Skotheim, J. Dumais, L. Mahadevan, *Nature* **2005**, 433, 421; b) E. Stokstad, *Science* **2016**, 352, 756.

[4] P. Fratzl, F. G. Barth, *Nature* **2009**, 462, 442.

[5] a) M. Yamada, M. Kondo, J.-i. Mamiya, Y. Yu, M. Kinoshita, C. J. Barrett, T. Ikeda, *Angew. Chem. Int. Ed.* **2008**, 47, 4986; b) X. Zhang, Z. Yu, C. Wang, D. Zarrouk, J.-W. T. Seo, J. C. Cheng, A. D. Buchan, K. Takei, Y. Zhao, J. W. Ager, J. Zhang, M. Hettick, M. C. Hersam, A. P. Pisano, R. S. Fearing, A. Javey, *Nat. Commun.* **2014**, 5, 2983; c) Y. Hu, G. Wu, T. Lan, J. Zhao, Y. Liu, W. Chen, *Adv. Mater.* **2015**, 27, 7867.

[6] a) Z. Pei, Y. Yang, Q. Chen, E. M. Terentjev, Y. Wei, Y. Ji, *Nat. Mater.* **2014**, 13, 36; b) C. S. Haines, M. D. Lima, N. Li, G. M. Spinks, J. Foroughi, J. D. W. Madden, S. H. Kim, S. Fang, M. Jung de Andrade, F. Göktepe, Ö. Göktepe, S. M. Mirvakili, S. Naficy, X. Lepró, J. Oh, M. E. Kozlov, S. J. Kim, X. Xu, B. J. Swedlove, G. G. Wallace, R. H. Baughman, *Science* **2014**, 343, 868.

[7] a) S. Palagi, A. G. Mark, S. Y. Reigh, K. Melde, T. Qiu, H. Zeng, C. Parmeggiani, D. Martella, A. Sanchez-Castillo, N. Kapernaum, F. Giesselmann, D. S. Wiersma, E. Lauga, P. Fischer, *Nat. Mater.* **2016**, 15, 647; b) D. Rus, M. T. Tolley, *Nature* **2015**, 521, 467; c) C. Larson, B. Peele, S. Li, S. Robinson, M. Totaro, L. Beccai, B. Mazzolai, R. Shepherd, *Science* **2016**, 351, 1071; d) H.-W. Huang, M. S. Sakar, A. J. Petruska, S. Pané, B. J. Nelson, *Nat. Commun.* **2016**, 7, 12263.

[8] J.-a. Lv, Y. Liu, J. Wei, E. Chen, L. Qin, Y. Yu, *Nature* **2016**, 537, 179.

[9] a) K. M. Lee, M. L. Smith, H. Koerner, N. Tabiryan, R. A. Vaia, T. J. Bunning, T. J. White, *Adv. Funct. Mater.* **2011**, 21, 2913; b) K. Kumar, C. Knie, D. Bléger, M. A. Peletier, H. Friedrich, S. Hecht, D. J. Broer, M. G. Debije, A. P. H. J. Schenning, *Nat. Commun.* **2016**, 7, 11975.

[10] M. Ma, L. Guo, D. G. Anderson, R. Langer, *Science* **2013**, 339, 186; b) R. Tang, Z. Liu, D. Xu, J. Liu, L. Yu, H. Yu, *ACS Appl. Mater. Interfaces* **2015**, 7, 8393.

[11] T. H. Ware, M. E. McConney, J. J. Wie, V. P. Tondiglia, T. J. White, *Science* **2015**, 347, 982.

[12] a) N. Hosono, T. Kajitani, T. Fukushima, K. Ito, S. Sasaki, M. Takata, T. Aida, *Science* **2010**, 330, 808; b) T. J. White, D. J. Broer, *Nat. Mater.* **2015**, 14, 1087; c) C. Ohm, M. Brehmer, R. Zentel, *Adv. Mater.* 2010, 22, 3366; d) H. Yu, T. Ikeda, Adv. Mater. 2011, 23, 2149; e) T. Seki, *J. Mater. Chem.* C **2016**, 4, 7895.

[13] a) Y. Yu, M. Nakano, T. Ikeda, *Nature* **2003**, 425, 145; b) C. L. van Oosten, C. W. M. Bastiaansen, D. J. Broer, *Nat. Mater.* **2009**, 8, 677.

[14] J. J. Wie, M. R. Shankar, T. J. White, *Nat. Commun.* **2016**, 7, 13260.

[15] R. R. Kohlmeyer, J. Chen, *Angew. Chem. Int. Ed.* **2013**, 52, 9234.

[16] C. Huang, J.-a. Lv, X. Tian, Y. Wang, Y. Yu, J. Liu, *Sci. Rep.* **2015**, 5, 17414.

[17] S. Iamsaard, S. J. Aßhoff, B. Matt, T. Kudernac, J. L. M. CornelissenJeroen, S. P. Fletcher, N. Katsonis, *Nat. Chem.* **2014**, 6, 229.

[18] a) D. Montarnal, M. Capelot, F. Tournilhac, L. Leibler, *Science* **2011**, 334, 965; b) M. Capelot, D. Montarnal, F. Tournilhac, L. Leibler, *J. Am. Chem. Soc.* **2012**, 134, 7664.

[19] Y. Yang, Z. Pei, Z. Li, Y. Wei, Y. Ji, *J. Am. Chem. Soc.* **2016**, 138, 2118.

[20] a) T. Ube, K. Kawasaki, T. Ikeda, *Adv. Mater.* **2016**, 28, 8212; b) Y. Li, O. Rios, J. K. Keum, J. Chen, M. R. Kessler, *ACS Appl. Mater. Interfaces* **2016**, 8, 15750.

[21] a) T. Yoshino, M. Kondo, J.-i. Mamiya, M. Kinoshita, Y. Yu, T. Ikeda, Adv. Mater. **2010**, 22, 1361; b) M. Kondo, Y. Yu, T. Ikeda, *Angew. Chem. Int. Ed.* **2006**, 45, 1378.

[22] a) H. Zhang, H. Xia, Y. Zhao, J. Mater. Chem. **2012**, 22, 845; b) H. Zhang, Y. Zhao, *ACS Appl. Mater. Interfaces* **2013**, 5, 13069.

[23] K. M. Lee, D. H. Wang, H. Koerner, R. A. Vaia, L.-S. Tan, T. J. White, *Macromol. Chem, Phys.* **2013**, 214, 1189.

[24] R. J. Wojtecki, M. A. Meador, S. J. Rowan, *Nat. Mater.* **2011**, 10, 14.

[25] X. Chen, M. A. Dam, K. Ono, A. Mal, H. Shen, S. R. Nutt, K. Sheran, F. Wudl, *Science* **2002**, 295, 1698.

[26] T. F. Scott, A. D. Schneider, W. D. Cook, C. N. Bowman, *Science* **2005**, 308, 1615.

[27] R. Klajn, *Chem. Soc. Rev.* **2014**, 43, 148.

[28] H. Tian, S. Yang, *Chem. Soc. Rev.* **2004**, 33, 85.

[29] K. M. Lee, D. H. Wang, H. Koerner, R. A. Vaia, L.-S. Tan, T. J. White, *Macromol. Chem, Phys.* **2013**, 214, 1189.

2.2.5. Experimental Section

2.2.5.1. Materials

Unless otherwise stated, all solvents and reagents were purchased from Sigma Aldrich and used without further purification.

2.2.5.2. General Characterizations

Differential scanning calorimetry (DSC) experiments were carried out under nitrogen atmosphere on TA Instruments DSCQ2000 at a heating rate of 10 ℃ min^{-1}. For Wide-angle X-ray diffraction experiments, the samples were fixed on a homemade sample holder and mounted at room temperature on a Bruker APEX DUO X-ray diffractometer. A 30 second X-ray exposure time was used to record the diffraction pattern using the Cu micro-focus anode (1.54184 Å) and the CCD APEX II detector at a 45 mm distance. The stress–strain curves were recorded on an Instron 5965 machine with a 100 N load cell. The isostrain measurements (experimental setup being shown in Figure 2-S6) at room temperature for the unstretched and stretched films under UV irradiation were performed on an Instron 5965 system with a 10 N load cell using the stress-relaxation mode. By applying UV light (365 nm, normal incidence, light source 4 cm away) to a stripe-shaped sample (20 mm × 3.5 mm × 13 μm) held under constant strain (within 0.2%), the contractile force generated in the film can be sensed and measured. The photocontrolled motions of the ALCE-based smart devices were performed by using a UV Spot Curing System (Omnicure® Series 1000) equipped with UV light filter (365 nm) and visible light filter (550 nm). The light intensity was measured using a photometer (Oriel® Instruments).

2.2.5.3. Synthesis of ALCEs

4,4'-diglycidyloxy-azobenzene was synthesized according to the literature.[S1] The azobenzene liquid crystalline networks were synthesized through several steps (Figure 2-S1). Typically, a stoichiometric amount of 4,4'-diglycidyloxy-azobenzene (326 mg, 1.0 mmol), dodecanedioic acid (230 mg, 1.0 mmol) and 1,5,7-triazabicyclo[4.4.0]dec-5-ene catalyst (14 mg, 5 mol% to the COOH groups) were dissolved in anhydrous N,N'-

dimethylacetamide (2 mL) in a glass vial (20 mL). The resulting mixture was heated at 145 ℃ for 12 hours in an oil bath to yield orange-brown solid. The polymer was further dried under vacuum at 145 ℃ for 12 h.

2.2.5.4. Preparation of Stretched ALCE Films and ALCE-based Actuators

Thin films with desired thickness were obtained by hot-compressing the polymer granules at 180 ℃ , followed by cooling to room temperature. Then the films were stretched at 100 ℃ to different strain (100% or 200%) using the Instron machine mentioned above, followed by cooling to room temperature to keep the strains. Bilayer films were obtained by laminating the stretched ALCE film with a BOPP film. From the bilayer film, a rectangular strip (85 mm × 8.5 mm) was cut and then rolled around a glass tube (πd=85 mm) and end-to-end joined to form a wheel at 65 ℃ followed by cooling to fix the closed tubular shape, with the ALCE film either as the inner or outer layer. The spring was readily fabricated by twisting the film (around a cylindrical metal rod) into either left-handed or right-handed helical ribbon at 65 ℃ followed by cooling to fix the helical shape. Likewise, the ALCE could be set as either the inward or outward layer of the spring. The light-driven "vehicle" was assembled by linking the two ends of a helical ribbon with two wheels made with polyurethane foam.

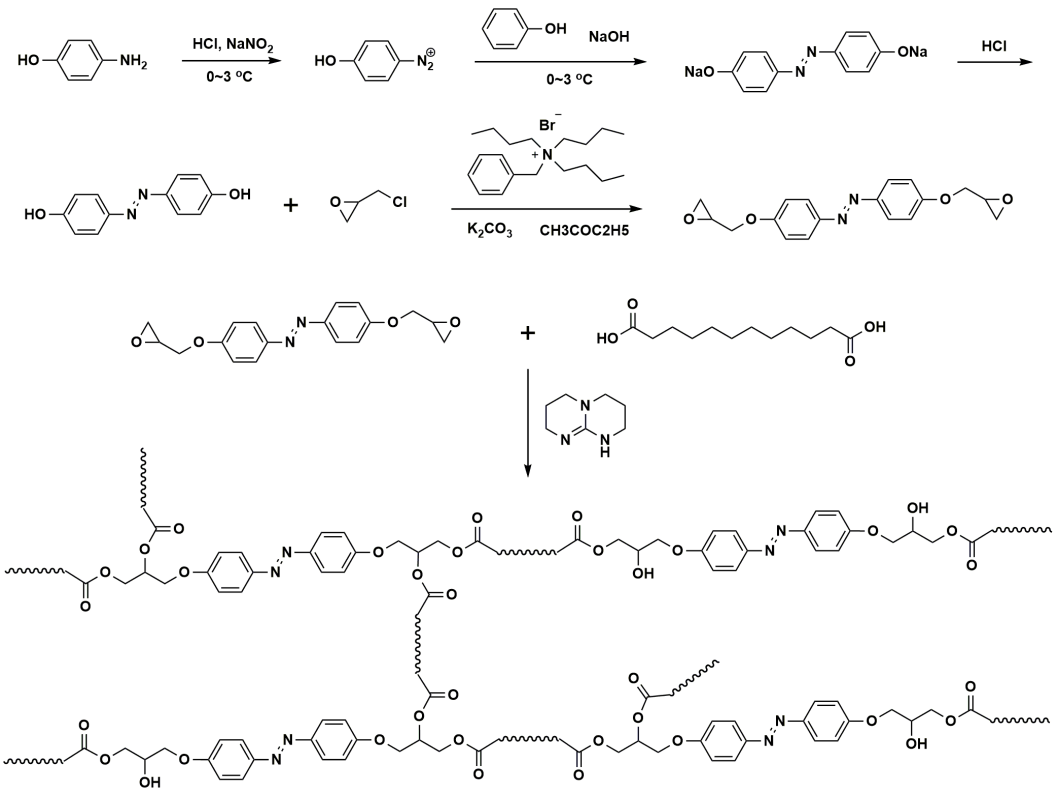

Figure 2-S1. Synthesis routes to the azobenzene liquid-crystalline elastomer.

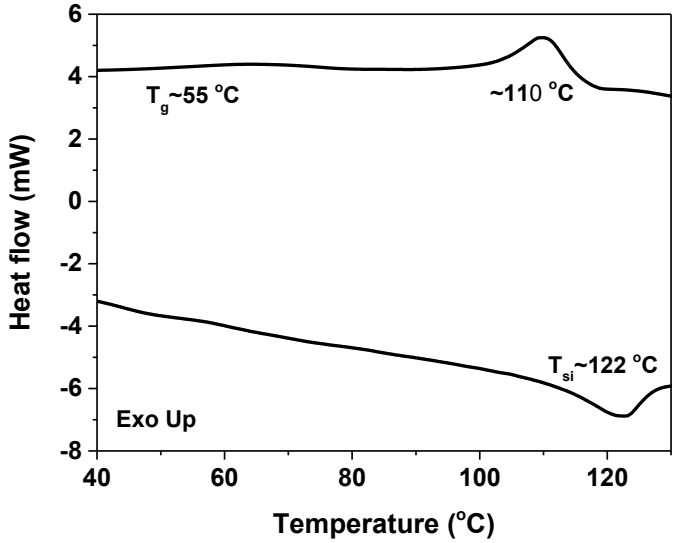

Figure 2-S2. DSC traces of both heating/cooling (rate of 10 ºC min^{-1}) of ALCE.

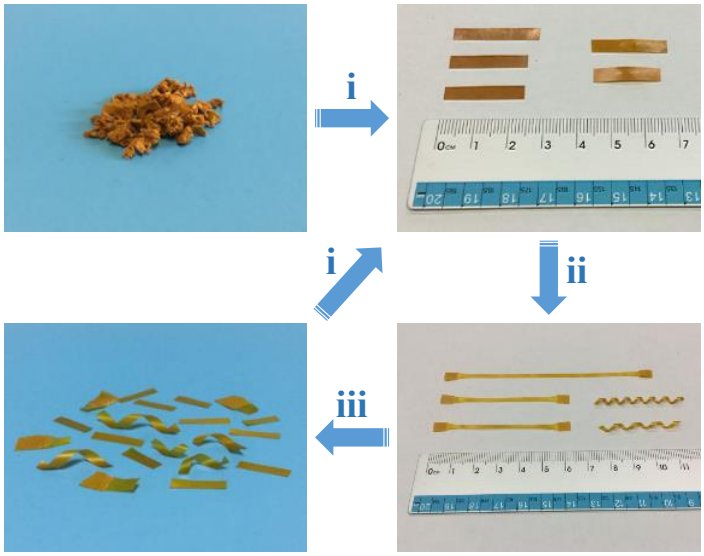

Figure 2-S3. Photographs showing recycling of ALCE: i) hot pressing: 3 MP, 180 ºC 30 min; ii) stretching at 100 ºC followed by cooling to room temperature, spring reshaping at 65 ºC; iii) cutting.

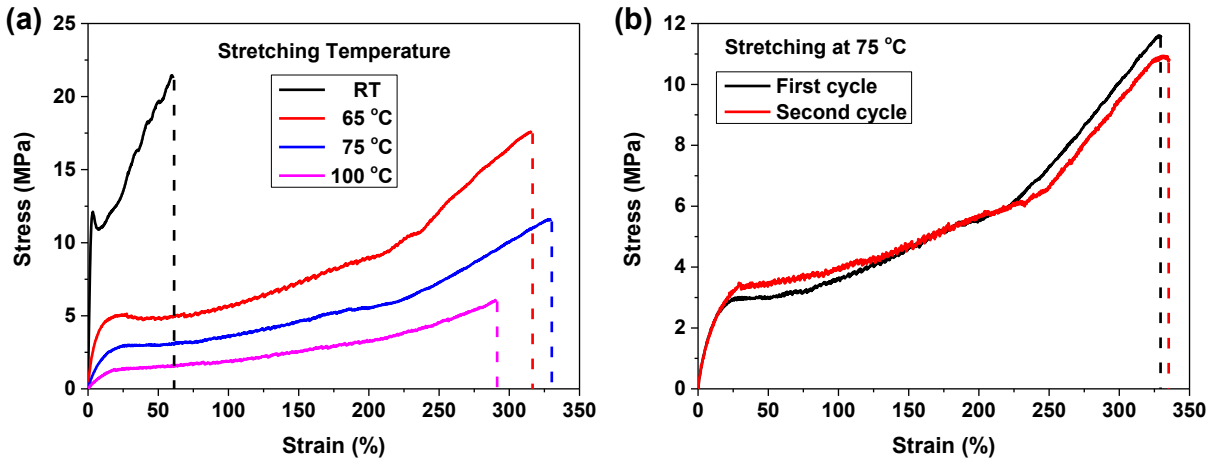

Figure 2-S4. a) Stress–strain curves of the ALCEs at different stretching temperatures. b) Stress–strain curves at 75 ºC for the initial and remolded ALCEs, showing similar mechanical properties.

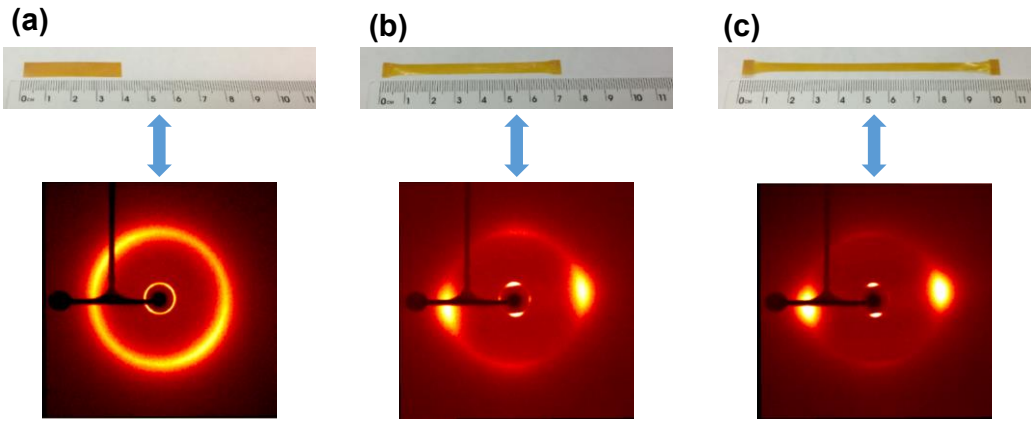

Figure 2-S5. Wide-angle X-ray diffraction patterns of (a) unstretched ALCE film and stretched films with (b) 100% strain and (c) 200% strain. Patterns (b) and (c) show high orientation of smectic layers (small-angle scattering) and high orientation of mesogens and chain backbone (wide-angle scattering).

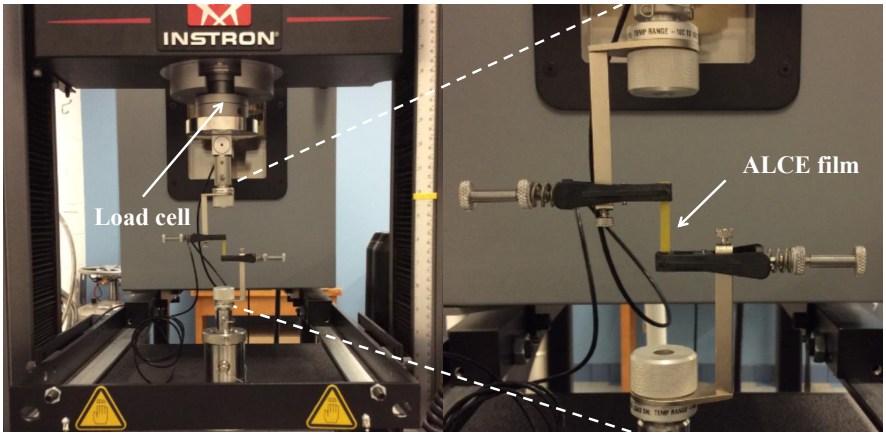

Figure 2-S6. Photographs of the experimental setup used for measuring photoinduced contraction force under the isostrain condition.

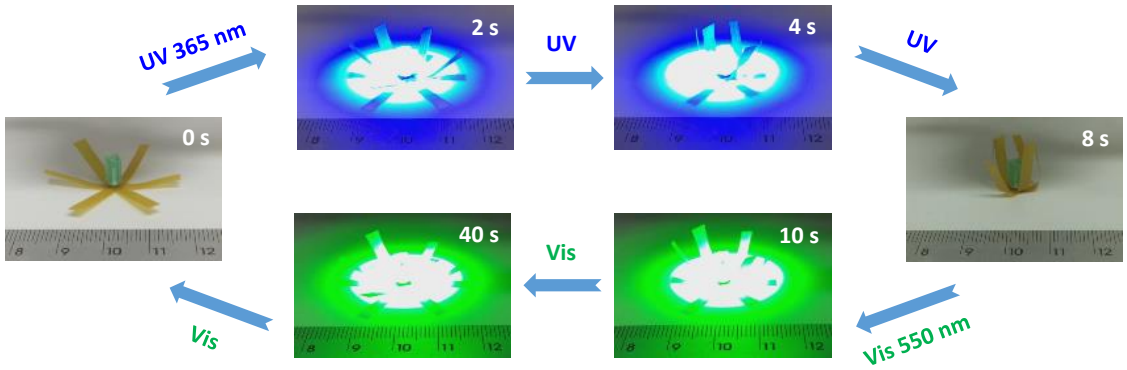

Figure 2-S7. Photographs showing the closing and blooming of an ALCE flower upon exposure to UV light (365 nm, 60 mW cm^{-2}) and Vis light (550 nm, 20 mW cm^{-2}) respectively.

Additional notes: The photothermal effect and surface temperature of ALCE films upon UV light irradiation was measured using an infrared camera. The surface temperature can reach and keep constant at about 60 °C after UV light irradiation for 5 s at an intensity of 100 mW cm^{-2} (as shown in the Additional Figure).

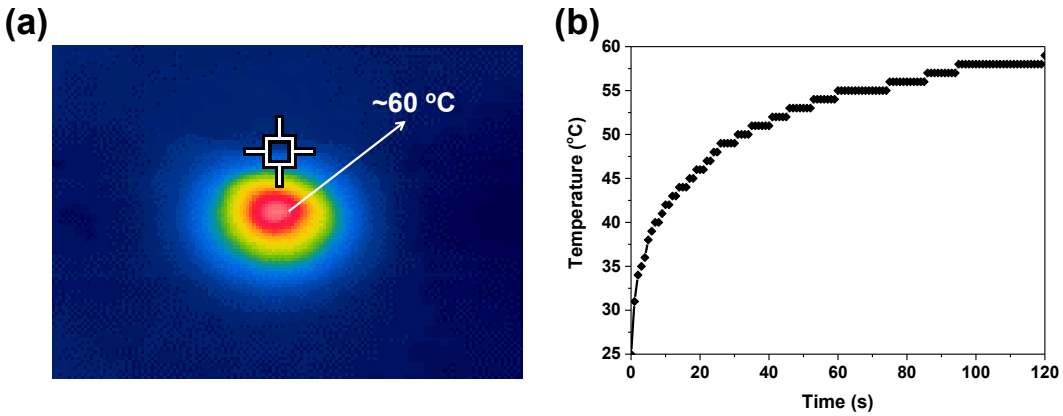

Additional Figure. a) Infrared thermal images recorded the surface temperature of an ALCE film (20 μm) after UV light (100 mW cm^{-2}) irradiation for 5 s. b) Temperature of the back of an ALEC film as a function of UV light (100 mW cm^{-2}) exposure time. The temperature was measured by sandwiching the probe of a digital thermometer between two ALCE films.

The photothermal effect was also shown in Figure 1e and f, the most part of recoverable actuation stress originates from photothermal effect. And the other part of stress that can drop to zero only upon exposure to Vis light is attributed to isomerization of azobenzene. It is very important to keep the temperature between Tg and Tsi. If the light power is too strong, the resulting high temperature will cause some irreversible chain relaxation or irreversible contraction of the film. And it will make irreversible deformation of the devices and prevent the continuous motion. For example, if the wheel is deformed into a non-circular shape, it will find a balance position to keep still. But if the power is too weak, it can't drive the object move.

The surface temperature of ALCE films upon UV light irradiation was determined with a FLIR infrared camera (TG165). The temperature of the back of ALEC films was measured by sandwiching the probe of a digital thermometer (Fisher Scientific™ Traceable™ Expanded-Range Thermometers) between two ALCE films.

[S1] J.-a. Lv, W. Wang, J. Xu, T. Ikeda, Y. Yu, *Macromol. Rapid Commun.* **2014**, 35, 1266.

2.3. Summary of the Project

In this project, we synthesized a mouldable liquid crystal epoxy-acid derived network (denoted as ALCE) with azobenzene mesogens located in the chain backbone using transesterification-based dynamic covalent crosslinking. Very thin films (10~20 μm) can easily be obtained by hot-compressing the polymer granules at high temperature owing to the dynamic feature of the exchangeable bonds. We found that pre-stored mechanical strain energy in ALCE films could largely amplify the photoinduced mechanical stress to as high as ~7 MPa as a result of the phototriggered release of the stored energy in addition to the direct optical to mechanical energy conversion stemming from the trans-cis photoisomerization of azobenzene. Furthermore, we made use of these energy-storing films to fabricate large-size polymer photo-actuators in the form of wheels or spring-like "motors". The moving speed and directions of the moving objects could be tuned (from ~0.33 to ~1 cm s^{-1}) and controlled (moving towards or away from light) by adjusting the amount of pre-stored strain energy in the ALCE films and changing the architectures of the objects, respectively. We also tested how far the light-driven motion could go for the wheel in Figure 51c. The results showed that there was no sign of decreased speed or sensitivity for the wheel even after 100 rotations. This continuous rolling, together with the winding/unwinding (or vice versa) motion of the helical ribbons under on/off of vertical UV light exposure, implies that the photoisomerization and photothermal effect in this ALCE could work synergistically to provide stability for stored strain energy and produce recoverable stress.

CHAPITRE 3. LIQUID-CRYSTALLINE DYNAMIC NETWORKS DOPED WITH GOLD NANORODS SHOWING ENHANCED PHOTOCONTROL OF ACTUATION

3.1. About the Project

Smart polymer actuators are capable of mechanical reconfiguration or motions by translating the energy contained within chemical or physical stimuli into macroscopic shape changes. Despite the many progresses made in recent years, it is still very challenging to simultaneously apply photochemical reaction and photothermal effect to control photomechanical actuations in one device to execute sophisticated motion tasks and to do useful work. Besides, stimuli-responsive LCP actuators that are able to exhibit controllable, robust, self-propelling (continuous), macroscopic motions, especially locally-programmable and concerted robot-like motions, needs further exploration. In this study, we expect to address the challenges by employing gold nanorods (AuNRs)/LCP composites to creat novel sophisticated motions.

This work was published in *Advanced Materials*, **2018**, 30, 1706597 by Xili Lu, Hu Zhang, Guoxia Fei, Bing Yu, Xia Tong, Hesheng Xia and Yue Zhao. This research work was conducted in the Université de Sherbrooke under the supervision of Prof. Zhao and co-supervision of Prof. Xia. I designed and performed the experiments described in this study. Hu Zhang helped me with the synthesis of gold nanorods. Guoxia Fei and Bing Yu gave me a lot of useful suggestions and assisted me with the data and figures processing. Xia Tong assisted me with some characterizations. I wrote the first draft of the manuscript. Prof. Zhao finalized the manuscript with revision contributions from Prof. Xia.

3.2. Paper Published in Advanced Materials, 2018, 30, 1706597.

Liquid‐Crystalline Dynamic Networks Doped with Gold Nanorods Showing Enhanced Photocontrol of Actuation

Xili Lu[a,b], Hu Zhang[b], Guoxia Fei[a], Bing Yu[b], Xia Tong[b], Hesheng Xia[*a] and Yue Zhao[*b]

[a]State Key Laboratory of Polymer Materials Engineering, Polymer Research Institute, Sichuan University, Chengdu 610065, China. E-mail: xiahs@scu.edu.cn

[b]Département de chimie, Université de Sherbrooke, Sherbrooke, Québec, J1K 2R1, Canada. Email: yue.zhao@usherbrooke.ca.

Keywords: photocontrolled motions, polymer actuators, azobenzene, liquid crystalline dynamic networks, gold nanocomposites

3.2.1. Abstract

A near-infrared light (NIR) and UV light-responsive polymer nanocomposite is synthesized by doping polymer-grafted gold nanorods into azobenzene liquid crystalline dynamic networks (AuNR-ALCNs). The effects of two different photoresponsive mechanisms, i.e., the photochemical reaction of azobenzene and the photothermal effect from the surface plasmon resonance of AuNRs, are investigated by monitoring both NIR and UV light-induced contraction force of oriented AuNR-ALCNs. By taking advantage of the material's easy processability, bilayer-structured actuators can be fabricated to display photocontrollable bending/unbending directions as well as localized actuations through programmed alignment of azobenzene mesogens in selected regions. Versatile and complex motions enabled by the enhanced photocontrol of actuation are demonstrated, including plastic "athletes" that can execute light-controlled push up or sit up, and light-driven caterpillar-inspired walker that can crawl forward on a ratcheted substrate at a speed of about 13 mm min^{-1}. Moreover, the photomechanical effects arising from the two types of light-triggered molecular motions, i.e., the *trans-cis* photoisomerization and liquid crystalline-isotropic phase transition of azobenzene mesogens, are added up to design a polymer "crane" that is capable of performing lightcontrolled, robot-like, concerted macroscopic motions including grasping, lifting up, lowering down, and releasing an object.

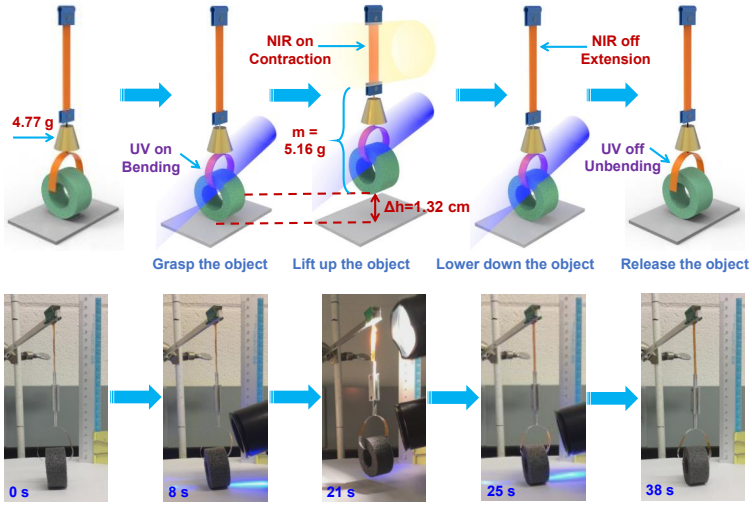

3.2.2. Introduction

Smart materials-based actuators have been attracting much interest in recent years because of their envisioned applications in the fields of soft robots,[1] sensors,[2] artificial muscles,[3] programmable origami,[4] motors,[5] oscillators,[6] and energy generators.[7] They can exhibit reversible shape changes in response to external stimuli (such as light, moisture, pH, heat and electrical current) to accomplish a function or carry out a work, for example, mimicking plant motions[8] or serving as energy transducers. Among those versatile smart materials, liquid crystalline polymer (LCP) actuator that can self-organize its molecular alignment represents arguably the most promising candidate for realizing the potential applications.[9] On the one hand, by making use of the order–disorder, generally nematic–isotropic, thermal phase transition, LCPs can be utilized to fabricate artificial muscles,[3b,10] reversible shape memory devices[11] and 3D reconfigurable objects,[12] where the smart actuators serve as thermal or optical to mechanical energy transducers. In order to control the actuation of LCPs in a remotely-controlled and precisely-manipulated way, light has been employed to trigger the order–disorder transition of liquid crystal mesogens. To this end, using photothermal effect is effective and convenient, which consists in doping LCP matrix with a light-absorbing and heat-releasing active species such as carbon nanotubes (CNTs),[13] graphene,[14] polydopamine nanoparticles,[15] organic dyes,[16] conjugated polymers[17] and gold nanocrystals.[18] On the other hand, for LCPs azobenzene mesogens, the reversible *trans-cis* photoisomerization of the photoswitch has been extensively explored for polymer LC actuators that can perform sophisticated biomimetic motions such as bending,[19] rolling,[5,20] walking,[21] swimming,[1a,22] oscillating,[6] twisting,[20,23] and making waves.[24] Many state-of-the-art light-driven intelligent devices including artificial flytrap,[25] photocontrolled fluid slugs,[26] soft microrobots[1a] and wave-making machines[24] have been developed. LCP actuators are generally liquid crystalline elastomers (LCEs) or networks (LCNs) because polymer chain crosslinking is required for reversible actuation.

Despite the recent exciting progress achieved in the field of light-driven LCP actuators, few attempts[16,27] have been made to take advantage of both photochemical reaction and photothermal effect in one single LCP. Notably, Yu et al. demonstrated triple shape

memory polymer by adding azobenzene and graphene oxide (GO) in a polyurethane matrix, which exhibits photomechanical motion under UV irradiation typical to azobenzene polymers and photothermally triggered shape transition upon near infrared (NIR) light exposure due to absorption by GO.[27b] Therefore, simultaneously applying photochemical reaction and photothermal effect to control photomechanical actuations in one device to execute sophisticated motion tasks and to do useful work remains a major scientific challenge. Besides, stimuli-responsive LCP actuators that are able to exhibit controllable, robust, self-propelling (continuous), macroscopic motions, especially locally-programmable and concerted robot-like motions, needs further exploration. Herein, we demonstrate an approach to address the challenges by doping polymer-grafted gold nanorods (AuNRs) into dynamic azobenzene liquid crystalline networks (ALCNs) to endow the polymers with both near-infrared (NIR) light and UV light responsiveness, enabling enhanced photocontrol of actuations. By programming the alignment of azobenzene mesogens in localized and different regions of bilayer films, we show that the plastic "athletes" can perform different physical exercise motions, such as push up and sit up. Moreover, combining the actions from two mechanisms—photothermally induced phase transition and *trans-cis* photoisomerization of azobenzene mesogens, we demonstrate that a LC polymer crane configured with an artificial muscle arm and a gripper is capable of executing robot-like motion tasks including grasping, lifting up, lowering down and releasing an object.

3.2.3. Results and Discussion

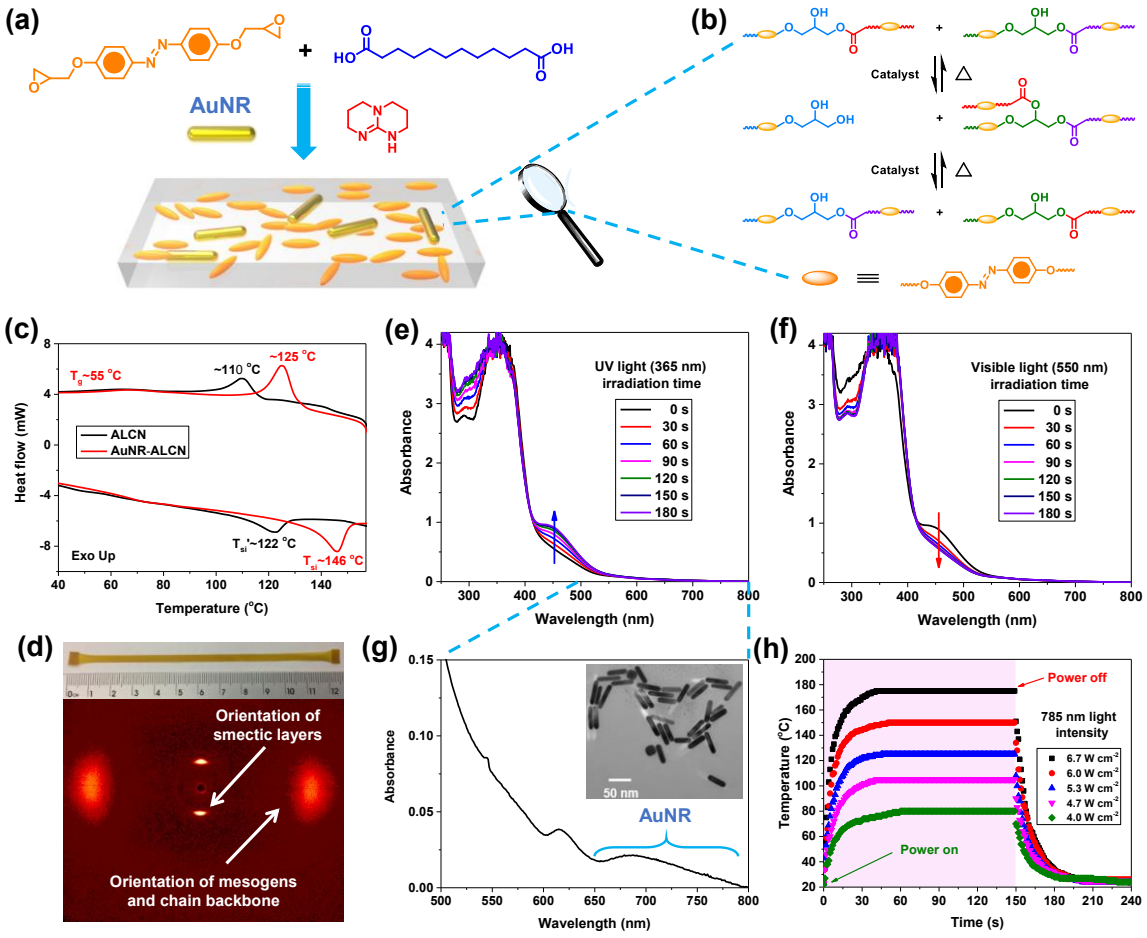

Figure 3-1. (a) Synthesis route to the AuNR-ALCN composite. (b) Schematic illustrations of the reversible transesterification reaction. (c) DSC traces of both heating/cooling (rate of 10 ºC min^{-1}) of ALCN and AuNR-ALCN. d) X-ray diffraction (XRD) image of a stretched AuNR-ALCN film (inserted picture, 200% strain). (e) Changes in the absorption spectra of a stretched AuNR-ALCN film (10 μm thick) upon direct irradiation with UV light (365 nm, 100 mW cm^{-2}) for different times. (f) Changes in the absorption spectra of the UV-pre-illuminated AuNR-ALCN film (film of Figure 1e) upon exposure to Visible light (550 nm, 20 mW cm^{-2}) for different times. (g) The amplified figure of absorption spectra of the AuNR-ALCN film shows the longitudinal surface plasmon resonance absorption band of AuNR. (h) Near infrared (NIR) light induced temperature rise of the AuNR-ALCN film at different light intensities.

The general synthesis procedure for azobenzene liquid crystalline networks doped with AuNRs (hereafter referred to as AuNR-ALCNs) is shown in **Figure 3-1**a. Firstly, AuNRs were surface-functionalized with thiol-terminated poly(N,N'-dimethylacrylamide) to enable homogeneous dispersion in organic solvent. The transmission electron microscopy (TEM) image shows the average dimension of AuNRs is about 50 nm×10 nm in length and diameter, respectively (inset picture of Figure 3-1g). The AuNR-ALCN composites were synthesized by curing AuNRs (0.05wt%), 4,4'-diglycidyloxyazobenzene and dodecanedioic acid (1:1) in the presence of triazobicyclodecene (TBD) as the catalyst for transesterification (see Supporting Information for detailed synthesis and samples preparation, Figure 3-S1).[28] It is reported that the curing reaction between di-epoxy and dicarboxylic acid includes several steps: the reaction between epoxy and acid takes place firstly to generate esters and hydroxyl groups, then the hydroxyl groups can continue to react with either epoxy or acid, leading to the formation of a network.[29] Upon heating, the catalytic transesterification reaction takes place and allows rearrangements of the epoxy-acid-derived network without change of the numbers of links and average functionality, thus affording the moldable and easy processing properties (Figure 3-1b). According to differential scanning calorimetry (DSC) measurements (Figure 3-1c), the AuNR-ALCN composite displays a glass transition temperature (T_g) at ≈55 °C and a broad smectic–isotropic phase transition (T_{si}) at ≈146 °C upon heating, which is higher than that of the neat polymer by ≈24 °C owing to heterogeneous nucleation effect,[30] where the rod-like structure of AuNRs can stabilize the smectic LC structure of AuNR-ALCN. Similar to ALCN alone,[5a] it is very easy to prepare thin films by hot-compressing the nanocomposite granules at 180 °C, followed by cooling to room temperature; then the film can be stretched at a temperature between T_g and T_{si} (110 °C for this study) to 200% strain with a thickness of 20 μm (Figure 3-1d, unless otherwise stated, the strain and thickness of the stretched film used in this study are 200% and ~ 20 μm respectively). Upon cooling to room temperature, the extensional state of polymer chains and networks is fixed by both oriented azobenzene mesogens in the smectic phase and T_g. As can be seen from the 2D image of X-ray diffraction (XRD) recorded on the stretched film, the stretching leads to the formation of well-aligned monodomain structure of azobenzene mesogens and chain

backbones oriented along the strain direction, while the smectic layers remain in the stretched film with the layer normal aligned along the strain direction (Figure 3-1d).

Furthermore, thin stretched AuNR-ALCN films (~10 μm thick) were utilized to record the UV–Vis spectra. Upon exposure to UV light for different times (unless otherwise stated, 365 nm UV light of 100 mW cm^{-2} intensity), the absorption band in the 430-500 nm region (absorption of *cis* azobenzene) of the AuNR-ALCN film increases owing to the *trans-cis* photoisomerization of the azobenzene moieties (Figure 3-1e); while subsequently under visible light irradiation (550 nm, 20 mW cm^{-2}), the absorption band can gradually decrease to the original value with time (Figure 3-1f), indicating the reversible *cis-trans* back-isomerization. The magnified spectrum in the 500-800 nm region for the AuNR-ALCN film reveals a broad absorption band (from 650 nm to 800 nm) which arises from the longitudinal surface plasmon resonance (SPR) absorption of AuNRs (Figure 3-1g). It should be noted that: AuNRs in water solution show a narrow longitudinal SPR absorption peak at ~853 nm (Figure 3-S2, Supporting Information), while the longitudinal SPR absorption of AuNRs in polymer matrix shifts to smaller wavelength and becomes broad. Upon exposure to NIR light (785 nm) with different intensities, the SPR-generated photothermal effect of AuNRs elevates the temperature of the nanocomposite film quickly until it reaches a thermal equilibrium value, which is proportional to the light intensity (Figure 3-1h). For example, when the light intensity is about 6.7 W cm^{-2}, the temperature rises rapidly from 25 °C to ≈175 °C in about 40 s, and then remains unchanged. Once the NIR light is tuned off, the temperature of AuNR-ALCN film drops quickly. It can be concluded from the above results that the stretched AuNR-ALCN films reacts to both great UV–Vis as a result of the *trans-cis* photoisomerization of azobenzene and NIR light due to absorption by AuNRs and heat release.

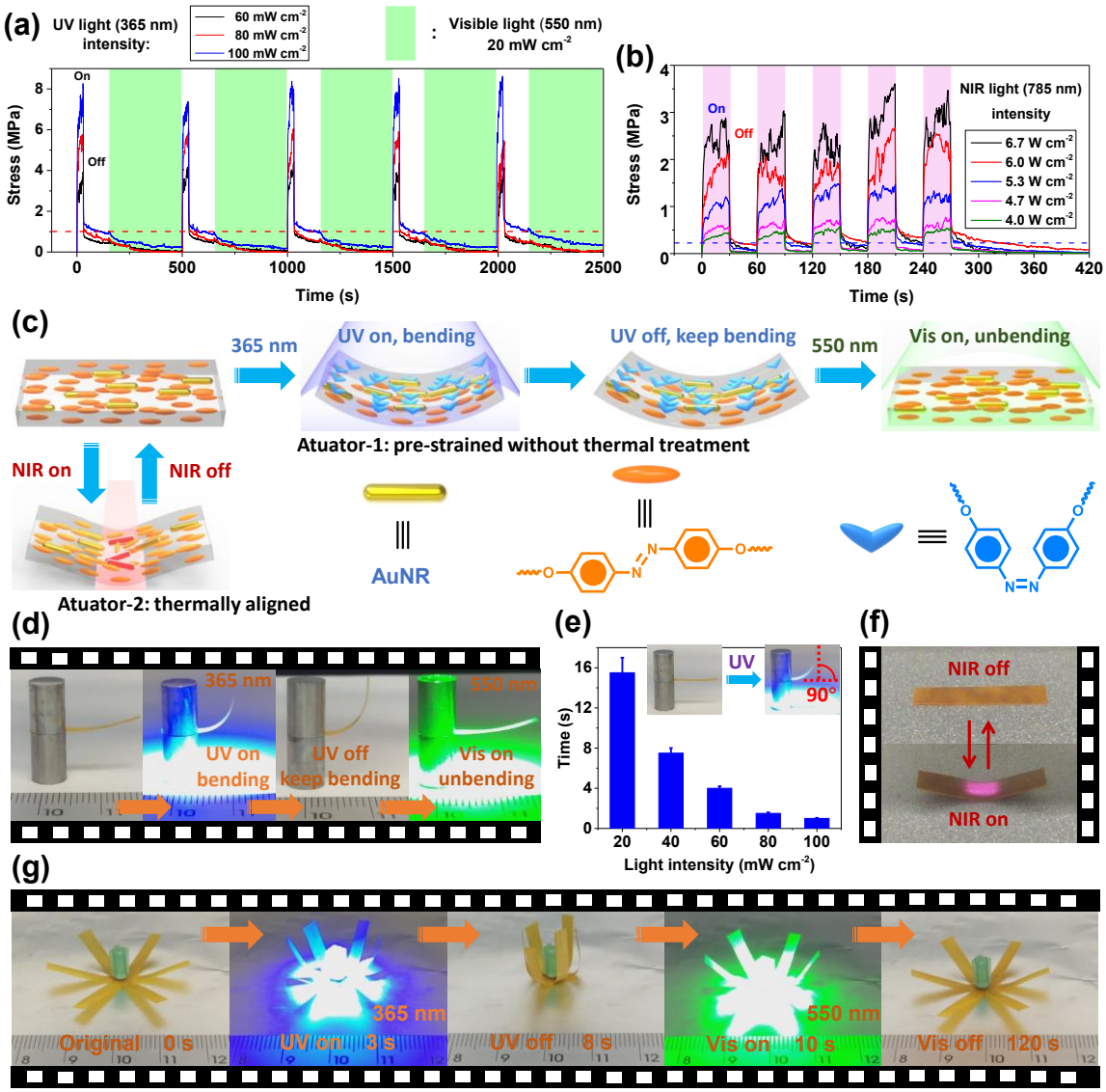

Figure 3-2. (a) Actuation stress as a function of time as UV light (with different intensities) is periodically turned on (time, 30 s) and off (time, 120 s) on the film (200% strain, 20 mm × 3.5 mm × 20 μm), followed by illumination with visible light for 350 s in each cycle. (b) Actuation stress as a function of time as NIR light (785 nm) is periodically turned on (time, 30 s) and off (time, 30 s) on the film (20 mm × 3 mm × 0.15 mm). (c) Schematic illustration of the two acting mechanisms for different bending behaviors triggered by UV-Vis and NIR light respectively. (d) Photographs showing the bending and unbending of the film under irradiation with UV light (365 nm, 100 mW cm^{-2}) and Vis light (550 nm, 20 mW cm^{-2}) respectively. (e) UV irradiation time required for 90° bending angle as a function of UV light intensity. f) Photographs showing the fast bending and unbending shape change

shift upon turning on and off NIR light (785 nm, 6.7 W cm^{-2}). (g) Photographs showing the closing and blooming of an AuNR-ALCE "flower" upon exposure to UV light (365 nm, 40 mW cm^{-2}) and Vis light (550 nm, 20 mW cm^{-2}) respectively.

In a previous work[5a] we showed that photoinduced release of strain energy from ALCN can generate a mechanical force that adds up to the photomechanical effect arising from azobenzene mesogens. With stretched AuNR-ALCN nanocomposite, we investigated the photoinduced mechanical force under both UV-Vis and NIR light irradiation. We carried out the isostrain measurements at room temperature to monitor the light-generated force of the stretched AuNR-ALCN film (namely **Actuator-1**) by applying UV light to a strip-shaped sample (20 mm × 3.5 mm × 20 μm) held under constant strain in the sample holder of a tensile tester (Instron 5965, experimental setup in Figure 3-S3, Supporting Information); the contractile force generated in the sample sheet can be sensed and measured. As is shown in **Figure 3-2**a, upon irradiation with UV light, **Actuator-1** generated a large stress that increases with the light intensity, reaching ~ 4 MPa, close to 6 MPa and more than 8 MPa for the light intensity of 60 mW cm^{-2}, 80 mW cm^{-2} and 100 mW cm^{-2} respectively, which is much higher than the photoinduced forces usually found in ALCEs.[31] Upon turning off the UV light, the force dropped with a significant amount of stress (about 1 MPa for the light intensity of 100 mW cm^{-2}) remaining at the UV-off state rather than declined to the original level. However, upon exposure of Vis light (550 nm, 20 mW cm^{-2}), the stress started to drop again to approach zero. The cycle of force up and down under UV light on and UV off followed by Vis on, respectively, can be repeated for many times with the remaining force decreased slightly over time (Figure 3-2a; Figure 3-S4, Supporting Information). On the other hand, by following the previously reported approach to prepare the uniform aligned monodomain dynamic LCNs,[12b] it is very easy to obtain photothermally responsive AuNR-ALCN actuators (namely **Actuator-2**) by making use of the catalytic transesterifcation. With this actuator in hand, we also measured the NIR light-induced force using the same isostrain testing method. By applying NIR light (785 nm) to a strip-shaped sample (20 mm × 3 mm × 0.15 mm) held under constant strain in the same experiment setup, similarly, **Actuator-2** generated a stress that increases with light intensity, and the cycle of force up and down can also be repeated for many times

upon NIR light on and off respectively (Figure 2b). However, the actuation stress (about 3 MPa) of **Actuator-2** is smaller than that of **Actuator-1** even when the NIR light intensity is as high as 6.7 W cm^{-2}. Besides, in contrast to the actuation force induced by UV light, the force generated under NIR irradiation dropped to near the original level after turning off the NIR light, implying that only the photothermal effect is at the origin of the induced contractile stress. It can be seen that significant force appeared at NIR intensity of 5.3 W cm^{-2} or higher when the temperature reached the broad LC-isotropic phase transition.

On the basis of the above results from both the UV–Vis spectroscopy studies and the isostrain force measurements, the following points can be made to explain the different phenomenon of photoactuated stress between this two kinds of actuators. (1) It should be noted that the remaining UV light induced stress of **Actuator-1** (~1 MPa) is smaller than that of the neat ALCN film (~ 2.2 MPa),[5a] which is probably caused by more *cis–trans* thermal relaxation of azobenzene mesogens in the AuNR-ALCN due to a greater photothermal effect under UV light irradiation in the presence of AuNRs. (2) For **Actuator-1**, the UV light-induced contraction force originates from both *trans–cis* photoisomerization of azobenzene and photothermally induced polymer chain relaxation. Therefore, after turning off the UV light, the contraction force does not drop completely due to the remaining *cis* state of azobenzene, and the remaining force can diminish only upon visible light irradiation. On the other hand, the actuation force of **Actuator-2** only depends on the shape contraction when heated above its LC phase transition temperature by NIR light and thus is smaller than that of **Actuator-1**. Because the reversible shape change based on LC phase transitions can easily take place just by turning on and turning off NIR light to heat and cool the AuNR-ALCN sheet, the photoactuated force of **Actuator-2** can drop close to the original level upon removal of NIR light.

Based on the above analysis, we assume that **Actuator-1** can undergo bending motions under UV light irradiation and keep the bending state unless exposure to Vis light to diminish the remaining stress; while **Actuator-2** can display bending and unbending motions just by turning on and off the NIR light. The two mechanisms of photoinduced bending but different behaviors are illustrated in Figure 3-2c. It is known that on exposure to UV light most incident photons (up to 99%) are absorbed within 1 μm of the surface

layer due to the high extinction coefficient of azobenzene moieties (about 2.0×10^4 L mol^{-1} cm^{-1} at 365 nm).[31] Therefore, change in orientation of the azobenzene mesogens induced by *trans–cis* photoisomerization and photothermal effect should take place only in the film surface region. As a result, an uneven distribution of the anisotropic deformation is formed and the bending motion of the film can be achieved. Different from the donor-acceptor-substituted azobenzene drivatives whose *cis-trans* back-isomerization rates (at room temperature) are very rapid owing to low barriers to isomerization,[32] the 4,4'-alkoxy-azobenzene used in our polymer can keep its relatively stable *cis* state[19,31b] and the photoinduced stress, thus allowing the bending state to be retained until irradiation with Vis light (Figure 3-2d; Movie 3-S1, Supporting Information). Knowing that the strain energy stored in **Actuator-1** could largely amplify the photoinduced contraction force,[5a] we studied the relationship between the UV light intensity and the bending speed by calculating the time that it takes to bend the film from horizontal to vertical direction (Figure 3-2e). The results show that the bending speed increases with light intensity, and it takes only about 1 s to bend the film with an angle of 90° at light intensity of 100 mW cm^{-2} (Figure 3-2e). This rapid motion speed is consistent with the robust UV-light triggered contraction force, which allows for the fabrication of high photosensitive actuators. For **Actuator-2**, under irradiation with NIR light, the AuNRs absorb light energy and convert it into thermal energy to heat the illuminated region above the LC phase transition temperature. Owing to the light attenuation, a diminishing temperature gradient occurs in the illuminated region from top surface to bottom surface. Therefore, the order–disorder LC phase transition only takes place in the high temperature top surface of **Actuator-2**, leading to an uneven distribution of the anisotropic deformation and bending motion (Figure 3-2f; Movie 3-S2, Supporting Information). Upon removal of the NIR light, the temperature of **Actuator-2** drops quickly, which allows for the rapid disorder-smectic phase transition and unbending motions. The integration of both NIR and UV light responsiveness into one single material can provide the AuNR-ALCN with multifunction for potential applications. For example, it can be employed to act as switches for some inaccessible and touchless circuits or other electronic devices with a remote control modality by making use of either of the two photomechanical deformation and motion mechanisms. It can also be utilized to fabricate smart devices that display rapid and

continuous motions by taking advantages of photothermally induced LC phase transition, such as artificial muscles and soft motors. In particular, a biomimetic AuNR-ALCN "flower" that can undergo repeated closing and blooming in response to UV (365 nm, 40 mW cm^{-2}) and Vis light (550 nm, 20 mW cm^{-2}) respectively was fabricated (Figure 3-2g; Movie 3-S3, Supporting Information).

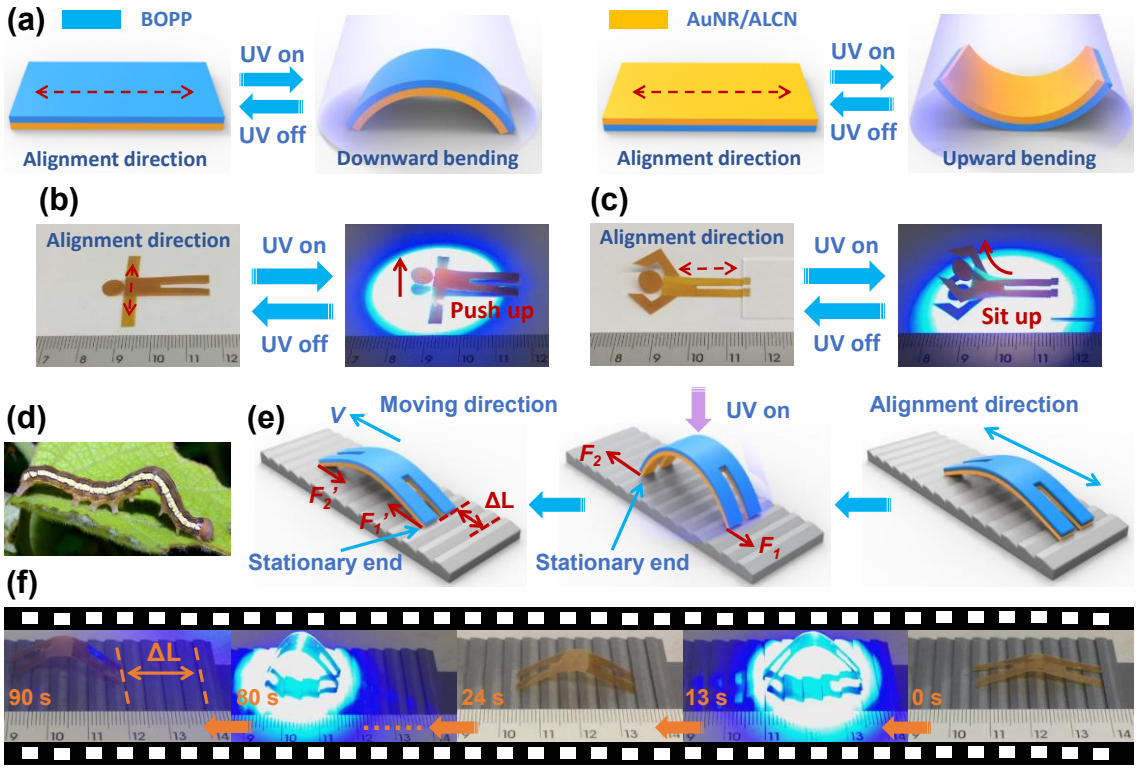

Figure 3-3. (a) Schematic illustration of two different reversible motion modes of the bilayer film upon turning on and off UV light. Photographs showing the plastic "athletes" performing different physical exercise motions, such as (b) push up and (c) sit up, upon on-off UV light illumination cycles (365 nm, 100 mW cm^{-2}). (d) The photo image of a caterpillar. (e) Schematic illustration of the force analysis for a light-driven caterpillar-inspired walker. (f) Photographs showing caterpillar-inspired walker crawling forward on a ratcheted substrate upon on-off UV light illumination cycles (365 nm, 100 mW cm^{-2}).

Sophisticated light-controlled motions can be achieved using our AuNR-ALCN nanocomposite material. On the one hand, it is known that rapid shape change recovery is essential for creating continuous material motions. Previous studies show that bilayer

structures can afford LC actuators with more tunable motion parameters, such as fast shape change recover rate, controllable moving direction and self-propelling motion modality.[5,13] On the other hand, for many plants and animals, sensing environmental changes and converting environmental stimuli (e.g., humidity, light or touch) into motions based on the localized, well-defined, hierarchical orientations of cellulose microfibrils,[8] myosin and actin filaments,[33] is an essential function for living activities. Being inspired by the above, we adapted the bilayer structure to enhance the photoresponsiveness of AuNR-ALCN and used the bilayer films to fabricate smart actuators that can execute localized, programmable and specified motion tasks. To this end, an AuNR-ALCN film was stretched to 200% strain and then laminated with a flexible transparent polypropylene film (biaxially oriented polypropylene, hereafter referred to as BOPP, ~ 45 μm in thickness, commercial transparent scotch-tape), leading to a bilayer film, namely AuNR-ALCN/BOPP. As schematized in **Figure 3-3**a, upon vertical UV light illumination, different bending directions can be achieved with the bilayer film bending downwards or upwards just by setting the AuNR-ALCN film as bottom layer or top layer, respectively. In the former case, upon receiving the UV light passed through the BOPP top layer, the bottom AuNR-ALCN layer reacts to contract while the bilayer interface tends to keep the length, which leads to the downward bending of the bilayer film. Because the UV-light-induced contraction (photoisomerization of the azobenzene moieties) only occurs in the surface region (within 1 μm) of the AuNR-ALCN film around the bilayer interface, a recoverable stress leading to an unbending force, with the help of the elastic recovery of the BOPP layer, may allow the bilayer film to recover the initial shape when turning off the UV light. While in the latter case, the bilayer film bends towards to the UV light as a result of the direct illumination on the top AuNR-ALCN layer. In both cases, the bending and unbending motions can repeat many times according to the repeated actuation cycles (Figure 3-2a,b). Based on these bending-direction-controllable bilayer films, we fabricated some plastic “athletes” that are capable of executing designed specific motions, such as push up (Figure 3-3b; Movie 3-S4, Supporting Information) and sit up (Figure 3-3c; Movie 3-S5, Supporting Information), by locally programming the alignment of azobenzene mesogens in the athlete’s arms and waist respectively. Furthermore, the excellent properties of the bilayer actuator were used in the demonstration of biomimetic

applications. Figure 3-3d,e shows the schematic illustration of a light-driven caterpillar-inspired walker that can crawl forward on a ratcheted substrate. Upon irradiation with UV light, the caterpillar walker undergoes downward bending, and the force analysis is shown in Figure 3-3e. Because of the ratcheted substrate surface, the front edge bearing larger frictional force (F_2>F_1) acts as a stationary end and thus the downward bending of the bilayer film leads to the forward moving of the back part of the caterpillar walker. Upon removal of the UV light, a recoverable unbending force due to the elastic recovery of the BOPP layer, may allow caterpillar walker to recover the original shape. In this case, the back edge bears larger frictional force (F_1'>F_2') and acts as a stationary end to allow for the caterpillar walker's forward moving of its front part, thus leading to caterpillar-like crawl along the ratcheted substrate at a speed of about 13 mm min^{-1} (Figure 3-3f; Movie 3-S6, Supporting Information).

Finally, the two different photoactuation behaviors of AuNR-ALCN were added up to demonstrate a proof-of-concept application by making a polymer crane that performs sophisticated photomechanical functions to produce useful work. To this end, a photo-manipulated LCP crane was fabricated by connecting a bilayer-film-made gripper to the end of a polymer telescopic arm, which was made of an AuNR-ALCN artificial muscle (**Actuator-2**, 50 mm × 5 mm × 0.17 mm) with a high heavy-lift capability that can lift up a load of ~ 90 times its own weight with a maximum contraction of 32% original length (Movie 3-S7, Supporting Information). It should be noted that a burden of 4.77 g was imposed on the telescopic arm (**Figure 3-4**a) in order to keep it vertical during the phototriggered contraction/extension movements. The schematic illustration (Figure 3-4a) and photographs (Figure 3-4b) show the photo-operated polymer crane executing a series of concerted robot-like motion tasks, including grasping, lifting up, lowering down, and releasing a tubular-shape polyurethane foam (Movie 3-S8, Supporting Information). Under illumination with UV light, the gripper grasps and firmly holds the tubular-shape object as a result of the two different bending modes of the bilayer film (Figure 3-3a). And then, upon illumination with a continuous-wave NIR light source (Flash Torch, Wicked Lasers, which provides >90% of the light in the NIR region, 1.6 W cm^{-2}),[13] the telescopic arm undergoes a rapid contraction in length due to the photothermally induced LC-isotropic

phase transition and lifts up the object by 1.32 cm, thus producing a work of 6.68×10^{-4} J (Figure 3-4a, g=9.803 m s^{-2}, the total weight of the burden is about 5.16 g, which is about 135 times heavier than the telescopic arm's own weight). At last, after removal of the NIR and UV light in sequence, the telescopic arm returns to its original state (extension) and the gripper liberates the object.

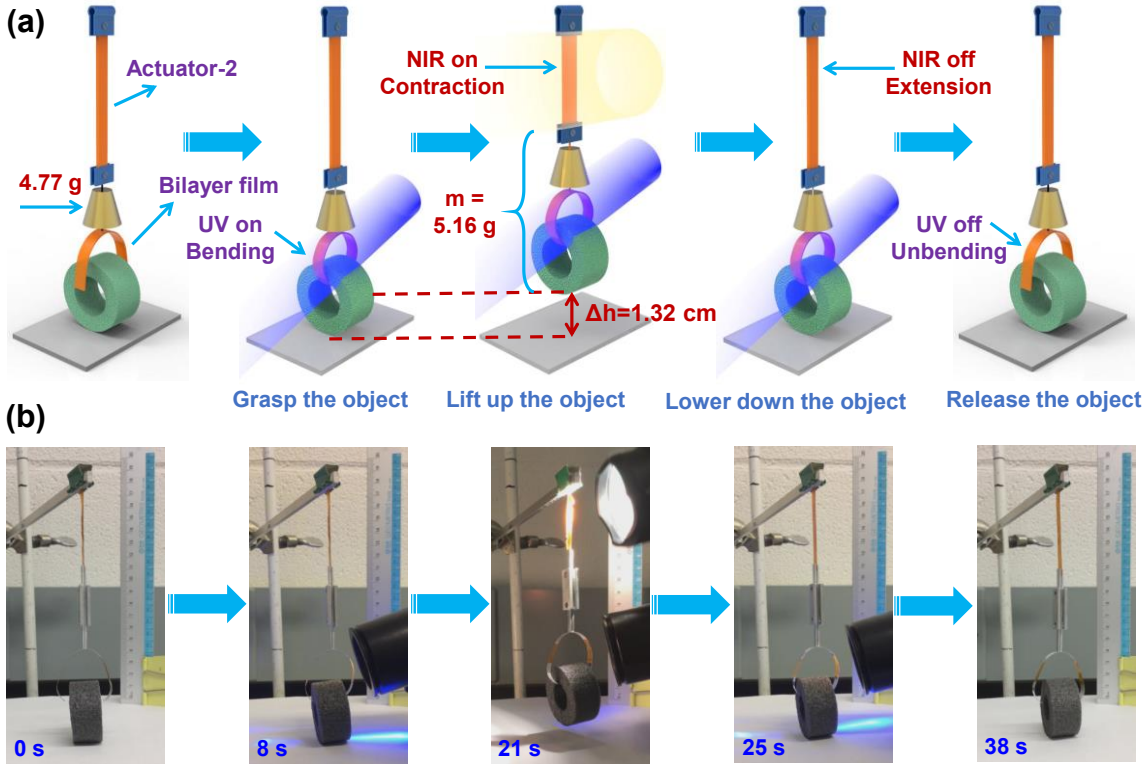

Figure 3-4. (a) Schematic illustration and (b) photographs showing the polymer "crane" executing a series of combinational light-driven robot-like motion tasks, including grasping, lifting up, lowering down, and releasing a tubular-shape object, along with producing a useful work of 6.68×10^{-4} J.

Before concluding this work, we mention some thoughts on the parameters that influence the photoinduced motions and that should be taken into consideration in the future modeling effort. Except the contraction/extension of the polymer arm in the "crane" (Figure 3-4), which is induced by the LC-isotropic phase transition across the sample due to the intense photothermal effect, the various types of macroscopic motions of our AuNR-ALCN actuators (Figures 3-2 to 3-4) are based on a photoinduced bending motion.

Generally, the extent of bending can be analyzed using a bilayer actuator model based on the linear beam theory,[34] in which the bending curvature is mainly determined by the ratio of the thicknesses of the two layers, the ratio of the moduli of the two layers and the mismatch strain at the interface between the two layers. In the present study, the situation is more complex. On the one hand, under UV light irradiation, considering that the *trans-cis* photoisomerization of azobenzene moieties takes place within 1 μm of the surface layer due to the high extinction coefficient (about 2.0×10^4 L mol^{-1} cm^{-1} at 365 nm),[31] the AuNR-ALCN film can be regarded as a bilayer actuator composed of a photoresponsive surface layer and a bottom layer. However, because the photochemical reaction of azobenzene is gradually diminishing due to the light attenuation along the thickness direction, the photoresponsive layer should have a gradient of contractile force, a gradient of modulus and a gradient of mismatched strain with respect to the bottom layer. On the other hand, for the bending based on photothermal effect, the absorption of NIR light by AuNR should undergo a similar attenuation effect and, as a result, there should be a temperature gradient along the actuator thickness direction. With this mechanism, the photoresponsive layer is defined by the depth where the actual heating raises the temperature above the LC-isotropic phase transition temperature. However, the bottom layer may still have a temperature gradient that changes the modulus along the thickness direction. In other words, bilayer actuator models with two definite layer thicknesses, layer moduli and one definite strain mismatch at the layer interface cannot by applied directly to the photoinduced bending motion of our AuNR-ALCN actuator under either UV light induced *trans-cis* photoisomerization of azobenzene or NIR light induced order-disorder phase transition. Actually, the situation is even more complicated by the lamination of the AuNR-ALCN with a polypropylene film. Nevertheless, the above analysis highlights the theoretical background of the photoinduced bending motion and points out the issues that need to be addressed in future modeling studies.

3.2.4. Conclusions

In summary, we have synthesized an AuNRs hybrid azobenzene liquid crystalline dynamic network with excellent processability and enhanced photocontrol for actuations, i.e., sensitive NIR and UV-Vis light responsiveness. The two different photoresponsive

mechanisms of AuNR-ALCNs, being the *trans-cis* photoisomerization of azobenzene as well as SPR absorption of NIR and heat release by AuNR, were investigated by employing the isostrain experiment to measure the phototriggered contraction force. Moreover, by taking advantages of bilayer structures, we successfully controlled the motion directions of AuNR-ALCNs. Based on this enhanced photocontrol of actuation, we could manipulate plastic "athletes" to execute designed specified motion tasks, such as push up and sit up, by locally inscribing molecular alignments in different regions of the bilayer actuators. Besides, a light-driven caterpillar-inspired walker that can crawl forward on a ratcheted substrate was demonstrated as a biomimetic application by making use of the rapid shape-change recover property of the bilayer film. Finally, the effects of the two light-triggered molecular changes, i.e., LC-isotropic phase transition and photoisomerization of azobenzene, were added up to design a polymer "crane" that is capable of performing light-controlled sophisticated, concerted robot-like, macroscopic motions to produce useful work. This work not only unveils a new method for the fabrication of photoresponsive LCP actuators based on two mechanisms but also takes a significant step forward towards their potential applications in artificial muscle and biomimetic soft robots.

Acknowledgements

Y. Zhao acknowledges the financial support from the Natural Sciences and Engineering Research Council of Canada (NSERC) and le Fonds de recherche du Québec: Nature et technologies (FRQNT). X. Lu, H. Zhang and B. Yu thank China Scholarship Council (CSC) for scholarship allowing them to study in Canada. H. Xia acknowledges the financial support of National Natural Science Foundation of China (51433006, 51473094). Y. Zhao is a member of the Centre québécois sur les matériaux fonctionnels (CQMF) funded by FQRNT.

Reference

[1] a) S. Palagi, A. G. Mark, S. Y. Reigh, K. Melde, T. Qiu, H. Zeng, C. Parmeggiani, D. Martella, A. Sanchez-Castillo, N. Kapernaum, F. Giesselmann, D. S. Wiersma, E. Lauga, P. Fischer, *Nat. Mater.* **2016**, 15, 647; b) H.-W. Huang, M. S. Sakar, A. J. Petruska, S. Pané, B. J. Nelson, *Nat. Commun.* **2016**, 7, 12263.

[2] C. Larson, B. Peele, S. Li, S. Robinson, M. Totaro, L. Beccai, B. Mazzolai, R. Shepherd, *Science* **2016**, 351, 1071.

[3] a) C. S. Haines, M. D. Lima, N. Li, G. M. Spinks, J. Foroughi, J. D. W. Madden, S. H. Kim, S. Fang, M. Jung de Andrade, F. Göktepe, Ö. Göktepe, S. M. Mirvakili, S. Naficy, X. Lepró, J. Oh, M. E. Kozlov, S. J. Kim, X. Xu, B. J. Swedlove, G. G. Wallace, R. H. Baughman, *Science* **2014**, 343, 868; b) L. Liu, M.-H. Liu, L.-L. Deng, B.-P. Lin, H. Yang, *J. Am. Chem. Soc.* **2017**, 139, 11333.

[4] J. Mu, C. Hou, H. Wang, Y. Li, Q. Zhang, M. Zhu, *Sci. Adv.* **2015**, 1, 1500533.

[5] a) X. Lu, S. Guo, X. Tong, H. Xia, Y. Zhao, *Adv. Mater.* **2017**, 29, 1606467; b) M. Yamada, M. Kondo, J.-i. Mamiya, Y. Yu, M. Kinoshita, C. J. Barrett, T. Ikeda, *Angew. Chem. Int. Ed.* **2008**, 47, 4986.

[6] a) K. Kumar, C. Knie, D. Bléger, M. A. Peletier, H. Friedrich, S. Hecht, D. J. Broer, M. G. Debije, A. P. H. J. Schenning, *Nat. Commun.* **2016**, 7, 11975; b) A. H. Gelebart, G. Vantomme, E. W. Meijer, D. J. Broer, *Adv. Mater.* **2017**, 29, 1606712.

[7] a) M. Ma, L. Guo, D. G. Anderson, R. Langer, Science **2013**, 339, 186; b) R. Tang, Z. Liu, D. Xu, J. Liu, L. Yu, H. Yu, *ACS Appl. Mater. Interfaces* **2015**, 7, 8393.

[8] P. Fratzl, F. G. Barth, *Nature* **2009**, 462, 442.

[9] a) T. J. White, D. J. Broer, Nat. Mater. **2015**, 14, 1087; b) C. Ohm, M. Brehmer, R. Zentel, *Adv. Mater.* **2010**, 22, 3366.

[10] D. L. Thomsen, P. Keller, J. Naciri, R. Pink, H. Jeon, D. Shenoy, B. R. Ratna, *Macromolecules* **2001**, 34, 5868.

[11] a) S. V. Ahir, A. R. Tajbakhsh, E. M. Terentjev, *Adv. Funct. Mater.* **2006**, 16, 556; b) I. A. Rousseau, P. T. Mather, *J. Am. Chem. Soc.* **2003**, 125, 15300.

[12] a) T. H. Ware, M. E. McConney, J. J. Wie, V. P. Tondiglia, T. J. White, *Science* **2015**, 347, 982; b) Z. Pei, Y. Yang, Q. Chen, E. M. Terentjev, Y. Wei, Y. Ji, *Nat. Mater.* **2014**, 13, 36.

[13] R. R. Kohlmeyer, J. Chen, *Angew. Chem. Int. Ed.* **2013**, 52, 9234.

[14] Y. Yang, W. Zhan, R. Peng, C. He, X. Pang, D. Shi, T. Jiang, Z. Lin, *Adv. Mater.* **2015**, 27, 6376.

[15] Z. Li, Y. Yang, Z. Wang, X. Zhang, Q. Chen, X. Qian, N. Liu, Y. Wei, Y. Ji, *J. Mater. Chem. A* **2017**, 5, 6740.

[16] M. Wang, B.-P. Lin, H. Yang, *Nat. Commun.* **2016**, 7, 13981.

[17] W. Liu, L.-X. Guo, B.-P. Lin, X.-Q. Zhang, Y. Sun, H. Yang, *Macromolecules* **2016**, 49, 4023.

[18] H. Yang, J.-J. Liu, Z.-F. Wang, L.-X. Guo, P. Keller, B.-P. Lin, Y. Sun, X.-Q. Zhang, *Chem. Commun.* **2015**, 51, 12126.

[19] Y. Yu, M. Nakano, T. Ikeda, *Nature* **2003**, 425, 145.

[20] J. J. Wie, M. R. Shankar, T. J. White, *Nat. Commun.* **2016**, 7, 13260.

[21] Y. Liu, B. Xu, S. Sun, J. Wei, L. Wu, Y. Yu, *Adv. Mater.* **2017**, 29, 1604792.

[22] C. Huang, J.-a. Lv, X. Tian, Y. Wang, Y. Yu, J. Liu, *Sci. Rep.* **2015**, 5, 17414.

[23] a) S. Iamsaard, S. J. Aßhoff, B. Matt, T. Kudernac, J. L. M. CornelissenJeroen, S. P. Fletcher, N. Katsonis, *Nat. Chem.* **2014**, 6, 229; b) S. J. Aßhoff, F. Lancia, S. Iamsaard, B. Matt, T. Kudernac, S. P. Fletcher, N. Katsonis, *Angew. Chem. Int. Ed.* **2017**, 56, 3261.

[24] A. H. Gelebart, D. Jan Mulder, M. Varga, A. Konya, G. Vantomme, E. W. Meijer, R. L. B. Selinger, D. J. Broer, *Nature* **2017**, 546, 632.

[25] O. M. Wani, H. Zeng, A. Priimagi, *Nat. Commun.* **2017**, 8, 15546.

[26] J.-a. Lv, Y. Liu, J. Wei, E. Chen, L. Qin, Y. Yu, *Nature* **2016**, 537, 179.

[27] a) Z. Cheng, T. Wang, X. Li, Y. Zhang, H. Yu, *ACS Appl. Mater. Interfaces* **2015**, 7, 27494; b) L. Zhou, Q. Liu, X. Lv, L. Gao, S. Fang, H. Yu, *J. Mater. Chem. C* **2016**, 4, 9993.

[28] M. Capelot, M. M. Unterlass, F. Tournilhac, L. Leibler, *ACS Macro Letters* **2012**, 1, 789.

[29] a) D. Montarnal, M. Capelot, F. Tournilhac, L. Leibler, *Science* **2011**, 334, 965; b) M. Capelot, D. Montarnal, F. Tournilhac, L. Leibler, *J. Am. Chem. Soc.* **2012**, 134, 7664.

[30] H. N. Beck, H. D. Ledbetter, *J. Appl. Polym. Sci.* **1965**, 9, 2131.

[31] a) T. Yoshino, M. Kondo, J.-i. Mamiya, M. Kinoshita, Y. Yu, T. Ikeda, *Adv. Mater.* **2010**, 22, 1361; b) M. Kondo, Y. Yu, T. Ikeda, *Angew. Chem. Int. Ed.* **2006**, 45, 1378.

[32] D. G. Whitten, P. D. Wildes, J. G. Pacifici, G. Irick, *J. Am. Chem. Soc.* **1971**, 93, 2004.

[33] a) H. Yin, M. D. Wang, K. Svoboda, R. Landick, S. M. Block, J. Gelles, *Science* **1995**, 270, 1653; b) N. Hirokawa, *Science* **1998**, 279, 519; c) R. D. Vale, R. A. Milligan, *Science* **2000**, 288, 88.

[34] a) M. Christophersen, B. Shapiro, E. Smela, Sens. *Actuators, B* **2006**, 115, 596; b) F. Greco, V. Domenici, A. Desii, E. Sinibaldi, B. Zupancic, B. Zalar, B. Mazzolai, V. Mattoli, *Soft Matter* **2013**, 9, 11405; c) S. Taccola, F. Greco, E. Sinibaldi, A. Mondini, B. Mazzolai, V. Mattoli, *Adv. Mater.* **2015**, 27, 1668.

3.2.5. Supporting Information

3.2.5.1. Materials

Unless otherwise stated, all solvents and reagents were purchased from Sigma Aldrich and used without further purification.

3.2.5.2. General characterizations

Differential scanning calorimetry (DSC) measurements were carried on a TA DSCQ2000 instrument. Samples were heated from 30 °C to 150 °C at a rate of 10 °C min^{-1} under nitrogen flow with a rate of 50 mL min^{-1}. X-ray diffraction (XRD) pattern was collected with a Bruker AXS Nanostar system equipped with a Microfocus Copper Anode at 45 kV/0.65 mA, MONTAL OPTICS and a VANTEC 2000 2D detector at 85.5 mm distance, from the samples calibrated with a Silver Behenate standard. UV-Vis-NIR absorption spectra were taken using a Varian 50 Bio spectrophotometer. The temperature of ALCE-ALCN upon NIR (785 nm) light irradiation was measured by sandwiching the probe of a digital thermometer (Fisher Scientific™ Traceable™ Expanded-Range Thermometers) between two ALCE-ALCN sheets. The isostrain measurements (experimental setup being shown in Figure 3-S3) at room temperature for **Actuator-1** and **Actuator-2** under UV (365 nm) and NIR (785 nm) light irradiation respectively, were performed on an Instron 5965 system with a 10 N load cell using the stress-relaxation mode. By applying UV or NIR light (normal incidence, light source 4 cm away) to a stripe-shaped sample held under constant strain (within 0.2%), the contractile force generated in the film can be sensed and measured. The UV-light-responsive motions of the ALCE-ALCN-based smart devices were performed by using a UV Spot Curing System (Omnicure® Series 1000) equipped with UV light filter (365 nm) and visible light filter (550 nm). The NIR-light-driven actuations of the ALCE-ALCN were conducted using a PM-785 laser with a wavelength of 785 nm and a tunable power output from 0 W to 1 W (Changchun New Industries Optoelectronics Tech. Co., Ltd). The light intensity was measured using a photometer (Oriel® Instruments). The muscle-like contraction/extension behaviors of **Actuator-2** were controlled using a continuous-wave NIR light source (Flash Torch, Wicked Lasers), which provides >90% of the light in the NIR region.

3.2.5.3. Synthesis of AuNRs stabilized with CTAB

Gold nanorods (AuNRs) stabilized with hexadecyltrimethylammonium bromide (CTAB) were synthesized based on a seed mediated growth procedure according to literature[S1]. The process was briefly stated as follows. Gold seed solution was firstly prepared in a 10 mL round flask, 365 mg CTAB was dissolved in 10 mL water. 100 μL $HAuCl_4$ stock solution (25 mmol L^{-1}) was added to this CTAB solution, and the mixture was vigorously stirred (1200 rpm) at room temperature. Then, 0.6 mL of ice-cold solution of 10 mmol L^{-1} $NaBH_4$ was added quickly to the above mixture and further stirred for 2 min. These seeds were aged for 2 h before use. The second step is the growth procedure. 3644.5 mg CTAB was dissolved in 100 mL water in a 250 mL round bottom flask. Other reagents were added to this solution in the following order: 1.0 mL of 10 mmol L^{-1} silver nitrate solution, 2.0 mL of 25 mmol L^{-1} aqueous $HAuCl_4$ stock solution, 0.2 mL of 1 mol L^{-1} HCl solution and 0.70 mL of 78.8 mmol L^{-1} L-ascorbic acid. This mixture was stirred gently (400 rpm) for 30 s. Afterwards 120 μL of seed solution was added, stirred for 30 s and left undisturbed overnight. The temperature of the growth step was kept constant at 29 °C during the whole process. The 100 mL fabricated AuNRs was centrifuged and the precipitate was redispersed in 5 mL of water.

3.2.5.4. Synthesis of AuNRs stabilized with PDMA

Poly(N,N-dimethylacrylamide) (PDMA M_n=2563 g mol^{-1}, PDI=1.15) was synthesized via RAFT polymerization[S2] using 2-cyano-2-propyl benzodithioate (CPDB) as RAFT agent and 2,2'-azobis(2-methylpropionitrile) (AIBN) as initiator. Then, PDMA was aminolysized by n-butylamine to yield thiol-terminated PDMA according to literatures.[S3] PDMA stabilized AuNRs were prepared by ligand exchange. Briefly, a 250 mL beaker was filled with 1 g thiol-terminated PDMA and 100 ml H_2O with a magnetic stirring bar. After the polymer was completely dissolved, the above-prepared concentrated AuNRs was added dropwise into this polymer solution. The whole mixture was further stirred for 6 h. Finally the solution was centrifuged and redissolved in N,N-dimethylformamide to obtain the final AuNR solution.

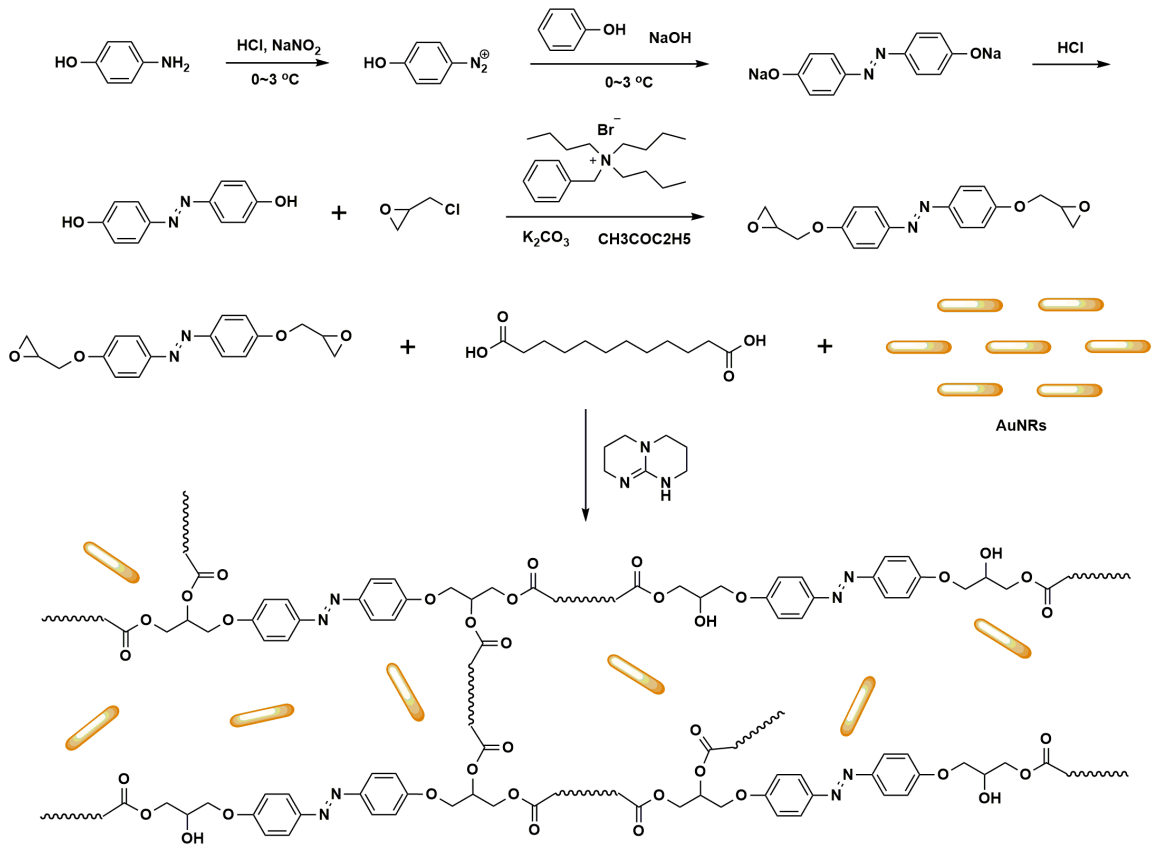

Figure 3-S1. Synthesis routes to the AuNR hybrid azobenzene liquid-crystalline networks (AuNR-LCNs).

3.2.5.5. Synthesis of AuNR-ALCNs

4,4'-diglycidyloxy-azobenzene was synthesized according to the literature[S4]. The azobenzene liquid crystalline networks were synthesized through several steps (Figure 3-S1). Typically, a stoichiometric amount of AuNRs solution (285 μL, 1 mg mL^{-1}) (the Au content of the nanocmposite is ~0.05wt%), 4,4'-diglycidyloxy-azobenzene (326 mg, 1.0 mmol), dodecanedioic acid (230 mg, 1.0 mmol) and 1,5,7-triazabicyclo[4.4.0]dec-5-ene catalyst (14 mg, 5 mol% to the COOH groups) were dissolved in anhydrous N,N'-dimethylacetamide (2 mL) in a glass vial (20 mL). The resulting mixture was heated at 145 °C for 12 hours in an oil bath to yield brown solid. The nanocomposite was further dried under vacuum at 145 °C for 12 h.

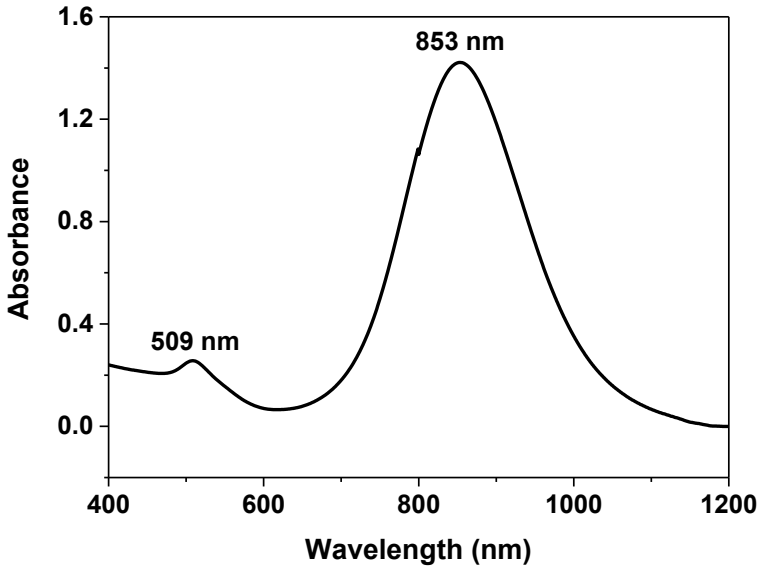

Figure 3-S2. The absorption spectrum of AuNRs solution (stabilized with CTAB). The absorption peaks at 509 nm and 853 arise from the transverse and longitudinal surface plasmon resonance (SPR) respectively.

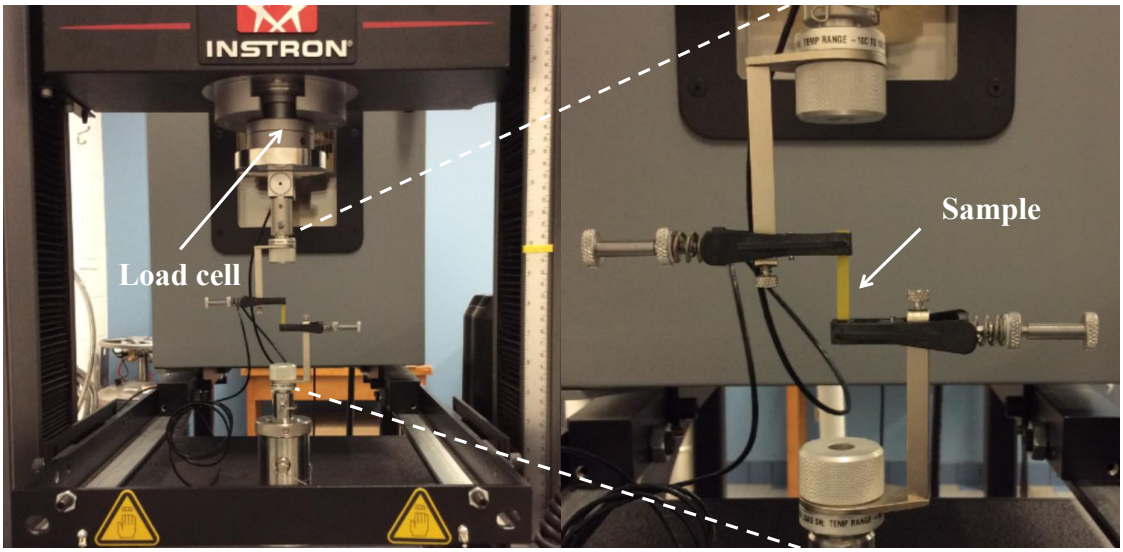

Figure 3-S3. Photographs of the experimental setup used for measuring photoinduced contraction force under the isostrain condition.

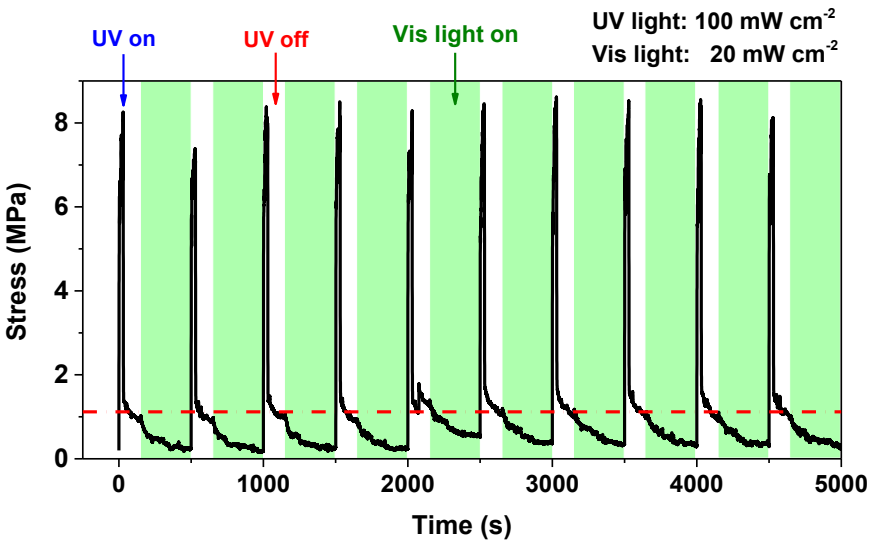

Figure 3-S4. Actuation stress as a function of time as UV light (with different intensities) is periodically turned on (time, 30 s) and off (time, 120 s) on the film (200% strain, 20 mm × 3.5 mm × 20 μm), followed by illumination with visible light for 350 s in each cycle.

[S1]B. Nikoobakht, M. A. El-Sayed, *Chem. Mater.* **2003**, 15, 1957; b) Z. Guo, C. Gu, X. Fan, Z. Bian, H. Wu, D. Yang, N. Gu, J. Zhang, *Nanoscale Res. Lett.* **2009**, 4, 1428.

[S2] J. Chiefari, Y. K. Chong, F. Ercole, J. Krstina, J. Jeffery, T. P. T. Le, R. T. A. Mayadunne, G. F. Meijs, C. L. Moad, G. Moad, E. Rizzardo, S. H. Thang, *Macromolecules* **1998**, 31, 5559.

[S3] 1) V. Lima, X. Jiang, J. Brokken-Zijp, P. J. Schoenmakers, B. Klumperman, R. Van Der Linde, *J. Polym. Sci., Part A: Polym. Chem.* **2005**, 43, 959; 2) D. L. Patton, M. Mullings, T. Fulghum, R. C. Advincula, *Macromolecules* **2005**, 38, 8597. 3) X.-P. Qiu, F. M. Winnik, *Macromol. Rapid Commun.* **2006**, 27, 1648; 4) J. Xu, J. He, D. Fan, X. Wang, Y. Yang, *Macromolecules* **2006**, 39, 8616; 5) X.-P. Qiu, F. M. Winnik, *Macromolecules* **2007**, 40, 872; 6) A. P. Vogt, B. S. Sumerlin, *Soft Matter* **2009**, 5, 2347.

[S4] J.-a. Lv, W. Wang, J. Xu, T. Ikeda, Y. Yu, *Macromol. Rapid Commun.* **2014**, 35, 1266.

3.3. Summary of the Project

In the present work, we took a significant step forward in designing azobenzene based LCNs and actuators. We synthesized, for the first time, near-infrared light (NIR) and UV light responsive polymer nanocomposite by doping polymer-grafted gold nanorods into azobenzene liquid crystalline dynamic networks (AuNR-ALCNs). Both the NIR and UV light-triggered contraction force of oriented AuNR-ALCNs specimens was measured using the isostrain experiment, showing the action of the two different photoresponsive mechanisms through the photochemical reaction of azobenzene and the photothermal effect due to the surface plasmon resonance (SPR) absorption of NIR by AuNRs, respectively. Moreover, taking advantage of the easy processability, bilayer actuators of AuNR-ALCNs can be fabricated, of which the photoinduced bending/unbending directions can be controlled, and localized actuations can be realized through programmed alignment of azobenzene mesogens in selected regions. A series of versatile and complex motions making use of the enhanced photocontrol of actuation were demonstrated. These include plastic "athletes" that can execute light-controlled motion tasks such as push up and sit up, as well as light-driven, caterpillar-inspired walker that can crawl forward on a ratcheted substrate at a speed of about 13 mm min^{-1}. Finally, the effects of the two types of light-triggered molecular motions, i.e., LC-isotropic phase transition and photoisomerization of azobenzene mesogens, were added up to design a polymer "crane" that is capable of performing light-controlled, concerted, robot-like motions including grasping, lifting up, lowering down and releasing an object. Our approach to preparing azobenzene LCN based actuators that are responsive to both NIR and UV-visible lights in addition to be easily processable, is general and extensible.

CHAPITRE 4. GENERAL DISCUSSION AND PERSPECTIVES

Equation Chapter 4 Section 1

The research work presented in this thesis is centered on developing novel reprocessable polymers that are capable of stimuli-controlled shape memory, self-healing and motions. The research targets designing new molecular structures, exploring novel stimulation methods and creating sophisticated motions.

In the first project, we present ultrasound-healable shape memory dynamic polymers via a precise polymer architecture design that simultaneously integrates superior mechanical properties, ultrasound responsiveness, shape memory and self-healing ability into one material. The polymers are designed as polyurethane (PU) networks with poly(ε-caprolactone) (PCL) and Diels-Alder (DA) adducts (furan-maleimide) alternatively positioned in the backbone of polymer chains between adjacent crosslinking points. The choice of these components is driven by their ability to deliver specific functions. PU as a class of high-performance polymeric materials can provide desired combination of stiffness, strength, extensibility and toughness (162,163); PCL as a reversible phase can afford shape memory effect to close the cracks; and DA adducts provide HIFU sensitivity to undergo reversible bond breaking and reformation across fractured surfaces to allow self-healing. We conducted the SAXS experiments to study the relationship between the mechanical properties and microstructures of the polymer. The microphase-separated structures endow the dynamic polymers with excellent mechanical properties, such as high Young's modulus and elongation. Furthermore, we used small-molecule analogues to demonstrate the HIFU-responsiveness of the DA bonds, and the results show that furan and maleimide groups are responsible for the re-building of the damaged polymer structure owing to its dynamic and exchangeable features upon exposure to HIFU. We also demonstrated the high healing efficiency of the designed polymer by comparing with two control polymers. To our knowledge, no studies on the use of ultrasound to trigger shape memory-assisted self-healing of covalently cross-linked dynamic polymers were reported previously. The distinct advantages of this novel stimulation modality over thermally or optically healable systems include: 1) localized, on-demand repair can be easily achieved in a remote and controlled way; 2) ultrasound can penetrate much deeper into the interior of the materials than light; and 3) due to the non-invasive and non-radiative property of HIFU, this strategy has potential applications in the field of biomedical device engineering,

such as triggering shape memory and/or self-healing of implants like pacemakers, artificial hip and knee to avoid the secondary injury during removal of implant materials.

In the second project, we developed azobenzene liquid crystalline elastomer actuators displaying light-controlled continuous motions by pre-storing strain energy in the dynamic polymer films. The polymers are designed as epoxy-acid derived network with azobenzene mesogens located in the chain backbone using transesterification-based dynamic covalent crosslinking. There are two unique features in the rational polymer design. On the one hand, azobenzene mesogens not only can undergo order-disorder transition (LC phase to isotropic phase transition) upon heating but also can experience *trans-cis* photoisomerization under UV light irradiation, allowing more stimuli-responsiveness (photothermal effect and photo mechanical effect) to conduct shape change and motions. On the other hand, different from other thermally reversible bond (such as DA bond) that undergo bond breaking at high temperature, the catalytic transesterification reaction used in this study takes place without modification of the numbers of ester links and average functionality, thus promising good mechanical properties of the polymer even at high temperature. We demonstrated that by pre-storing mechanical strain energy in ALCE films, unprecedented contraction force can be generated. The relationship between the storing-strain energy, actuation force, motion speed of ALCE actuator was studied. Moreover, the motion direction and mode of the ALCE actuator was also explored.

Based on the second research project, we prepared AuNR-ALCNs nanocomposites with both NIR and UV-Vis responsiveness in order to further enhance the photocontrol of liquid crystal polymer. We studied the two different photoresponsive behaviors and mechanisms, as well as the relationship between the actuator structure and motion direction, motion location, and motion mode. In addition, the effects of the two types of light-triggered molecular motions, i.e., LC-isotropic phase transition and photoisomerization of azobenzene mesogens, were added up to fabricate actuators that was capable of performing novel sophisticated motions.

4.1. General Discussion

4.1.1. Ultrasound-Healable Dynamic SMPs

Self-healing materials based on dynamic covalent bonds, such as Diels-Alder bond, disulfide, trithiocarbonate and transesterification chemistry, can repair themselves via reversible breaking and reformation of dynamic bonds that build up their structures. Using direct heating to initiate exchangeable or reshuffling reactions in dynamic polymers to achieve self-healing is the most common and convenient way. However, direct heating is not applicable or inefficient in many application circumstances. For example, if the polymer implants are made of SHPs, it is unpractical to take them out for repairing. One way to solve this problem consists in incorporating some stimuli-responsive bonds into the polymer structure or embedding some stimuli-responsive fillers into the polymer matrix. These reversible bonds or fillers are able to absorb other forms of energy, such as electrical, optical or magnetic energies to initiate bond breaking and reformation to repair the polymer. Those stimuli can provide special features for triggering self-healing of materials that direct heating does not have. For instance, light can offer the possibility of controlling the self-healing process remotely, meaning that the stimuli can be applied from a source located far from the dynamic polymers. This feature is particularly important for some conceivable application circumstances like in space, deep sea or even human body.

Using ultrasound, compared to the previously developed stimuli as mentioned above, offers some unique advantages in repairing materials. Firstly, the ultrasound induced thermal effect, which is based on viscous shearing motion and friction of polymer chains during ultrasonic wave propagation, can be directly employed to trigger the exchange or reshuffling reaction of thermally reversible dynamic bonds to create thermal effect similar to direct heating. There is no need to incorporate additional fillers or compounds into the polymer system, which makes the preparation of self-healing polymers easier and has no need to consider the properties changes caused by the addition of the fillers. Secondly, since the ultrasound waves can be focused into a small spot (~ 3 mm in diameter for HIFU), localized, on-demand repair can be easily achieved in a remote and spatially controlled way. Moreover, even comparing with light, ultrasound can go deep into human body in a non-invasive and non-radiative way, which is an important advantage for biomedical applications. As a matter of fact, ultrasound has already been an well-developed technology for

the treatment of tumors. It can be imagined that the repairing of inserted tubes, stents or artificial organs made of SHPs can be readily controlled at any part of the human body and at any time using ultrasound.

On the basis of our findings, both the thermal and mechanical effects of HIFU are crucial for efficient ultrasound induced temperature rise and initiating the dynamic feature of DA bonds. Since vigorous polymer chain oscillation, friction and vibrations can take place in many viscoelastic polymers upon exposure to ultrasound, the method can be applied to a wide range of dynamic materials that are thermosensitive and/or mechano-responsive. To this regard, reversible chemical bonds, either covalent or non-covalent, or even "mechanophores" can be used to construct the polymer network, and they may be labile to thermal effect or mechanical force generated by ultrasound. To our knowledge, no studies on the use of ultrasound to trigger self-healing of covalently cross-linked dynamic polymers were reported previously. This is also something that is not achievable using other stimuli, because all of them are based on temperature rise induced by incorporated functional fillers, involving no polymer chain movement during the heating procedure. Upon ultrasound irradiation, the thermal, mechanical and cavitation effects will trigger dynamic bonds or mechanophores to undergo exchangeable or reshuffling reactions and cause a concomitant reversible degradation of the polymer network, which is followed by wetting, diffusion and re-entanglement of polymer chains in the crack region. The reformation of the dynamic bonds or mechanophores then takes place when the HIFU is switched off, resulting in self-healing in a selected area with accuracy and minimum side effects on the undamaged region.

On the other hand, with the self-healing materials developed so far, small cracks can be repaired but the deformation and deformation-induced large cracks resulting from external force are difficult to heal. In most situations, damage is caused or accompanied by plastic deformation. For example, the deformation and damage of automobile bumper caused by car crash is difficult to repair by employing microcapsule self-healing materials or single dynamic self-healing materials. Deformed parts usually require manual operation to recover their original shapes. In certain situations, the deformed parts cannot even be removed for repairing. Moreover, if the original shape cannot be recovered, the damages separated by cracks will not be repaired. In order to resolve this problem, shape memory function was introduced into the materials to assist the self-healing effect, as demonstrated in our study.

4.1.2. Photocontrolled Motions of LCE Actuators

Light-driven azobenzene liquid crystalline elastomer (denoted as ALCE) actuators have been attracting broad and growing interest in recent years because of their versatility in creating material motions, such as bending, rolling, walking, oscillating and twisting. However, there are still two challenges that need to be addressed. On the one hand, the ALCEs are usually covalently cross-linked polymers, which show large deformation and fast response. In ALCEs, the conformation of polymer chains is strongly coupled with the alignment of mesogens, and once crosslinked, the change in conformation can be largely amplified into macroscopic deformation. On the other hand, reprocessing is a common challenge in cross-linked systems such as elastomers, resins, and gels as they are insoluble and infusible. Leibler and co-workers developed a novel epoxy resin with ester bonds undergoes transesterification in the presence of catalysts, which allows reshaping and remolding of the polymers even after the formation of network structures. Ji and co-workers made use of this transesterification by incorporating mesogens into epoxy-based vitrimers. The incorporation of dynamic covalent bonds enables fabrication of cross-linked LCEs with good processability and high alignment of the mesogens. To our knowledge, no studies exploring dynamic ALCEs have been reported when we started this project. Therefore, we employed transesterification chemistry to enable fabrication of crosslinked systems with high processability, allowing infinite designs of functional materials. On the other hand, reversible deformations or motions of ALCE actuators stem from the combination of the reversible trans-cis photoisomerization of azobenzene moieties and the cooperative motion of liquid crystal mesogens. Although it works well in many cases as reported in the literature, how to convert a change in molecular geometry (e.g., azobenzene after photoisomerization) into an efficient macroscopic motion remains challenging. Any light-driven motion requires a photoinduced mechanical force. This force in azobenzene LCEs or LCNs (liquid crystalline polymer networks) is small, partly due to the very low achievable efficiency of the optical to mechanical energy conversion. Therefore, the photoinduced force arising from direct optical to mechanical energy conversion may not be strong enough to allow robust (fast and continuous) motion of large-size polymer actuators, which needs large forces. In this study, we made use of pre-storing mechanical strain energy in ALCE films to greatly amplify the photoinduced mechanical force. Upon exposure to UV light, unprecedented contraction force can be generated in the ALCE films as a result of the

phototriggered release of the stored strain energy as well as the direct optical to mechanical energy conversion stemming from the trans-cis photoisomerization of azobenzene.

Mechanical responsiveness to environmental stimuli, an intrinsic property of plants, enables the performance of diverse vital tasks and activities, such as seed dispersal (164,165), self-protection (166,167) and food acquisition (168,169). These mechano-responsive motions stem from the internal microscopic helical structure (166,170,171) of the plants. For example, torsional movements, including the twisting of wood cells (172), helical motion of tendrils (173) and coiling of awns (174), strongly rely on the orientation of cellulose fibrils embedded in a matrix of hemicellulose, lignin, pectin, and structural proteins. Inspired by this improved understanding of the structure-response relationships in plants, people can manipulate the microscopic structure of the ALCE to provide the actuator with controllable motion direction and mode by controlling the orientation of the azobenzene mesogens.

4.1.3 Enhanced Photocontrol of Actuations Motions of AuNR-ALCN Actuators

Stimuli-responsive liquid crystalline polymer networks (LCNs) actuators are a class of "smart" polymer systems that are capable of receiving stimuli from the external environment such as temperature, light, pH, electric fields, magnetic fields, humidity and chemicals to induce change of their own molecular alignment or liquid crystal phase, thus affecting their physical and chemical properties and then triggering the corresponding macroscopic deformations or motions. Many researches show that photoresponsive LCN incorporating with azobenzene mesogens (ALCN) are among the most promising materials for applications in the fields of artificial muscles, sensors and flexible robots. However, even numerous progress achieved in the field of photoresponsive ALCN actuators, there are still some issues that remain in adding up the effects of the two light-triggered molecular changes, i.e., LC-isotropic phase transition and photoisomerization of azobenzene, into one actuation behavior. On the other hand, near-infrared (NIR) light (with a wavelength of about 700 to 1000 nm) is often used as the stimulus for drug release in the field of biomaterials, due to its good penetrability, non-contaminative and non-destructive properties, as well as its harmless feature to healthy human cells compared to UV light. In this study, we successfully enhanced the photocontrolled actuations of LCNs by doping the polymer with gold nanorods to endow the materials with NIR light responsiveness due to the surface plasmon resonance (SPR) absorption

of AuNRs. Besides, the moving direction, actuation location and motion mode have very important relationships with the actuator structure. We employed bilayer structure to control the motion direction of AuNR-ALCN actuators. Furthermore, we successfully achieved localized actuations through programmed alignment of azobenzene mesogens in selected regions. Our approach to preparing ALCN based actuators that are responsive to both NIR and UV-visible lights in addition to be easily processable, is general and extensible.

4.2. Future Studies

Monomer-Recyclable Azobenzene Liquid Crystalline Polymer Actuators

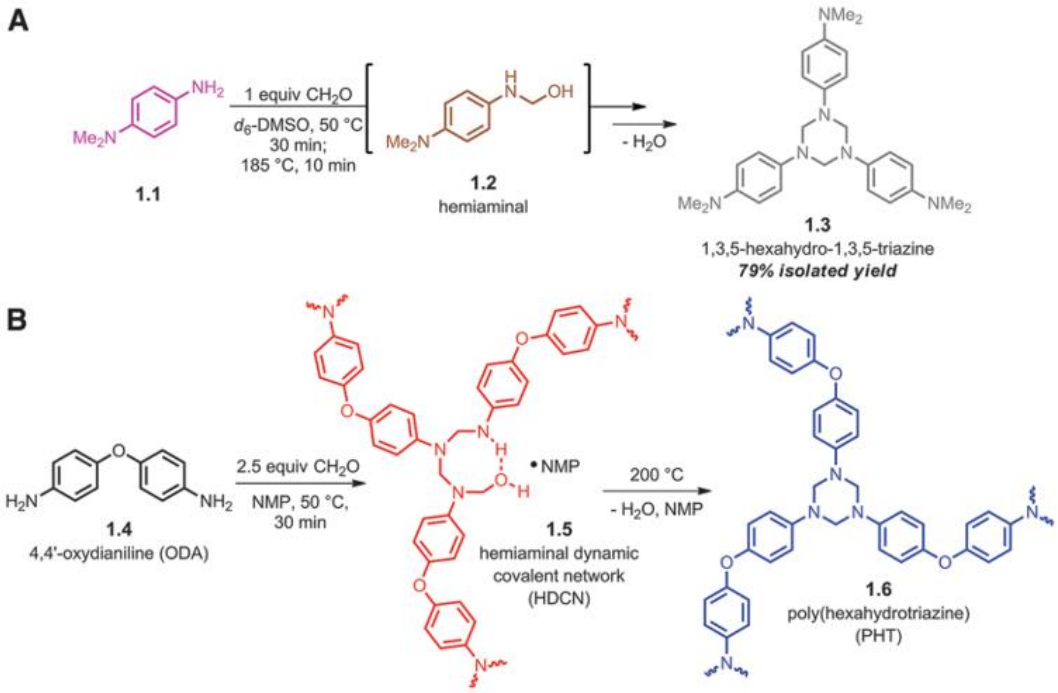

Figure 4-1. (A) Representative model reaction between N,N-dimethyl-*p*-phenylene diamine (1.1) and stoichiometric paraformaldehyde. Hemiaminal 1.2 is an intermediate to hexahydrotriazine 1.3 (isolated in 79% yield). (B) Polycondensation of ODA and paraformaldehyde. At low temperatures, an HDCN formed, plasticized with ~27% NMP and water. At higher temperatures, the PHT formed. [175]

Due to the high stake of development and applications of azobenzene LCE actuators, research on these smart functional materials will remain intense for still many years to come. On the basis of

the knowledge generated by this thesis, many future studies are worth being conducted. As discussed above, the development of remoldable or self-healing ALCE actuators is still in an early stage and few strategies have been explored until now. Recently, Hedrick and coworkers (175) developed hemiaminal dynamic covalent networks (HDCNs) using a simple one-pot, low-temperature polycondensation between paraformaldehyde and 4,4′-oxydianiline (ODA) (Figure 4-1 and 4-2). The HDCNs could further cyclize at high temperatures, producing poly(hexahydrotriazine)s (PHTs). Both materials possess mechanical properties comparable to strong thermosetting polymers, and the PHTs have very high Young's moduli (up to ~14.0 GPa and up to 20 GPa when reinforced with surface-treated carbon nanotubes), excellent solvent resistance, and resistance to environmental stress cracking. Moreover, both HDCNs and PHTs could undergo degradation at low pH (<2) to recover the bisaniline monomers.

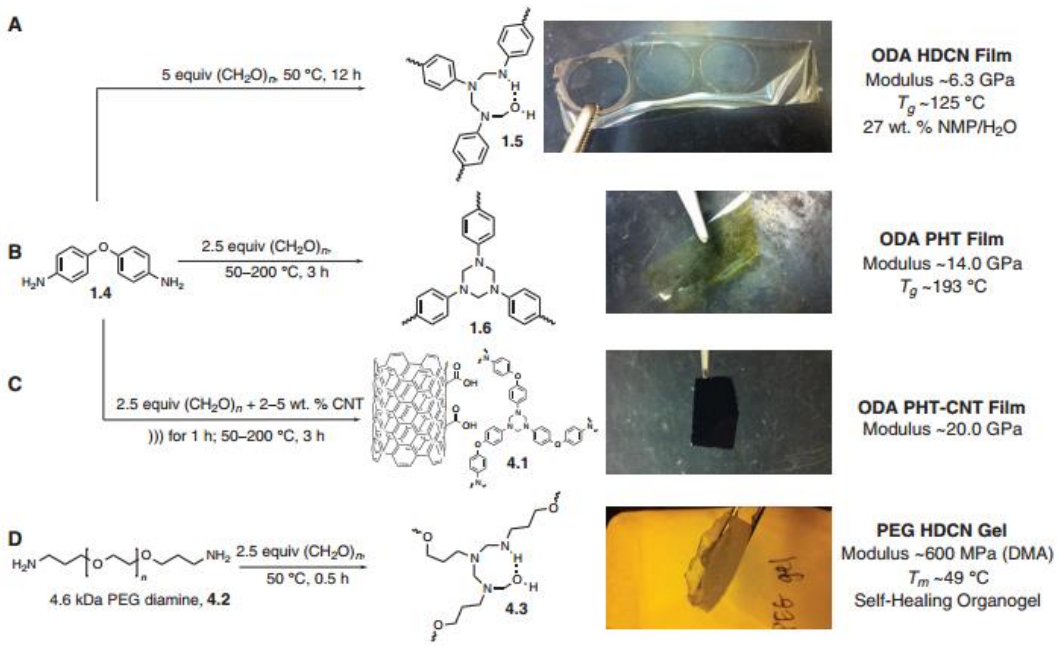

Figure 4-2. (A) ODA HDCNs are cross-linked polymer networks plasticized with NMP and water that show high modulus (~6.3 GPa), are flexible, and processable. The T_g was ~125 °C and films underwent decomposition into monomers in strongly acidic solutions (pH <2) within an hour. (B) ODA PHTs exhibited a modulus of ~14.0 GPa, are robust materials, and are resistant to bases, oxidants, and solvents. Rigid PHTs showed a T_g of ~192 ℃ and degraded at ~300°C. PHTs degraded into monomers after long exposure (>24 hours) to strong acid. (C) PHT film reinforced with 2 wt % of multiwalled, surface-oxidized CNTs exhibited a Young's modulus of ~20.0 GPa.

(D) An HDCN derived from 4.6-kD PEG diamine formed a self-healing organogel, which was reversible in neutral water after 24 hours. [175]

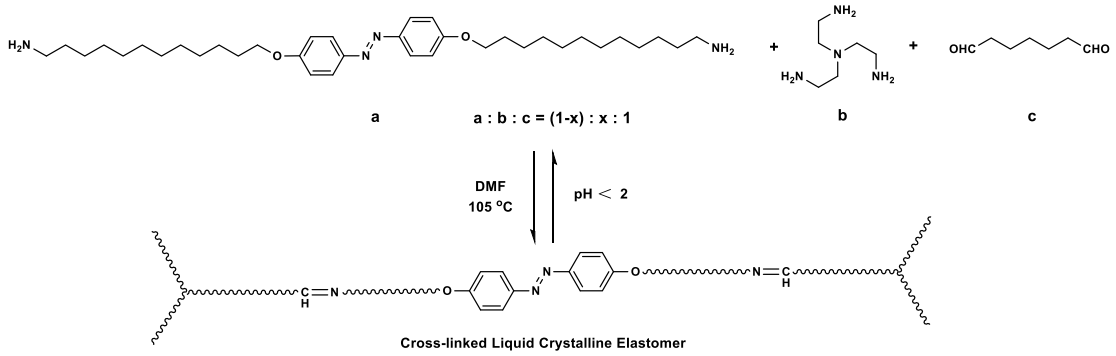

Figure 4-3. Synthesis and illustration of monomer-recyclable azobenzene liquid crystalline elastomers.

Inspired by this recent progress, we design a monomer-recyclable dynamic azobenzene LCEs which could decompose at low pH (<2) to recover the liquid crystal monomers. This may represent a future direction in this research field. As illustrated in Figure 4-3, the cross-linked liquid crystalline elastomer with dynamic imine bond is synthesized through the Schiff base reaction among azobenzene monomer **a**, tri-amine **b** and glutaraldehyde **c**. The cross-linking density can be tuned by changing the content of tri-amine **b**. It is reported that imine bond not only can be used to synthesize thermally malleable polymer network (176) but also can be employed to prepare dynamic materials that undergo decomposition and re-polymerization at pH＜4 and pH＞4 respectively (67). At high temperature, this dynamic cross-linked ALCEs can be re-programed or re-processed into desired shapes for the fabrication of polymer actuators owing to the exchanged or reshuffling reactions of the imine bonds. And at low pH, this ALCEs can decompose to recover the liquid crystal monomers **a**, and the liquid compounds **b** and **c** can be removed very easily. Based on this unique feature, the azobenzene monomers a can be re-used to prepare ALCE nanocomposite incorporated with CNTs, AuNPs or AuNRs, enabling the cyclic utilization from pure polymers to polymer nanocomposites, which is difficult for other dynamic LCEs or ALCEs as it is very difficult to disperse the nano-fillers into the pure polymer networks. Furthermore, such dynamic ALCEs can be used to fabricate polymer actuators with complex structures that can respond to light to exhibit sophisticate motions.

CONCLUSIONS

The research works reported in this thesis were focused on the design, fabrication and investigation of reprocessable polymers using dynamic covalent bonds that display the smart functionalities of stimuli-controlled shape memory, self-healing and motions. The results leading to the publication of three papers in top materials chemistry journals, have contributed to advancing the fundamental knowledge and understanding on design, novel stimulation methods and control of stimuli-responsive polymer materials. On one hand, we demonstrated for the first time that ultrasound (HIFU) could be used as a novel stimulus to trigger shape memory assisted self-healing of covalently cross-linked dynamic polymers. We found that high mechanical strength and toughness, excellent ultrasound responsiveness and efficient shape memory assisted self-healing property can be endowed to the same polymer based on rational material design using Diels–Alder bonds in the polymer structure. Rapid and prominent temperature rise in ultrasound-exposed region was observed, as the dynamic polymer could be heated above T_m (~58 ºC) from room temperature within several seconds (HIFU power output 5 W), leading to fast crack closure by shape recovery. The dynamic motifs embedded in the polymer can respond to HIFU to undergo bond breaking and reformation to realize the self-healing. Moreover, as one of the distinct features of HIFU-triggered self-healing, the localized and directed repairing can be achieved in a remote and controlled manner. This novel modality can be potentially applied for long term load-bearing engineering components, as well as anti-fatigue medical devices like pacemakers, artificial hip and knee used in the biomedical engineering.

The second part of the thesis work was dedicated to developing novel malleable azobenzene liquid crystalline elastomers using transesterification-based dynamic covalent crosslinking. We demonstrated that by pre-storing mechanical strain energy in ALCE films, unprecedented contraction force can be generated by UV light irradiation as a result of the synergistic effect between the phototriggered release of the stored energy and the photomechanical effect stemming from the trans-cis photoisomerization of azobenzene. Furthermore, by making use of the energy-storing ALCE films, we have been able to construct large polymer photo-actuators in the form of wheels or spring-like “motors” and adjust the amount of pre-stored strain energy in the polymer to achieve a variety of robust light-driven motions with tunable rolling or moving direction and speed.

The last part of the thesis aims at enhancing the photocontrolled motion of ALCN actuators and providing the actuators with more sophisticated motion modes. In this section, we propose a strategy by doping polymer-grafted AuNRs into dynamic ALCNs to enable NIR light and UV light responsive actuations and adopting bilayer structure to provide the actuators with different moving direction and localized motion mode. In addition, we simultaneously applied the photothermal and photochemical effects of ALCNs in one intelligent device to trigger actuators to execute sophisticated motion tasks and to do useful work. This work not only provides new insight into the manufacture of liquid crystal actuators for multiple responses, but also makes light-responsive polymer actuators an important step in the application of artificial muscles and bionic flexible robots.

In conclusion, we have made significant contributions to stimuli-responsive polymers through development of rationally designed material structures and new stimulation methods. Our studies show that using ultrasound to trigger shape recovery assisted self-healing is attractive by virtue of its advantages over other stimuli. Moreover, our demonstrated strategy for generating large photoinduced mechanical force to enable robust photocontrolled motions as well as the approach to preparing reprocessable liquid crystalline elastomer actuators also added fundamentally new knowledge to the related fields and may have a lasting impact. Further basic research for understanding these stimuli-responsive polymers as well as a sustained effort for their application exploitation are needed.

BIBLIOGRAPHIE

1. M. A. C. Stuart, W. T. S. Huck, J. Genzer, M. Muller, C. Ober, M. Stamm, G. B. Sukhorukov, I. Szleifer, V. V. Tsukruk, M. Urban, F. Winnik, S. Zauscher, I. Luzinov and S. Minko, *Nat. Mater.*, **2010**, 9, 101-113.
2. P. Theato, B. S. Sumerlin, R. K. O'Reilly and I. I. I. T. H. Epps, *Chem. Soc. Rev.*, **2013**, 42, 7055-7056.
3. R. J. Wojtecki, M. A. Meador and S. J. Rowan, *Nat. Mater.*, **2011**, 10, 14-27.
4. D. Habault, H. Zhang and Y. Zhao, *Chem. Soc. Rev.*, **2013**, 42, 7244-7256.
5. Y. Yang and M. W. Urban, *Chem. Soc. Rev.*, **2013**, 42, 7446-7467.
6. A. Lendlein and S. Kelch, *Angew. Chem. Int. Ed.*, **2002**, 41, 2034-2057.
7. R. Mohr, K. Kratz, T. Weigel, M. Lucka-Gabor, M. Moneke and A. Lendlein, *PNAS*, **2006**, 103, 3540-3545.
8. A. Lendlein, H. Jiang, O. Junger and R. Langer, *Nature*, **2005**, 434, 879-882.
9. G. Li, G. Fei, H. Xia, J. Han and Y. Zhao, *J. Mater. Chem.*, **2012**, 22, 7692-7696.
10. W. M. Huang, B. Yang, L. An, C. Li and Y. S. Chan, *Appl. Phys. Lett.*, **2005**, 86, 114105.
11. L. Wu, C. Jin and X. Sun, *Biomacromolecules*, **2011**, 12, 235-241.
12. J. S. Sodhi and I. J. Rao, *Int. J. Eng. Sci.*, **2010**, 48, 1576-1589.
13. H. Zhang, H. Xia and Y. Zhao, *J. Mater. Chem.*, **2012**, 22, 845-849.
14. H. Zhang, J. Zhang, X. Tong, D. Ma and Y. Zhao, *Macromol. Rapid Commun.*, **2013**, 34, 1575-1579.
15. H. Zhang and Y. Zhao, *ACS Appl. Mater. Interfaces*, **2013**, 5, 13069-13075.
16. H. Zhang, H. Xia and Y. Zhao, *ACS Macro Letters*, **2014**, 3, 940-943.
17. H. Koerner, G. Price, N. A. Pearce, M. Alexander and R. A. Vaia, *Nat. Mater.*, **2004**, 3, 115-120.
18. Y. Liu, J. K. Boyles, J. Genzer and M. D. Dickey, *Soft Matter*, **2012**, 8, 1764-1769.
19. L. Fang, S. Chen, T. Fang, J. Fang, C. Lu and Z. Xu, *Compos. Sci. Technol.*, **2017**, 138, 106-116.
20. L. Fang, T. Fang, X. Liu, S. Chen, C. Lu and Z. Xu, *Macromol. Mater. Eng.*, **2016**, 301, 1111-1120.
21. W. Small Iv, T. S. Wilson, W. J. Benett, J. M. Loge and D. J. Maitland, *Opt. Express* **2005**, 13, 8204-8213.
22. R. R. Kohlmeyer, M. Lor and J. Chen, *Nano Lett.*, **2012**, 12, 2757-2762.

23. K. C. Hribar, R. B. Metter, J. L. Ifkovits, T. Troxler and J. A. Burdick, *Small*, **2009**, 5, 1830-1834.
24. J. R. Kumpfer and S. J. Rowan, *J. Am. Chem. Soc.*, **2011**, 133, 12866-12874.
25. D. J. Maitland, M. F. Metzger, D. Schumann, A. Lee and T. S. Wilson, *Lasers Surg. Med.,* **2002**, 30, 1-11.
26. G. M. Baer, W. Small, T. S. Wilson, W. J. Benett, D. L. Matthews, J. Hartman and D. J. Maitland, *BioMed. Eng. OnLine*, **2007**, 6, 43.
27. D. J. Maitland, I. V. W. Small, J. M. Ortega, P. R. Buckley, J. Rodriguez, J. Hartman and T. S. Wilson, *BIOMEDO*, **2007**, 12, 030504-030504-030503.
28. S. Eustis and M. A. El-Sayed, *Chem. Soc. Rev.*, **2006**, 35, 209-217.
29. N. C. Bigall, W. J. Parak and D. Dorfs, *Nano Today*, **2012**, 7, 282-296.
30. H. Chen, L. Shao, Q. Li and J. Wang, *Chem. Soc. Rev.*, **2013**, 42, 2679-2724.
31. C. J. Murphy, A. M. Gole, J. W. Stone, P. N. Sisco, A. M. Alkilany, E. C. Goldsmith and S. C. Baxter, *Acc. Chem. Res.*, **2008**, 41, 1721-1730.
32. E. C. Dreaden, A. M. Alkilany, X. Huang, C. J. Murphy and M. A. El-Sayed, *Chem. Soc. Rev.*, **2012**, 41, 2740-2779.
33. A. Golbang and M. Kokabi, *Eur. Polym. J.*, **2011**, 47, 1709-1719.
34. M. Ma, Y. Wu, J. Zhou, Y. Sun, Y. Zhang and N. Gu, *J. Magn. Magn. Mater.*, **2004**, 268, 33-39.
35. C. M. Yakacki, N. S. Satarkar, K. Gall, R. Likos and J. Z. Hilt, *J. Appl. Polym. Sci.*, **2009**, 112, 3166-3176.
36. Y. Xiongjun, Z. Shaobing, Z. Xiaotong, G. Tao, X. Yu and S. Botao, *Nanotechnology*, **2009**, 20, 235702.
37. J. Leng, H. Lu, Y. Liu and S. Du, *Appl. Phys. Lett.*, **2008**, 92, 204101-204103.
38. J. W. Cho, J. W. Kim, Y. C. Jung and N. S. Goo, *Macromol. Rapid Commun.*, **2005**, 26, 412-416.
39. I. S. Gunes, F. Cao and S. C. Jana, *Polymer*, **2008**, 49, 2223-2234.
40. C. Bartholome, P. Miaudet, A. Derré, M. Maugey, O. Roubeau, C. Zakri and P. Poulin, *Compos. Sci. Technol.*, **2008**, 68, 2568-2573.
41. M. Nishikawa, K. Wakatsuki and N. Takeda, *J. Mater. Sci.*, **2010**, 45, 3957-3960.
42. K. Jud, H. H. Kausch and J. G. Williams, *J. Mater. Sci.*, **1981**, 16, 204-210.
43. S. R. White, N. R. Sottos, P. H. Geubelle, J. S. Moore, M. R. Kessler, S. R. Sriram, E. N. Brown and S. Viswanathan, *Nature*, **2001**, 409, 794-797.
44. Y. Chen, A. M. Kushner, G. A. Williams and Z. Guan, *Nat. Chem.*, **2012**, 4, 467-472.

45. A. Phadke, C. Zhang, B. Arman, C.-C. Hsu, R. A. Mashelkar, A. K. Lele, M. J. Tauber, G. Arya and S. Varghese, *PNAS*, **2012**, 109, 4383-4388.
46. J. Cui and A. d. Campo, *Chem. Commun.*, **2012**, 48, 9302-9304.
47. J. Liu, G. Song, C. He and H. Wang, *Macromol. Rapid Commun.*, **2013**, 34, 1002-1007.
48. K. Haraguchi, K. Uyama and H. Tanimoto, *Macromol. Rapid Commun.*, **2011**, 32, 1253-1258.
49. N. Holten-Andersen, M. J. Harrington, H. Birkedal, B. P. Lee, P. B. Messersmith, K. Y. C. Lee and J. H. Waite, *PNAS*, **2011**, 108, 2651-2655.
50. Z. Shafiq, J. Cui, L. Pastor-Pérez, V. San Miguel, R. A. Gropeanu, C. Serrano and A. del Campo, *Angew. Chem.*, **2012**, 124, 4408-4411.
51. S. Burattini, B. W. Greenland, D. H. Merino, W. Weng, J. Seppala, H. M. Colquhoun, W. Hayes, M. E. Mackay, I. W. Hamley and S. J. Rowan, *J. Am. Chem. Soc.*, **2010**, 132, 12051-12058.
52. S. Burattini, B. W. Greenland, W. Hayes, M. E. Mackay, S. J. Rowan and H. M. Colquhoun, *Chem. Mater.*, **2011**, 23, 6-8.
53. S. Burattini, H. M. Colquhoun, J. D. Fox, D. Friedmann, B. W. Greenland, P. J. F. Harris, W. Hayes, M. E. Mackay and S. J. Rowan, *Chem. Commun.*, **2009**, 44, 6717-6719.
54. A. B. South and L. A. Lyon, *Angew. Chem.*, **2010**, 122, 779-783.
55. Q. Wang, J. L. Mynar, M. Yoshida, E. Lee, M. Lee, K. Okuro, K. Kinbara and T. Aida, *Nature*, **2010**, 463, 339-343.
56. J.-Y. Sun, X. Zhao, W. R. K. Illeperuma, O. Chaudhuri, K. H. Oh, D. J. Mooney, J. J. Vlassak and Z. Suo, *Nature*, **2012**, 489, 133-136.
57. T. L. Sun, T. Kurokawa, S. Kuroda, A. B. Ihsan, T. Akasaki, K. Sato, M. A. Haque, T. Nakajima and J. P. Gong, *Nat. Mater.*, **2013**, 12, 932-937.
58. Z. Wei, J. He, T. Liang, H. Oh, J. Athas, Z. Tong, C. Wang and Z. Nie, *Polymer Chemistry*, **2013**, 4, 4601-4605.
59. T. Kakuta, Y. Takashima, M. Nakahata, M. Otsubo, H. Yamaguchi and A. Harada, *Adv. Mater.*, **2013**, 25, 2849-2853.
60. M. Nakahata, Y. Takashima, H. Yamaguchi and A. Harada, *Nat. Commun.*, **2011**, 2, 511.
61. D. C. Tuncaboylu, M. Sari, W. Oppermann and O. Okay, *Macromolecules*, **2011**, 44, 4997-5005.
62. E. B. Murphy and F. Wudl, *Prog. Polym. Sci.*, **2010**, 35, 223-251.
63. X. Chen, M. A. Dam, K. Ono, A. Mal, H. Shen, S. R. Nutt, K. Sheran and F. Wudl, *Science*, **2002**, 295, 1698-1702.

64. Y. Amamoto, H. Otsuka, A. Takahara and K. Matyjaszewski, *Adv. Mater.*, **2012**, 24, 3975-3980.
65. C. e. Yuan, M. Z. Rong, M. Q. Zhang, Z. P. Zhang and Y. C. Yuan, *Chem. Mater.*, **2011**, 23, 5076-5081.
66. J. Ling, M. Z. Rong and M. Q. Zhang, *Polymer*, **2012**, 53, 2691-2698.
67. G. Deng, C. Tang, F. Li, H. Jiang and Y. Chen, *Macromolecules*, **2010**, 43, 1191-1194.
68. M. Pepels, I. Filot, B. Klumperman and H. Goossens, *Polymer Chemistry*, **2013**, 4, 4955-4965.
69. Y.-X. Lu and Z. Guan, *J. Am. Chem. Soc.*, **2012**, 134, 14226-14231.
70. P. J. Boul, P. Reutenauer and J.-M. Lehn, *Org. Lett.*, **2004**, 7, 15-18.
71. R. C. Boutelle and B. H. Northrop, *J. Org. Chem.*, **2011**, 76, 7994-8002.
72. Y. Chujo, K. Sada and T. Saegusa, *Macromolecules*, **1990**, 23, 2636-2641.
73. A. Gandini, *Prog. Polym. Sci.*, **2013**, 38, 1-29.
74. S. R. Trenor, A. R. Shultz, B. J. Love and T. E. Long, *Chem. Rev.*, **2004**, 104, 3059-3078.
75. P. Froimowicz, H. Frey and K. Landfester, *Macromol. Rapid Commun.*, **2011**, 32, 468-473.
76. C.-M. Chung, Y.-S. Roh, S.-Y. Cho and J.-G. Kim, *Chem. Mater.*, **2004**, 16, 3982-3984.
77. J. Ling, M. Z. Rong and M. Q. Zhang, *J. Mater. Chem.*, **2011**, 21, 18373-18380.
78. B. Ghosh and M. W. Urban, *Science*, **2009**, 323, 1458-1460.
79. J. Canadell, H. Goossens and B. Klumperman, *Macromolecules*, **2011**, 44, 2536-2541.
80. Y. Amamoto, J. Kamada, H. Otsuka, A. Takahara and K. Matyjaszewski, *Angew. Chem.*, **2011**, 123, 1698-1701.
81. M. Burnworth, L. Tang, J. R. Kumpfer, A. J. Duncan, F. L. Beyer, G. L. Fiore, S. J. Rowan and C. Weder, *Nature*, **2011**, 472, 334-337.
82. B. Ghosh, K. V. Chellappan and M. W. Urban, *J. Mater. Chem.*, **2012**, 22, 16104-16113.
83. B. D. Fairbanks, S. P. Singh, C. N. Bowman and K. S. Anseth, *Macromolecules*, **2011**, 44, 2444-2450.
84. T. F. Scott, A. D. Schneider, W. D. Cook and C. N. Bowman, *Science*, **2005**, 308, 1615-1617.
85. H. Otsuka, S. Nagano, Y. Kobashi, T. Maeda and A. Takahara, *Chem. Commun.*, **2010**, 46, 1150-1152.
86. Y. Wang, E. Bolanos, F. Wudl, T. Hahn and N. Kwok, *Proc. SPIE*, **2007**, 6526, 1-12.
87. J. S. Park, K. Takahashi, Z. Guo, Y. Wang, E. Bolanos, C. Hamann-Schaffner, E. Murphy, F. Wudl and H. T. Hahn, *J. Compos. Mater.*, **2008**, 42, 2869-2881.
88. J.-P. Fortin, F. Gazeau and C. Wilhelm, *Eur. Biophys. J.*, **2008**, 37, 223-228.

89. T. A. Plaisted, A. Vakil Amirkhizi, D. Arbelaez, S. C. Nemat-Nasser and S. Nemat-Nasser, *Proc. SPIE*, **2003**, 5054, 372-381.
90. L. Ionov, *Langmuir*, **2015**, 31, 5015-5024.
91. T. Ikeda, J.-i. Mamiya and Y. Yu, *Angew. Chem. Int. Ed.*, **2007**, 46, 506-528.
92. C. Ohm, M. Brehmer and R. Zentel, *Adv. Mater.*, **2010**, 22, 3366-3387.
93. Y. Yu and T. Ikeda, *Angew. Chem. Int. Ed.*, **2006**, 45, 5416-5418.
94. H. Yu and T. Ikeda, *Adv. Mater.*, **2011**, 23, 2149-2180.
95. T. J. White and D. J. Broer, *Nat. Mater.*, **2015**, 14, 1087-1098.
96. T. Mirfakhrai, J. D. W. Madden and R. H. Baughman, *Mater. Today*, **2007**, 10, 30-38.
97. J. S. Randhawa, K. E. Laflin, N. Seelam and D. H. Gracias, *Adv. Funct. Mater.*, **2011**, 21, 2395-2410.
98. Y. Zhang and L. Ionov, *ACS Appl. Mater. Interfaces*, **2014**, 6, 10072-10077.
99. L. T. de Haan, C. Sánchez-Somolinos, C. M. W. Bastiaansen, A. P. H. J. Schenning and D. J. Broer, *Angew. Chem. Int. Ed.*, **2012**, 51, 12469-12472.
100. G. Stoychev, N. Puretskiy and L. Ionov, *Soft Matter*, **2011**, 7, 3277-3279.
101. A. Azam, K. E. Laflin, M. Jamal, R. Fernandes and D. H. Gracias, *Biomed. Microdevices* **2011**, 13, 51-58.
102. J. Hu, Y. Zhu, H. Huang and J. Lu, *Prog. Polym. Sci.*, **2012**, 37, 1720-1763.
103. Q. Zhao, H. J. Qi and T. Xie, *Prog. Polym. Sci.*, **2015**, 49–50, 79-120.
104. M. D. Hager, S. Bode, C. Weber and U. S. Schubert, *Prog. Polym. Sci.*, **2015**, 49–50, 3-33.
105. M. Behl, K. Kratz, J. Zotzmann, U. Nöchel and A. Lendlein, *Adv. Mater.*, **2013**, 25, 4466-4469.
106. M. Behl, K. Kratz, U. Noechel, T. Sauter and A. Lendlein, *PNAS*, **2013**, 110, 12555-12559.
107. H. Finkelmann, H.-J. Kock and G. Rehage, *Makromol. Chem. Rapid Commun.,* **1981**, 2, 317-322.
108. J. Küupfer and H. Finkelmann, *Macromol. Chem. Phys.*, **1994**, 195, 1353-1367.
109. R. Zentel and G. Reckert, *Makromol. Chem.,* **1986**, 187, 1915-1926.
110. R. Zentel and M. Benalia, *Makromol. Chem.,* **1987**, 188, 665-674.
111. D. J. Broer, H. Finkelmann and K. Kondo, *Makromol. Chem.,* **1988**, 189, 185-194.
112. J. Küpfer and H. Finkelmann, *Makromol. Chem. Rapid Commun.,* **1991**, 12, 717-726.
113. I. Kundler and H. Finkelmann, *Macromol. Chem. Phys.*, **1998**, 199, 677-686.
114. M. Tammer, J. Li, A. Komp, H. Finkelmann and F. Kremer, *Macromol. Chem. Phys.*, **2005**, 206, 709-714.
115. H. Finkelmann, S. T. Kim, A. Muñoz, P. Palffy-Muhoray and B. Taheri, *Adv. Mater.*, **2001**, 13, 1069-1072.

116. X.-Z. He, B.-Y. Zhang, F.-B. Meng and J.-R. Lin, *J. Appl. Polym. Sci.*, **2005**, 96, 1204-1210.
117. F.-B. Meng, B.-Y. Zhang, W.-Q. Xiao and T.-X. Hu, *J. Appl. Polym. Sci.*, **2005**, 96, 625-631.
118. M. Brehmer, R. Zentel, G. Wagenblast and K. Siemensmeyer, *Macromol. Chem. Phys.* , **1994**, 195, 1891-1904.
119. E. Nishikawa and H. Finkelmann, *Macromol. Chem. Phys.*, **1997**, 198, 2531-2549.
120. E. Gebhard and R. Zentel, *Macromol. Rapid Commun.*, **1998**, 19, 341-344.
121. E. Nishikawa and H. Finkelmann, *Macromol. Chem. Phys.*, **1999**, 200, 312-322.
122. H. M. Brodowsky, U.-C. Boehnke, F. Kremer, E. Gebhard and R. Zentel, *Langmuir*, **1999**, 15, 274-278.
123. W. Lehmann, H. Skupin, C. Tolksdorf, E. Gebhard, R. Zentel, P. Kruger, M. Losche and F. Kremer, *Nature*, **2001**, 410, 447-450.
124. J. J. Zanna, P. Stein, J. D. Marty, M. Mauzac and P. Martinoty, *Macromolecules*, **2002**, 35, 5459-5465.
125. K. Hiraoka, W. Sagano, T. Nose and H. Finkelmann, *Macromolecules*, **2005**, 38, 7352-7357.
126. P. Beyer and R. Zentel, *Macromol. Rapid Commun.*, **2005**, 26, 874-879.
127. S. Disch, H. Finkelmann, H. Ringsdorf and P. Schuhmacher, *Macromolecules*, **1995**, 28, 2424-2428.
128. M. Warner, K. P. Gelling and T. A. Vilgis, *J. Chem. Phys.*, **1988**, 88, 4008-4013.
129. Y. Mao, E. M. Terentjev and M. Warner, *Phys. Rev. E*, **2001**, 64, 041803.
130. O. Stenull and T. C. Lubensky, *Phys. Rev. Lett.*, **2005**, 94, 018304.
131. S. Krause, F. Zander, G. Bergmann, H. Brandt, H. Wertmer and H. Finkelmann, *C.R. Chim.*, **2009**, 12, 85-104.
132. T. H. Ware, M. E. McConney, J. J. Wie, V. P. Tondiglia and T. J. White, *Science*, **2015**, 347, 982-984.
133. K. D. Harris, C. W. M. Bastiaansen, J. Lub and D. J. Broer, *Nano Lett.*, **2005**, 5, 1857-1860.
134. B. T. Michal, B. M. McKenzie, S. E. Felder and S. J. Rowan, *Macromolecules*, **2015**, 48, 3239-3246.
135. H. Finkelmann, E. Nishikawa, G. G. Pereira and M. Warner, *Phys. Rev. Lett.*, **2001**, 87, 015501.
136. P. M. Hogan, A. R. Tajbakhsh and E. M. Terentjev, *Phys. Rev. E*, **2002**, 65, 041720.
137. J. Cviklinski, A. R. Tajbakhsh and E. M. Terentjev, *Eur. Phys. J. E*, **2002**, 9, 427-434.

138. T. Ikeda, M. Nakano, Y. Yu, O. Tsutsumi and A. Kanazawa, *Adv. Mater.*, **2003**, 15, 201-205.
139. Y. Yu, M. Nakano and T. Ikeda, *Nature*, **2003**, 425, 145-145.
140. Y. Yu, M. Nakano, A. Shishido, T. Shiono and T. Ikeda, *Chem. Mater.*, **2004**, 16, 1637-1643.
141. S. Iamsaard, S. J. Aßhoff, B. Matt, T. Kudernac, J. L. M. CornelissenJeroen, S. P. Fletcher and N. Katsonis, *Nat. Chem.*, **2014**, 6, 229-235.
142. E. Wang, M. S. Desai and S.-W. Lee, *Nano Lett.*, **2013**, 13, 2826-2830.
143. C. Yu, Z. Duan, P. Yuan, Y. Li, Y. Su, X. Zhang, Y. Pan, L. L. Dai, R. G. Nuzzo, Y. Huang, H. Jiang and J. A. Rogers, *Adv. Mater.*, **2013**, 25, 1541-1546.
144. T. G. Leong, A. M. Zarafshar and D. H. Gracias, *Small*, **2010**, 6, 792-806.
145. G. Stoychev, S. Zakharchenko, S. Turcaud, J. W. C. Dunlop and L. Ionov, *ACS Nano*, **2012**, 6, 3925-3934.
146. G. Stoychev, S. Turcaud, J. W. C. Dunlop and L. Ionov, *Adv. Funct. Mater.*, **2013**, 23, 2295-2300.
147. C. Heinzmann, C. Weder and L. M. de Espinosa, *Chem. Soc. Rev.*, **2016**, 45, 342-358.
148. L. Voorhaar and R. Hoogenboom, *Chem. Soc. Rev.*, **2016**, 45, 4013-4031.
149. C. D. Jones and J. W. Steed, *Chem. Soc. Rev.*, **2016**, 45, 6546-6596.
150. N. Gospodinova and E. Tomšík, *Prog. Polym. Sci.*, **2015**, 43, 33-47.
151. P. Wei, X. Yan and F. Huang, *Chem. Soc. Rev.*, **2015**, 44, 815-832.
152. C. Bohne, *Chem. Soc. Rev.*, **2014**, 43, 4037-4050.
153. C. J. Kloxin, T. F. Scott, H. Y. Park and C. N. Bowman, *Adv. Mater.*, **2011**, 23, 1977-1981.
154. K. Imato, M. Nishihara, T. Kanehara, Y. Amamoto, A. Takahara and H. Otsuka, *Angew. Chem. Int. Ed.*, **2012**, 51, 1138-1142.
155. M. Capelot, D. Montarnal, F. Tournilhac and L. Leibler, *J. Am. Chem. Soc.*, **2012**, 134, 7664-7667.
156. D. Montarnal, M. Capelot, F. Tournilhac and L. Leibler, *Science*, **2011**, 334, 965-968.
157. M. Röttger, T. Domenech, R. van der Weegen, A. Breuillac, R. Nicolaÿand L. Leibler, *Science*, **2017**, 356, 62-65.
158. C. J. Kloxin and C. N. Bowman, *Chem. Soc. Rev.*, **2013**, 42, 7161-7173.
159. Z. Pei, Y. Yang, Q. Chen, E. M. Terentjev, Y. Wei and Y. Ji, *Nat. Mater.*, **2014**, 13, 36-41.
160. R. NicolaÿJ. Kamada, A. Van Wassen and K. Matyjaszewski, *Macromolecules*, **2010**, 43, 4355-4361.
161. C. N. Bowman and C. J. Kloxin, *Angew. Chem. Int. Ed.*, **2012**, 51, 4272-4274.
162. S. M. Liff, N. Kumar and G. H. McKinley, *Nat. Mater.*, **2007**, 6, 76-83.

163. B. Fernández-d'Arlas, J. A. Ramos, A. Saralegi, M. Corcuera, I. Mondragon and A. Eceiza, *Macromolecules*, **2012**, 45, 3436-3443.
164. R. Elbaum, L. Zaltzman, I. Burgert and P. Fratzl, *Science*, **2007**, 316, 884-886.
165. D. Evangelista, S. Hotton and J. Dumais, *J. Exp. Biol.,* **2011**, 214, 521-529.
166. P. Fratzl and F. G. Barth, *Nature*, **2009**, 462, 442-448.
167. J. Dumais and Y. Forterre, *Annu. Rev. Fluid Mech.*, **2012**, 44, 453-478.
168. Y. Forterre, J. M. Skotheim, J. Dumais and L. Mahadevan, *Nature*, **2005**, 433, 421-425.
169. E. Stokstad, *Science*, **2016**, 352, 756-756.
170. K. Schulgasser and A. Witztum, *J. Theor. Biol.*, **2004**, 230, 281-288.
171. P. Fratzl and R. Weinkamer, *Prog. Mater Sci.*, **2007**, 52, 1263-1334.
172. P. Nayomi, L. Z. Samuel, S. S. Don and E. J. Joseph, *Smart Mater. Struct.*, **2013**, 22, 072001.
173. J.-S. Wang, G. Wang, X.-Q. Feng, T. Kitamura, Y.-L. Kang, S.-W. Yu and Q.-H. Qin, *Sci. Rep.*, **2013**, 3, 3102.
174. Y. Abraham, C. Tamburu, E. Klein, J. W. C. Dunlop, P. Fratzl, U. Raviv and R. Elbaum, *J. R. Soc. Interface*, **2012**, 9, 640-647.
175. J. M. García, G. O. Jones, K. Virwani, B. D. McCloskey, D. J. Boday, G. M. ter Huurne, H. W. Horn, D. J. Coady, A. M. Bintaleb, A. M. S. Alabdulrahman, F. Alsewailem, H. A. A. Almegren and J. L. Hedrick, *Science*, **2014**, 344, 732-735.
176. P. Taynton, K. Yu, R. K. Shoemaker, Y. Jin, H. J. Qi and W. Zhang, *Adv. Mater.*, **2014**, 26, 3938-3942.